

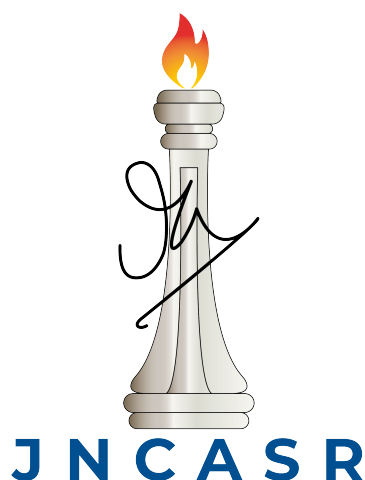
Kinetics of Phase Transitions in a few Systems with Long-range Interactions

A Thesis

Submitted for the Degree of
DOCTOR OF PHILOSOPHY
in the Faculty of Science

by

Soumik Ghosh



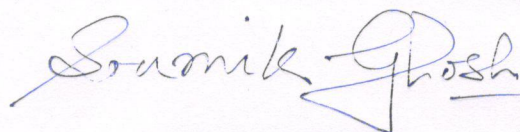
THEORETICAL SCIENCES UNIT
JAWAHARLAL NEHRU CENTRE FOR ADVANCED SCIENTIFIC RESEARCH
(A Deemed University)
Bangalore – 560 064

November 2024

DECLARATION

I hereby declare that the matter embodied in the thesis entitled “**Kinetics of Phase Transitions in a few Systems with Long-range Interactions**” is the result of investigations carried out by me at the Theoretical Sciences Unit, Jawaharlal Nehru Centre for Advanced Scientific Research, Bangalore, India under the supervision of **Prof. Subir K. Das**, and that it has not been submitted elsewhere for the award of any degree or diploma.

In keeping with the general practice in reporting scientific observations, due acknowledgment has been made whenever the work described is based on the findings of other investigators.



Soumik Ghosh

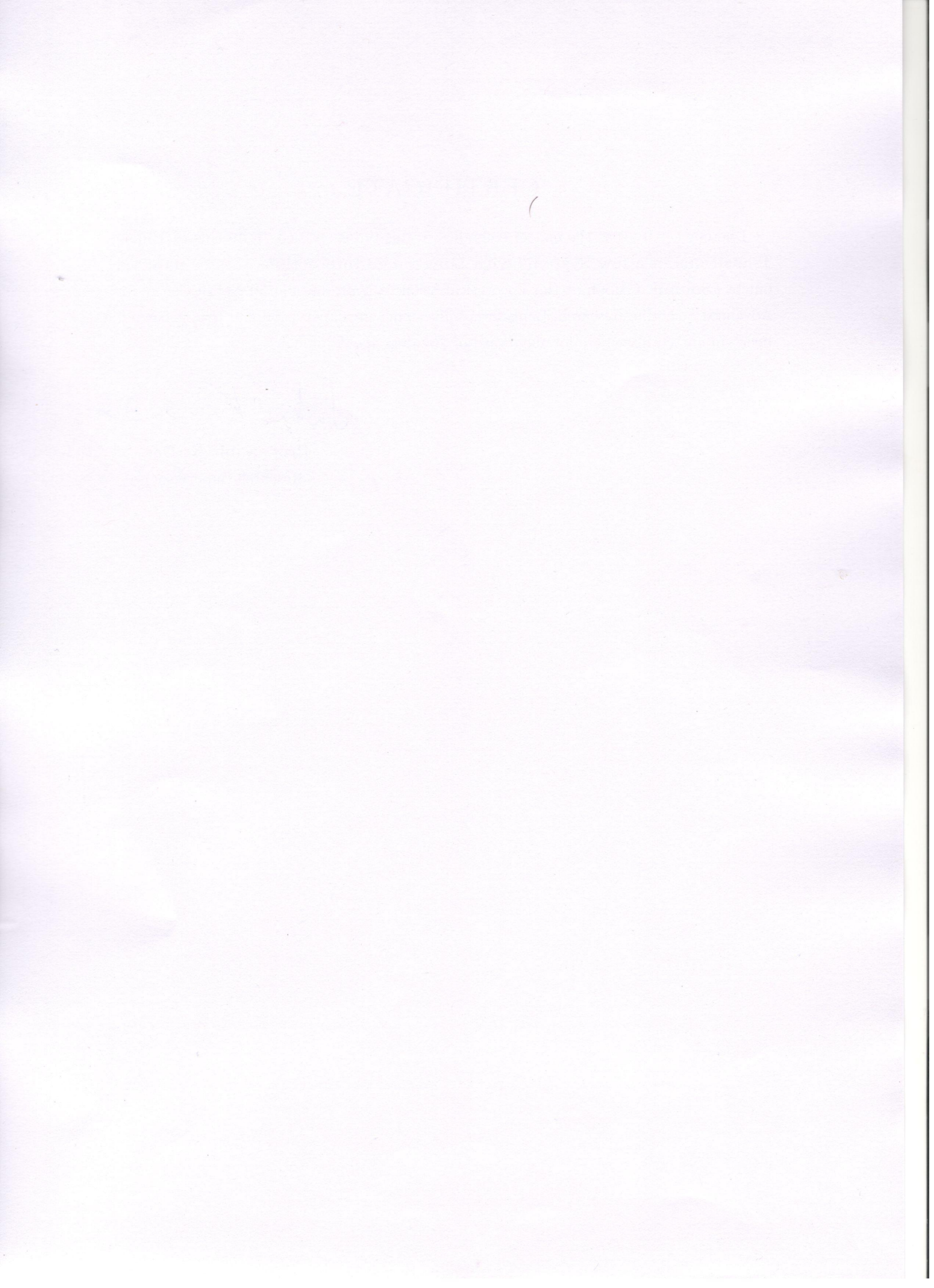
CERTIFICATE

I hereby certify that the matter embodied in this thesis entitled "**Kinetics of Phase Transitions in a few Systems with Long-range Interactions**" has been carried out by **Soumik Ghosh** at the Theoretical Sciences Unit, Jawaharlal Nehru Centre for Advanced Scientific Research, Bangalore, India under my supervision and that it has not been submitted elsewhere for the award of any degree or diploma.



Prof. Subir K. Das

(Research Supervisor)



Acknowledgements

First and foremost, I would like to thank my Ph. D. Supervisor, Prof. Subir K. Das, for his constant motivation, support and guidance throughout my Ph. D years.

I thank all my course instructors – Prof. Meher K. Prakash, Prof. Kavita Jain, Prof. Shobhana Narasimhan, Prof. Subir K. Das, Prof. Srikanth Sastry, and Prof. Rajesh Ganapathy. I also want to thank former TSU chair Prof. Swapan K. Pati and other TSU faculty members Prof. N.S. Vidhyadhiraja and Prof. K. B. Sinha for being a source of inspiration.

I would also like to thank my M.Sc. thesis Supervisor Dr. Malay Kumar Bandyopadhyay for his support and motivation.

I am thankful to the Graduate Students Advisory committee (GSAC) members, Prof. Rajesh Ganapathy and Prof. Diwakar, for their guidance.

I would like to thank all my past and present lab members - Dr. Nalina Vadakkayil, Dr. Koyel Das, Dr. Arabinda Bera, Dr. Sanat K. Singha, Dr. Tanay Paul, Soham, Purnendu, Sohini, Wasim, Mayukh, Kaushik, Shivam and Krishna - for their help and encouragement.

I thank all my outside-the-lab friends - Arpan, Bidhan, Prasenjit, abhishek, Koyel, Panda, Sinay, Oishika, Purnendu, Arijit, Souvik and Ritam.

I am deeply grateful to the members of my extended-family at JNCASR - Riddhimoy, Adrija, Supriti, Bitan and Darshana - for making the long journey memorable!

I would like to thank the Paramyukti supercomputing facility at JNCASR.

My sincere gratitude to all the staff from Library, Complab, Dhanvantari, Academics, Administration, Hostel, Hostel Mess, Dining hall, and Housekeeping.

I am grateful to JNCASR for the financial support.

A special thanks to Supriti (Dr. Dutta), for being a constant support throughout.

I express my heartfelt gratitude to my parents and few dearest family members who stood by my side in every situation.

Synopsis

This thesis contains results from studies aimed at exploring the structural and dynamical aspects of systems where inter-atomic interactions are long-range in nature . We have investigated phenomena associated with phase transitions in systems which are otherwise of different types. Below we provide a sketch of the thesis with brief discussions of the chapters.

In **Chapter 1** first we provide a basic picture of phase transitions. Following this, we introduce scaling properties related to aspects like structure, growth and aging. Relevant simulation methods in the broad domains of Monte Carlo (MC) and molecular dynamics (MD) are discussed. We have also incorporated descriptions of certain important methods of analysis in this chapter.

Chapters 2, 3, and 4 contain MC simulation results from the studies of phase separation kinetics in symmetric binary mixtures . For this purpose we have used the Ising model within which particles or spins interact via long-range potentials. With random initial arrangements of spins, mimicking a very high-temperature scenario, systems are quenched to a temperature inside the coexistence region. Our first focus has been on structure and growth. This was followed by the investigation of the aging phenomena, as the systems approach the equilibrium at the new state point. In order to study the kinetics, Kawasaki spin exchange Monte Carlo simulations were performed, in space dimension $d = 2$. It is observed that all the above-mentioned aspects depend upon the interaction range. Nevertheless, certain combination of the quantitative features exhibit universality.

In **Chapter 5**, we have undertaken a problem that remained a puzzle over millennia. A hotter body of water freezes faster than a colder one when kept inside the refrigerator - this counterintuitive fact is known as the Mpemba Effect (ME). We have carried out MD simulations using a realistic model of water. Following quenches of configurations prepared at temperatures above the freezing point to a fixed value lying deep inside the ice phase, we have noted the freezing times. Our results clearly indicate the presence of the fascinating ME for a wide range of initial temperatures.

Chapter 6 reports an investigation of the Mpemba-like effect in pure spin systems with long-range interaction. We have chosen the Ising model for a para-to-ferromagnetic transition. Configurations prepared at various temperatures above the Curie temperature T_c are quenched to a fixed temperature in the ferromagnetic region. Our MC simulations show that the ME exists in this case also.

Finally, in the **last Chapter** we have summarized the works and provided discussions by mentioning the future possibilities.

Contents

| | |
|--|------------|
| List of Publications | vii |
| 1 Introduction | 1 |
| 1.1 Phase Transition | 1 |
| 1.1.1 First-order Phase Transition | 1 |
| 1.1.2 Continuous Phase Transition | 2 |
| 1.2 Kinetics of Phase Transitions | 3 |
| 1.2.1 Correlation and Scaling | 6 |
| 1.3 More on Phase Transitions | 7 |
| 1.3.1 Ising Model | 7 |
| 1.3.2 Phase Transitions in Water | 8 |
| 1.4 Computational Methodologies | 10 |
| 1.4.1 Monte Carlo Simulation | 10 |
| 1.4.2 Molecular Dynamics Simulation | 13 |
| 1.4.3 Handling Long-range Forces | 16 |
| 1.5 Finite Size Scaling | 19 |
| 1.6 Overview of the Thesis | 20 |
| Bibliography | 21 |
| 2 Kinetics of Phase Separation in Systems with Long-range Interaction: Study of Domain Structure and Growth | 25 |
| 2.1 Introduction | 25 |
| 2.2 Model and Methods | 27 |
| 2.3 Results | 29 |
| 2.4 Conclusion | 38 |
| Bibliography | 41 |

| | |
|--|------------|
| 3 Kinetics of Phase Separation in Systems with Long-range Interaction: Study of Aging | 43 |
| 3.1 Introduction | 43 |
| 3.2 Model and Methods | 45 |
| 3.3 Results | 46 |
| 3.4 Conclusion | 53 |
| Bibliography | 57 |
| 4 Coarsening in the Long-range Ising Model with Conserved Dynamics | 59 |
| 4.1 Introduction | 59 |
| 4.2 Model and Methods | 61 |
| 4.3 Results | 62 |
| 4.4 Conclusion | 73 |
| Bibliography | 77 |
| 5 Mpemba Effect in WATER: A simulation study | 81 |
| 5.1 Introduction | 81 |
| 5.2 Model and Methods | 82 |
| 5.3 Results | 84 |
| 5.4 Conclusion | 93 |
| Bibliography | 95 |
| 6 Initial Temperature Dependence of Ordering in Long-range Ising Model | 97 |
| 6.1 Introduction | 97 |
| 6.2 Model and Methods | 98 |
| 6.3 Results | 99 |
| 6.4 Conclusion | 110 |
| Bibliography | 113 |
| 7 Summary of the Thesis | 115 |
| Bibliography | 119 |

List of Publications

1. “Nonuniversal aging during phase separation with long-range interaction”, **Soumik Ghosh** and Subir K. Das, Phys. Rev. E **109**, L052102 (2024).
2. “Simulations of Mpemba Effect in WATER, Lennard-Jones and Ising Models: Metastability vs Critical Fluctuations”, **Soumik Ghosh**, Purnendu Pathak, Sohini Chatterjee and Subir K. Das, arXiv:2407.06954 (2024).
3. “Mpemba effect in pure spin systems: Role of initial correlation and a universality”, Sohini Chatterjee, **Soumik Ghosh**, Nalina Vadakkayil, Tanay Paul, Sanat K. Singha and Subir K. Das, Phys. Rev. E **110**, L012103 (2024).
4. “Coarsening in the Long-range Ising Model with Conserved Dynamics”, **Soumik Ghosh** and Subir K. Das, arXiv:2407.06954 (2024).

List of Figures

- 1.1 Schematics of three different phases and their boundaries, for a typical chemical system, are drawn in Pressure vs Temperature plane. Critical point (T_c, P_c), as well as the triple point, are marked. 2
- 1.2 (a) Magnetization (m) is plotted versus temperature (T). The filled circle marks the location of the critical temperature, T_c . The direction of the atomic magnets inside the system at different temperatures are symbolically shown by up and down arrows. (b) A schematic diagram showing divergence of susceptibility (χ) with the variation of temperature (T). 3
- 1.3 A schematic phase diagram of a vapor-liquid transition in ρ vs. T plane is shown. The line separating the homogeneous phase from the phase-separated regime is a coexistence line. The point (ρ_c, T_c) is the critical point. This may describe phase behavior of an immiscible binary mixture as well, if ρ is replaced by the concentration/density of one of the participating species. Representative equilibrium snapshots from homogeneous and phase-separated regions are shown. 4
- 1.4 (a) Schematic phase diagram for Ice phases. Phases labeled with black Roman numerals are hydrogen-disordered phases; those labeled with red numerals are hydrogen-ordered phases; those labeled with blue numerals are metastable phases. The red solid arrows represent direct disorder-order transitions. The red dotted arrows represent disorder-order transitions that cross the stability range of another phase. Figure source: Thomas C. Hansen, Nature Communication **12**, 3161 (2021). (b) Model Ih ice structure (source: Wikipedia) is shown. Black spheres denote Oxygen positions, whereas, the white spheres are Hydrogens. 9

| | | |
|-----|--|----|
| 2.1 | Snapshots at different MC steps for an evolution with $\sigma = 0.6$, following quench of a random initial configuration to a temperature $T = 0.6T_c$. Locations of the particles are marked. These results are for $L = 256$ | 28 |
| 2.2 | Average domain length, ℓ , is plotted versus time t . We have included results for systems with $\sigma = 0.6$ and 0.95 | 31 |
| 2.3 | (a) Correlation functions, $C(r, t)$, from three different times, are plotted versus the distance r , for $\sigma = 0.6$. In (b), distance r is scaled by the domain lengths ℓ at corresponding times to obtain a collapse of the data. | 32 |
| 2.4 | (a) The inverse of the instantaneous exponent, α_i , for $\sigma = 0.6$ and different values of L , are plotted versus $1/t$. The solid line is a guide to the eyes, showing possible convergence of the data in the $t \rightarrow \infty$ limit. We have discarded some noisy data points at a very late time for a better visualization. (b) Same as in (a), but here the results are for $\sigma = 0.95$ and only one system size, viz., $L = 256$ | 33 |
| 2.5 | Plot of α as a function of σ . Results from both Theory (Th) and Simulations (Sim) are included. | 34 |
| 2.6 | (a) Structure factor, $S(k, t)$, from systems with two different σ values, viz., $\sigma = 0.6$ and 0.8 , are plotted against wave number k . The abscissa of the data from $\sigma = 0.8$ is shifted by hand for a clear view. Solid lines represent the expected power-law behavior. The rectangular box is drawn to capture the anomalous regions present. (b) Same plots as in (a), for systems with only $\sigma = 0.6$ and three different values of L | 35 |
| 2.7 | We plot X_i , for $\sigma = 0.6$, versus wave-number k , with $L = 256$. The upper horizontal line shows the maximum corresponding to a knee shown in Fig. 2.6. The lower one estimates the Porod exponent. The difference between these two is identified as Δ | 36 |
| 2.8 | Plot of Δ as a function of $(1 - \sigma)$ | 37 |

| | | |
|-----|---|----|
| 3.1 | Plots of the autocorrelation function, $C_{ag}(t, t_w)$, as a function of ℓ/ℓ_w , for the LRIM, with $\sigma = 0.6$. Results for several different ages have been included. (a) shows the original data with a jump that corresponds to the equilibration of domain magnetization. Results in (b) are scaled by a pre-factor, after discarding the jumps, such that C_{ag} smoothly approaches 1, as $\ell/\ell_w \rightarrow 1$, for most of the t_w values. Such a transformation does not affect the decay exponent. The solid line represents a power-law decay with the mentioned value of the exponent. The presented results are for $L = 256$, the unit being the lattice constant. | 47 |
| 3.2 | Instantaneous exponent, λ_i , are plotted versus t_w/t , for different σ and system sizes. Solid lines are the linear fits to the data sets from $L = 256$. Since λ_i is a noisy quantity, running averaging was carried out for data smoothening. | 48 |
| 3.3 | The estimated values of the aging exponent, λ , from the fits in Fig. 3.2, are shown against σ . These are calculated by considering t_w values from the scaling regimes. | 48 |
| 3.4 | Equal-time structure factors, $S(k, t)$, are plotted versus wave number k . The dashed and the solid lines are power-laws. System size, values of σ and exponents are mentioned in appropriate places inside the frame. | 50 |
| 3.5 | The quantity X_i is plotted versus k , for $\sigma = 0.6$ and 0.95 . Here, we have shown a small portion of the ordinate that is important for verifying the YRD bound. The horizontal dashed lines define the ceiling for the instantaneous exponent. The line colors are matched with the symbols to clearly identify the maxima for different values of σ | 51 |
| 3.6 | The quantity λ' , obtained from the calculated values of λ and theoretical predictions for α , is plotted versus σ | 52 |
| 3.7 | $C_{ag}(t, t_w) \times y^{\lambda'}$ is plotted versus y for $\sigma = 0.6$ an the nearest neighbor (NN) Ising model, with $L = 512$. The constant prefactors, A and B are introduced only for visual convenience. We have chosen $\lambda' = 1.1$ for both the cases. | 54 |

| | | |
|-----|--|----|
| 4.1 | Evolution snapshots of the 2D systems, with $L = 128$, when quenched to $0.6T_c$, from high temperature, are shown for (a) $\sigma = 1.5$ and (b) $\sigma = 0.6$. The locations of the particles are marked. For each σ value, in addition to the initial configuration, two well-grown configurations are displayed. | 62 |
| 4.2 | Domain length, $\ell(t)$, of systems with different σ values, are plotted against time t . The system size is mentioned inside the frame. | 63 |
| 4.3 | The upper left frame shows a snapshot taken during the evolution of a system with $\sigma = 1.5$. The lower left frame contains the same snapshot after removing the noise. See the text for discussion and reference related to the removal of noise. The right frame shows a comparison between domain lengths calculated by using snapshots with and without noise. These results are for $L = 128$ | 64 |
| 4.4 | (a) Instantaneous exponent, α_i , for different σ values, viz., $\sigma = 0.6$ and 0.9 , are plotted against $1/\ell$. (b) Same as (a), but here the results are for the nearest neighbor Ising model (NNIM). Inset shows the same plot for the LRIM with $\sigma = 1.5$. Various arrow-headed lines are guides to the eyes. All the data are presented after running averaging. Data earlier than the presented ones suffer from noise removal exercise. See text for a discussion on the latter fact. | 66 |
| 4.5 | (a) Plots of $\ell(t)$, versus t , for $\sigma = 0.6$, from three different system sizes. The dashed horizontal lines are our estimates for ℓ_{\max} . See text for the definition of the latter. | 68 |
| 4.6 | (a) Double-log plots of the finite-size scaling function, $Y(y)$, against the scaling variable y , for $\sigma = 0.6$. Data for a few different system sizes, viz., $L = 16, 24$, and 32 , are included. The dashed line represents Eq. (4.9) with $\alpha = 0.625$. The solid line is a fit of the simulation data to Eq. (4.11). See text for the best fit values of relevant parameters. (b) Eq. (4.12) (see the solid lines) is compared with direct growth data for $L = 16, 24$ and 32 . For the purpose of clear visualization, of comparison between simulation data and the analytical lines, we have thinned down the data sets in both parts (a) and (b). | 69 |

| | | |
|------|---|----|
| 4.7 | Plots of $\ell'(t)$ ($= \ell - \ell_0$), as a function of t' ($=t - t_0$), on a log-log scale, for (a) $\sigma = 0.6$ and (b) $\sigma = 0.8$. In each of the cases data from three different system sizes have been included. This is to show that the post-crossover bending is not due to finite-size effects. Solid lines are for the initial behavior of the growth and the dashed lines denote the later time, $\alpha = 1/(2 + \sigma)$, growth. | 72 |
| 4.8 | Scaling plot of $C(r, t)$, for $\sigma = 0.6$ and $L = 256$, using data from (a) early and (b) late times. | 73 |
| 4.9 | (a) Finite-size scaling exercise for $\sigma = 1.5$, using $\ell(t)$ data from different system sizes. The dashed line represents Eq. (4.9) with $\alpha = 0.32$ and the solid line is a fit of the simulation data to the analytical form in Eq. (4.11). (b) Same as Fig. 4.6(b) but here the demonstration is for $\sigma = 1.5$. The considered values of ℓ_{\max} for $L = 32, 64$ and 128 are $16, 32$ and 64 , respectively. Like in Fig. 4.6 here also we have thinned down the data sets, for visual clarity. | 74 |
| 4.10 | Both early-time and late-time values of the growth exponent α are plotted against σ . Simulation results are shown with symbols, whereas the relevant theoretical predictions (Th) are shown by dashed and dashed-dotted lines. The continuous line is a guide to the eye. The values of the late time exponents for $\sigma < 1$ are taken from Ref. [32]. For $\sigma > 1$, it was difficult to choose regions of data sets to estimate early and late time values of α . The overlapping numbers provide testimony to this fact. | 75 |
| 5.1 | Comparisons of phase behavior [15], obtained from simulations of two different models of water, viz., TIP4P and TIP4P/Ice, as well as from experiments. The circle is to highlight the convergence of the phase diagrams obtained via simulations of TIP4P/Ice model and that from experiments. | 83 |
| 5.2 | A schematic diagram of the TIP4P/Ice model of water. See text for the description. | 85 |
| 5.3 | Water molecules are arranged on a simple cubic lattice. The bond lengths and orientations within a molecule were taken from GitHub [25], to provide inputs to the LAMMPS [21] simulations. Oxygen atoms are shown in red and Hydrogens in grey. | 86 |

| | | |
|-----|--|-----|
| 5.4 | (a) Potential energy (PE), per molecule, is plotted for an equilibrium system at $400K$. (b) A typical configuration is shown from the equilibrium regime shown in (a). | 87 |
| 5.5 | Potential energy corresponding to a simulation run, with initial configuration prepared at $400K$, is shown following a quench to $230K$. Log scale for time is used in (a) to capture the fast decay in energy at small time limit. In (b), the time scale is kept linear so that the jump in the potential energy can be clearly seen. (c) A snapshot taken from the Ice regime is shown. Red dots denote the positions of the O atoms, whereas, H atoms are shown in gray. The arrangement of the atoms suggest a hexagonal Ice structure. | 88 |
| 5.6 | The temperature, T , of the system is plotted versus time, t , for the simulation in Fig. 5.5. | 90 |
| 5.7 | The probability distribution $P(q_6)$ of the sixth order local bond order q_6 is plotted. The blue curve corresponds to the periods after the energy jump seen in Fig. 5.5 (a) and (b). The location of the peak indicates a hexagonal Ice crystal. The red line is the same quantity but this is for supercooled/metastable water. | 91 |
| 5.8 | (a) Potential energy is plotted as a function of time for the TIP4P/Ice simulations. Results are shown for quenches to $T_f = 230K$, from a few starting temperatures, T_s . Data in each of the sets are thinned down for the sake of clarity. The symbols show the locations of jumps for simulation runs with certain other starting configurations. A unique color is used for a given T_s . The early parts of the energy decay are shown again in (b) by using a log scale for the abscissa. The horizontal lines stand for approximately the average values for intermediate metastable liquid and final Ice phase energies. | 92 |
| 5.9 | The freezing time, t_f , averaged over 8 runs for each T_s , is plotted as a function of T_s . The dashed line is a guide to the eye. | 92 |
| 6.1 | Snapshots of an evolving system, with $\sigma = 0.8$, taken at different times when quenched from a very high temperature to a final temperature $T_f = 0.3T_c$. Positions of the $+1$ spins are marked with red, while -1 spins are left unmarked. | 100 |

| | | |
|-----|--|-----|
| 6.2 | (a) Correlation function, $C(r, t)$, from three different times are plotted, versus distance, r , for $\sigma = 0.8$ and $L = 1024$. In (b), r is scaled by the domain length, ℓ , at corresponding times. | 101 |
| 6.3 | Average domain lengths, $\ell(t)$, in log-log scale, for $\sigma = 0.6$ and 0.8 , are plotted versus time, t . The ordinate of the data for $\sigma = 0.8$ is shifted artificially for better visualization of the difference in growth. These results have similarities with those in Ref. [12]. | 102 |
| 6.4 | The correlation function, $C(r, t)$, is plotted versus distance r for systems with two different σ values, viz., $\sigma = 0.6$ and 0.8 , as well as a nearest neighbor (NN) Ising model. The solid lines represent Ohta-Jasnow-Kawasaki function. | 104 |
| 6.5 | Equilibrium snapshots, prepared at two different starting temperatures, viz., $1.2T_c$ and ∞ , are shown. These results are for $\sigma = 0.8$ | 105 |
| 6.6 | Structure factor, $S(k, t)$, is plotted as a function of wavenumber, k . Results from three different initial temperatures are included. Note that the structure factor is defined as $S(k, t) = \langle \phi_k(t) \phi_{-k}(t) \rangle$ [19]. | 106 |
| 6.7 | Average domain lengths, $\ell(t)$, when quenched to a final temperature, $T_f = 0.3T_c$, from three different T_s are shown as a function of time t . The lower panel shows very early time data, whereas the upper panel shows data from late times. | 107 |
| 6.8 | The correlation function, $C(r, t)$, is plotted as a function of r/ℓ for three different starting temperatures, T_s . (a) Data from the pre-crossing time are shown. (b) Here scaling of data at a post-crossover time is shown. These results are for $\sigma = 0.8$ | 108 |
| 6.9 | Total energy per spin, E , is plotted against time, t , for three different starting temperatures, T_s . The upper and lower panels show data from early and late times, respectively. | 109 |

- 7.1 (a) The upper half shows a plot of the growth exponent, α , in the long time limit, for conserved order-parameter dynamics in the LRIM, that we have obtained from our simulations, as a function of σ . In the lower half, we have plotted the deviation, Δ , from the expected Porod exponent, in some intermediate wave number region, versus $(1 - \sigma)$. (b) Here, in the upper part, we have shown our estimated values of the aging exponent, λ , for the LRIM with conserved order-parameter dynamics, as a function of σ . The lower part shows the variation in the quantity λ' ($= \alpha\lambda$) with the variation in σ . (c) The simulation estimated early and late time values of α , for the same system as in (a) and (b), are plotted as a function of σ , with symbols. The lines correspond to the existing theoretical predictions. (d) Freezing times, t_f , for the TIP4P/Ice model, are shown as a function of the starting temperatures, T_s . The dashed line is drawn for a better visualization of the trend. (e) Decay of energy per spin, E , in the LRIM with nonconserved order-parameter dynamics, as a function of time, for different starting temperatures, T_s . The upper and lower halves show data from early and late time regimes, respectively. 116

Chapter 1

Introduction

1.1 Phase Transition

Phase transition is a phenomenon where a system transforms from one state to another depending on changes in external parameters like temperature (T), pressure (P), density (ρ), etc. [1–4]. From freezing of water to raft formation in cell membranes, phase transitions are common in nature.

Phase transition can be categorized in different ways. In the Ehrenfest [4,5] classification, it is done based on the discontinuity in different orders of derivatives of the relevant free energy. A first-order or discontinuous phase transition is identified when there is a discontinuity or jumps in the first derivative. Similarly, the presence of a discontinuity or singularity in the second derivative of the free energy, while having a continuous first derivative, marks a second-order or continuous phase transition. The points around which the second derivatives are discontinuous or diverge are commonly referred as the critical point [6].

1.1.1 First-order Phase Transition

For first-order phase transition, the Gibbs free energy (G), e.g., for a chemical system as in Fig. 1.1, is continuous across the phases, whereas its first derivatives are discontinuous. An important example of first-order phase transition is the formation of ice from liquid water. In Fig. 1.1, we have shown a schematic including three different phases in the pressure vs. temperature plane, for a normal chemical system. In this plane, all the three lines, separating one phase from another, meet at a point that is referred to as the triple point. The line separating the liquid and vapor phases is referred to as the vaporization line, and it terminates at a critical point. Beyond

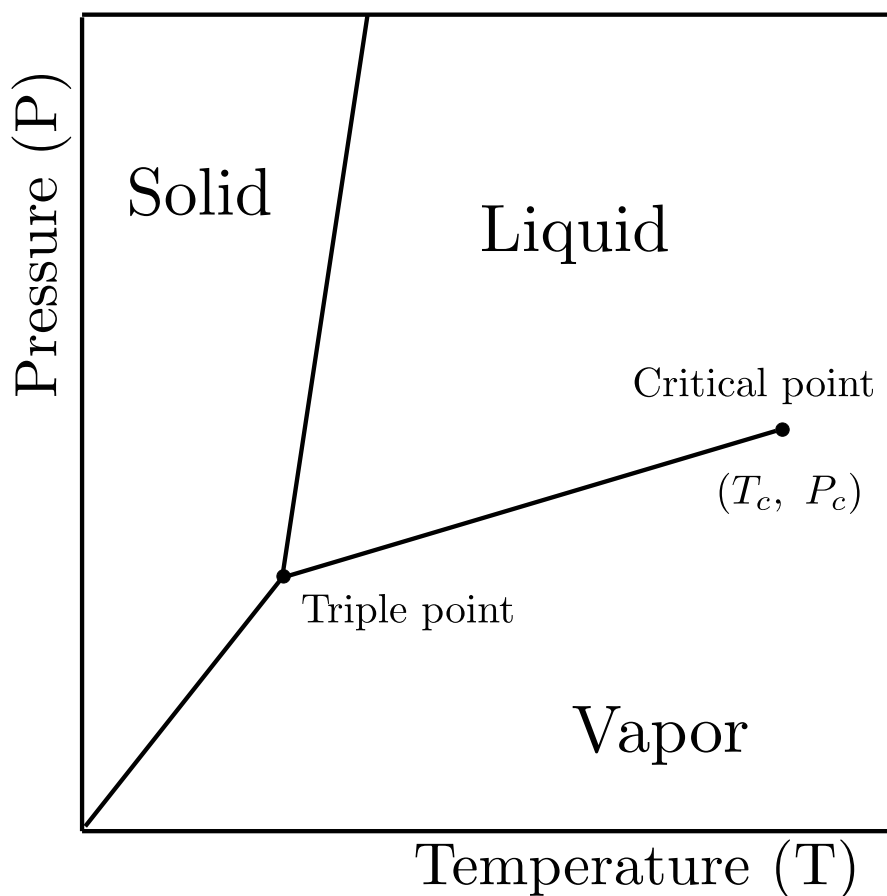


Figure 1.1: Schematics of three different phases and their boundaries, for a typical chemical system, are drawn in Pressure vs Temperature plane. Critical point (T_c, P_c) , as well as the triple point, are marked.

this, one has a homogeneous supercritical gaseous phase. The line separating the liquid phase from the solid one is referred to as the melting line. In the case of freezing of liquid water into ice, volume increases due to the formation of long-lasting hydrogen bonds, and so the slope of this curve is negative, as opposed to what is shown in the figure.

1.1.2 Continuous Phase Transition

An example of second-order or continuous phase transition is para- to ferromagnetic transition. For a magnetic system, temperature (T) and field (H) are the two independent thermodynamic quantities and Gibbs free energy $G = G(T, H)$. Then

the magnetization m and isothermal susceptibility χ can be written as [4]

$$m = - \left(\frac{\partial G}{\partial H} \right)_T; \quad \chi = - \frac{1}{V} \left(\frac{\partial^2 G}{\partial H^2} \right)_T, \quad (1.1)$$

where V is the volume. In the absence of any external field, a para-to-ferromagnetic transition occurs at the Curie temperature. Magnetization varies continuously across the phase boundary, whereas susceptibility shows a divergence at the critical point. In Fig. 1.2(a) magnetization (m) is schematically shown against temperature. Crit-

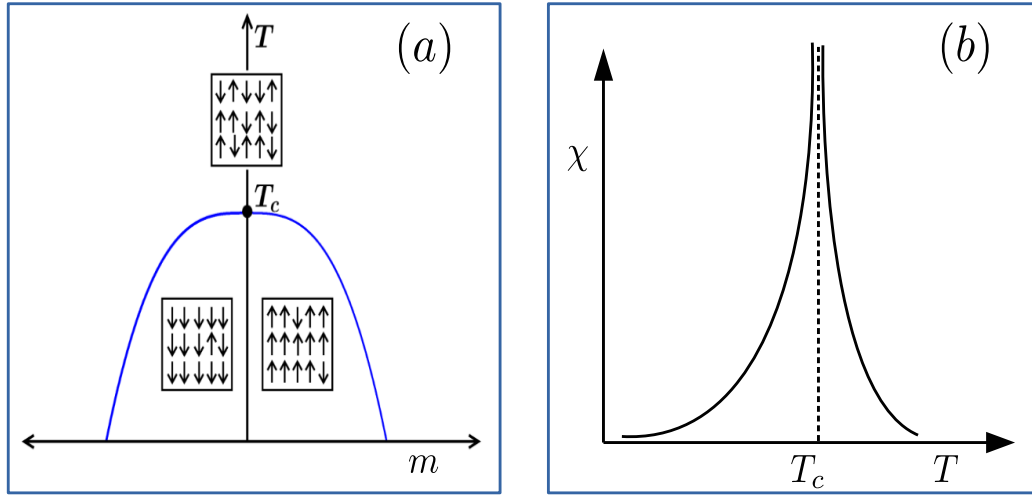


Figure 1.2: (a) Magnetization (m) is plotted versus temperature (T). The filled circle marks the location of the critical temperature, T_c . The direction of the atomic magnets inside the system at different temperatures are symbolically shown by up and down arrows. (b) A schematic diagram showing divergence of susceptibility (χ) with the variation of temperature (T).

ical or the Curie temperature (T_c) is marked, above which the system is in a homogeneous phase with $m = 0$. Below T_c , m increases continuously with decrease in T and reaches either $+1$ or -1 at very low temperatures. Susceptibility, χ , is plotted versus T in part (b) of the same figure. This quantity shows divergence at T_c .

1.2 Kinetics of Phase Transitions

For theoretical/computational studies of dynamics during phase transitions, typically a system is prepared in one phase and then “suddenly” quenched to a state point belonging to another phase. In the literature of statistical physics, a popular

case is to quench a homogeneous/disordered system into a region of the phase diagram where the system exhibits ordering or coexistence [1], as shown in Fig. 1.3, where T_c is the critical temperature and ρ_c is the critical density (concentration for a binary mixture). Appearances of a homogeneous system in the single phase re-

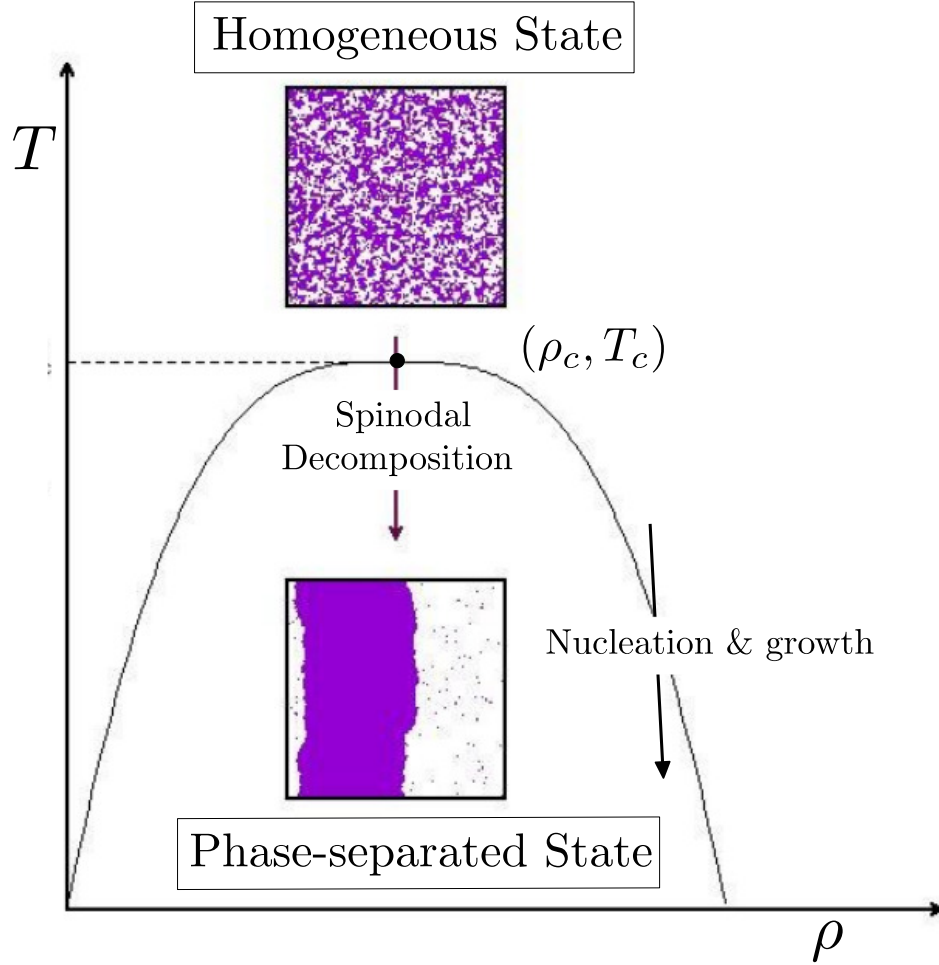


Figure 1.3: A schematic phase diagram of a vapor-liquid transition in ρ vs. T plane is shown. The line separating the homogeneous phase from the phase-separated regime is a coexistence line. The point (ρ_c, T_c) is the critical point. This may describe phase behavior of an immiscible binary mixture as well, if ρ is replaced by the concentration/density of one of the participating species. Representative equilibrium snapshots from homogeneous and phase-separated regions are shown.

gion and of a system containing coexisting phases, in equilibrium, in the immiscible region are pictorially demonstrated in this figure. A homogeneous system, after the quench, evolves [1, 7] with time and eventually reaches an equilibrium state where

two or more phases coexist, as depicted within the frame located inside the coexistence region. The curved line is similar to the magnetization curve in Fig. 1.2 but this here has a role of binodal line separating a homogeneous phase from the phase-segregated region corresponding to vapor-liquid or binary mixture transitions. The dynamical evolution towards the thermodynamic equilibrium occurs via the formation of domains rich in one type of particles or the other [1]. A quench with density at or near ρ_c leads to the formation of interconnected domains and is referred to as spinodal decomposition [8, 9]. On the other hand, if the same exercise is done relatively far away from the critical density, disconnected droplets of one species are formed [10, 11] in the background of the other species. Eventually, these droplets or domains grow with time. The average size of the domains at time t , $\ell(t)$, in general, can be expressed as a power-law [1, 7]:

$$\ell(t) \sim t^\alpha. \quad (1.2)$$

The quantity α , the growth exponent, depends on several factors [1, 12]. This and the related mechanism depend on the constraint on the *Order Parameter* (ϕ) [1], i.e., whether it is conserved or not, among other things. The latter quantity, for a system, is zero in the homogeneous regime and takes non-zero value(s) in the ordered phase. It can be a scalar, vector, or even a tensor [1, 12]. Depending on the constraints on its values, dynamics in systems can be broadly categorized into two classes, i.e., non-conserved and conserved order-parameter dynamics.

An example of conserved order-parameter dynamics is the kinetics of phase separation in an A+B binary mixture. A suitable order parameter in this system is the difference in densities of the components ($\rho_A - \rho_B$). In the homogeneous phase, the value of the order parameter is zero for a 50 : 50 mixture, but as the system is quenched inside the coexistence regime, domains of A-rich and B-rich particles start forming [1], inside which, however, the order parameter value differs from the constant global order-parameter. On the contrary, the total order-parameter of the system changes during nonconserved dynamics. The most common example of this is ordering in a magnetic system. In a para-to-ferromagnetic transition [1], the net magnetization of the system is the order-parameter that changes its value.

1.2.1 Correlation and Scaling

To probe the structures formed inside the systems, a common practice is to calculate the two-point equal time correlation function [1]:

$$C(\vec{r}, t) = \langle \phi(\vec{r}, t) \phi(0, t) \rangle. \quad (1.3)$$

Here $\phi(\vec{0}, t)$ and $\phi(\vec{r}, t)$ are order parameters at two different space points, at time t . The angular brackets denote the average over the initial points and also over different simulation runs with independent initial configurations. Furthermore, a spherical averaging considering isotropicity of the patterns will make the correlation depend upon the scalar distance r . The Fourier transformation of $C(r, t)$ is the experimentally relevant structure factor [1]:

$$S(k, t) = \langle \phi_k(t) \phi_{-k}(t) \rangle. \quad (1.4)$$

A scaling hypothesis states that during the evolution process, at late enough times, there exists a characteristic length scale, $\ell(t)$, such that the structures of the domains at two different times are statistically self-similar except for a difference in $\ell(t)$. The correlation function and the structure factor then have the scaling forms [1]:

$$\begin{aligned} C(r, t) &= f(r/\ell), \\ S(k, t) &= \ell^d g(k\ell), \end{aligned} \quad (1.5)$$

where the time independent master function, $g(y)$, is related to the other master function, $f(x)$, via a Fourier transformation, and d is the spatial dimension. In large k limit, $S(k, t)$ shows a power-law behavior, known as the Porod law [1]:

$$S(k, t) \sim k^{-(d+n)}, \quad (1.6)$$

n being the number of components in the order-parameter. On the other hand, in the limit $k \rightarrow 0$, one should observe [13]

$$S(k, t) \sim k^\beta. \quad (1.7)$$

Similar to the above discussed correlation function, which is a 2-point function in space, a 2-point correlation function in time can also be defined to quantify the relaxation of nonequilibrium systems following a quench. An example of the same

is the autocorrelation function [13–16]:

$$C_{ag}(t, t_w) = \langle \phi(\vec{r}, t) \phi(\vec{r}, t_w) \rangle. \quad (1.8)$$

Angular brackets indicate average over all space points inside the system. Here t_w is the time when the observation begins and is commonly referred to as the waiting time or the age of the system. On the other hand, t ($> t_w$) is the observation time. When a system is in equilibrium, if C_{ag} is plotted against $t - t_w$, for different t_w values, all of them should collapse on top of each other. This is not true for a nonequilibrium system. This relates to the fact that an older system relaxes slowly compared to a younger one [14]. Interesting limit is $\ell \gg \ell_w$, where ℓ and ℓ_w are the length scales at times t and t_w , respectively. For a large value of t_w and $t \gg t_w$, one investigates [14]:

$$C_{ag}(t, t_w) \sim (\ell/\ell_w)^{-\lambda} \sim (t/t_w)^{-\alpha\lambda}, \quad (1.9)$$

that implies a (type of) data collapse even in away-from-equilibrium situation. The exponent λ is referred to as the aging exponent [14]. There exists a theoretically predicted lower bound for λ , given by Yeung, Rao, and Desai [15]:

$$\lambda \geq \frac{d + \beta}{2}. \quad (1.10)$$

1.3 More on Phase Transitions

Here we discuss two cases relevant for this thesis.

1.3.1 Ising Model

A general form of the Hamiltonian of the Ising model is [16, 17]

$$H = -\frac{1}{2} \sum_i \sum_{j \neq i} J_{ij}(r) S_i S_j. \quad (1.11)$$

Here J_{ij} is the interaction strength between spins S_i and S_j , which can take values $+1$ or -1 , sitting at the lattice points i and j , respectively. A positive value of J_{ij} favors the parallel arrangement of spins, i.e., ferromagnetic ordering. Note that at high temperature thermal effect produces disorder, character of a paramagnet. Only below a critical temperature the ferromagnetic alignment occurs. Power-law variation of this quantity as a function of r , the inter-site distance, has been of

interest [17–21]:

$$J_{ij} = \frac{J}{r^{d+\sigma}}, \quad (1.12)$$

where J is a constant usually taken as 1 and σ is the parameter a value of which is expected to separate the long-range Ising universality class from the short-range one [12, 22]. Note here that this universality can be related to static critical phenomena [22–24] as well as kinetics [12, 16]. Setting σ very large leads essentially to a very short-range situation like in the nearest-neighbor Ising model where spins interact only with their neighboring sites. On the other hand, $\sigma = -d$ may mean a fully connected scenario where every spin interacts with all other sites with equal strength. Nearest-neighbour Ising Hamiltonian is probably the most explored model system in the domain of phase transitions due to its simplicity. Via incorporation of appropriate dynamics, a variety of phase transitions can be studied with this model.

Domains rich in one type of particles or the other, for conserved order-parameter dynamics, grow practically via diffusive transport for this model, and in such cases, the Renormalization Group (RG) predicts [12]:

$$\alpha = \begin{cases} \frac{1}{2+\sigma}, & \text{for } \sigma < 1 \\ \frac{1}{3}, & \text{when } \sigma > 1. \end{cases} \quad (1.13)$$

For systems with non-conserved order-parameter dynamics, the similar theoretically predicted value for the growth exponent α is [12]

$$\alpha = \begin{cases} \frac{1}{1+\sigma}, & \text{for } \sigma < 1 \\ \frac{1}{2}, & \text{when } \sigma > 1. \end{cases} \quad (1.14)$$

While the conserved dynamics may mimic phase transition in a binary mixture, the nonconserved order-parameter dynamics is relevant for kinetics of para-to-ferromagnetic transition. We have studied both the cases in this thesis.

1.3.2 Phase Transitions in Water

When fluid water is kept at a sub-zero temperature, it turns into ice. Fig. 1.4(a) shows a schematic phase diagram of water in such phase, in temperature vs. pressure plane, covering different structural possibilities in the solid form. Most of the ice found on Earth’s surface has a hexagonal crystal structure and is called ice ‘Ih’ [25] (shown in Fig. 1.4(b)). Ice formation from liquid water is much discussed

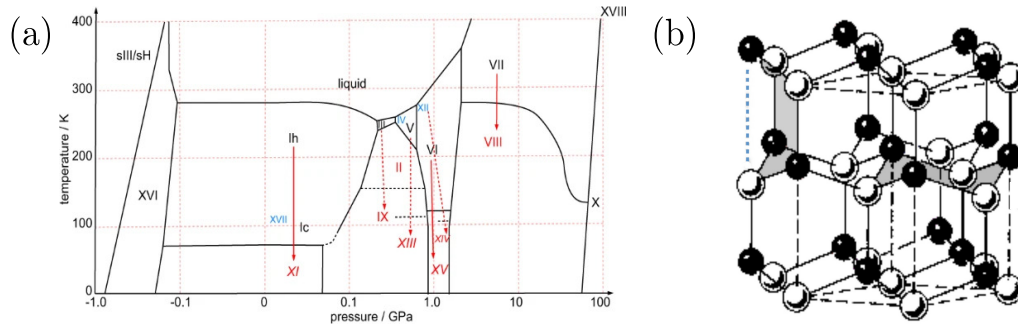


Figure 1.4: (a) Schematic phase diagram for Ice phases. Phases labeled with black Roman numerals are hydrogen-disordered phases; those labeled with red numerals are hydrogen-ordered phases; those labeled with blue numerals are metastable phases. The red solid arrows represent direct disorder-order transitions. The red dotted arrows represent disorder-order transitions that cross the stability range of another phase. Figure source: Thomas C. Hansen, *Nature Communication* **12**, 3161 (2021). (b) Model Ih ice structure (source: Wikipedia) is shown. Black spheres denote Oxygen positions, whereas, the white spheres are Hydrogens.

and very commonly encountered first-order phase transition. Even though this is everyday phenomena, the nucleation and growth process (and related understanding) of ice crystals inside water is not truly straightforward. When liquid water is cooled below 0°C , instead of crystallization, the system typically gets stuck in a supercooled metastable state. Although energetically a crystalline solid state is more favorable, unless there occurs an appropriate fluctuation, this supercooled water does not transform into a solid, if there is no external perturbation. This makes the simulation study of nucleation and growth of ice a difficult task. Efforts have grown into the study of ice crystallization, but most experimental, as well as theoretical/simulation, studies deal with heterogeneous condition [26, 27]. Matsumoto et. al. carried out an early study [28] of homogeneous nucleation and freezing of bulk water computationally using a realistic model of water [29]. In one of our following chapters, we have also studied the nucleation and growth of ice crystals from fluid water under nearly ambient pressure. We have also studied the effect of the initial temperature of the system on ice nucleation.

Mpemba Effect

When two copies of the same system prepared at two different temperatures, say, T_{hot} and T_{cold} , with $T_{\text{hot}} > T_{\text{cold}}$, are quenched to a final temperature T_f ($< T_{\text{cold}} < T_{\text{hot}}$), the one initially at higher temperature equilibrates faster than the one that started

from the lower temperature. This counterintuitive fact is generally referred to as the Mpemba effect (ME). This effect is discussed at least since the time of Aristotle as in his book *Meteorologica*, around 340 B.C., he wrote, “The fact that the water has previously been warmed contributes to its freezing quickly: for so it cools sooner.” While some experiments confirmed the presence of the effect in water [30], some questioned [31] its validity. When it comes to simulations, cooling and freezing of bulk water, even for a very small volume, in the absence of any impurity, is a difficult task. In one of the following chapters, we have studied homogeneous ice nucleation, starting from different initial temperatures. Similar study we have carried out for para- to ferromagnetic transitions as well.

1.4 Computational Methodologies

We have studied various structural and dynamical properties of the systems mentioned in the previous section via computer simulations. For this purpose, we have primarily used two different simulation techniques, namely, Molecular Dynamics and Monte Carlo. Brief descriptions of these methods are given in the following subsections.

1.4.1 Monte Carlo Simulation

Monte Carlo (MC) [32,33] is typically a stochastic process where systems are sampled from different parts of the phase/configuration space by generating random numbers and comparing them with certain probabilities. For an adequately large number of samples, average values of relevant quantities are calculated. The two most popular MC methods to study the dynamics of evolving systems, in Ising-like situations, are the Glauber spin-flip dynamics [32,34] and the Kawasaki spin-exchange kinetics [33]. These are used for studying nonconserved and conserved order-parameter systems, respectively.

The probability, P_n , for a system to be in state n with energy E_n can be written as [32]

$$P_n = \frac{\exp(-E_n/k_B T)}{Z}, \quad (1.15)$$

where T is the temperature of the system, k_B is the Boltzman constant and Z is the partition function. If another state m , with energy E_m , is considered, the transition between these two states will depend on the energy difference, or more

precisely, the factor $\exp(\Delta E/k_B T)$, where $\Delta E = E_m - E_n$. Satisfying the condition of detailed balance, the transition probability from one state to the other can be written, according to Metropolis-Hastings sampling, as [35]

$$W_{n \rightarrow m} = \min(1, \exp(-\Delta E/k_B T)). \quad (1.16)$$

The typical steps for the MC simulations are discussed in the following subsections.

Glauber Dynamics

For the simulations of the Ising model, with Glauber [34] spin-flip method, the below-mentioned steps are followed:

- (1) A random site on the lattice is chosen, and the spin there is flipped.
- (2) Energy cost ΔE is calculated.
- (3) A random number M is generated between 0 and 1.
- (4) If $M \leq$ acceptance probability (mentioned in Eq. 1.16), then the move is accepted; else, the spin is flipped back to its original state.
- (5) Steps (1 – 4) are repeated N times, where N is the total number of lattice sites/spins in the system. These N trial moves make one Monte Carlo step (MCS), typical unit of time.

Kawasaki Dynamics

For the Kawasaki [33] update scheme, spins of two neighboring sites are interchanged. The steps followed to implement the dynamics with the Ising model are:

- (1) A random site is selected first, and then one of the nearest neighbor sites is chosen at random.
- (2) Spin values of these two sites are interchanged.
- (3) Energy change due to the swap is calculated.
- (4) A random number (M) is generated between 0 and 1.
- (4) If $M \leq$ acceptance probability (see Eq. 1.16), the exchange of spins are accepted. Otherwise, the selected spins are swapped again to bring them back to their original positions.
- (5) Repetitions of steps (1 – 4) are performed N times to complete one MCS, where N again is the number of lattice points in the system.

Order-N Cluster Algorithm

Cluster algorithm is an important tool to equilibrate systems near the critical temperature, avoiding critical slowing down [36]. Though cannot be used to study the true dynamics, these are particularly important in studying equilibrium properties because of being fast algorithms. Each Monte Carlo sweep of a cluster algorithm consists of two primary steps. In the first step, clusters of like spins are mapped by checking all possible bonds and their probabilities. The second step is to flip the spins of a fraction of the clusters identified in the first step. The most commonly used cluster MC method to simulate systems with long-range interactions is the one proposed by Swendsen and Wang [37]. In this method, clusters are identified by inspecting all the bonds sequentially and then activating them with a probability $P_i = \delta_{S_i S_j} (1 - \exp(2\beta J_{ij}))$, where δ is the Kronecker delta function and $\beta = 1/k_B T$. Then, the clusters are flipped with a probability of $1/2$. Although the method is fairly simple, the $\mathcal{O}(N^2)$ search for the bonds makes it slow. So, we have used a faster, order $\mathcal{O}(N)$ MC algorithm, proposed by Fukui and Todo [38]. In this simulation method, instead of binary searches, Walker's alias list [38, 39] is used along with certain other smart techniques to reduce the simulation time as well as the memory consumption.

One MC sweep of this $\mathcal{O}(N)$ algorithm is performed as described below:

1. Generate a non-negative integer k according to a Poisson distribution with mean λ_{tot} , where $\lambda_{\text{tot}} = \sum_{\ell} \lambda_{\ell}$ and $\lambda_{\ell} = 2\beta J_{\ell}$.
2. The following steps are repeated k times:

(a) A bond ℓ is chosen with a probability

$$\frac{\lambda_{\ell}}{\lambda_{\text{tot}}} = \frac{J_{\ell}}{\sum_{\ell} J_{\ell}} \quad (1.17)$$

using Walker's method of alias [39]. This is simply done by choosing a random site i on the lattice and then choosing another site j with a probability $J_{\ell} / \sum_{\ell} J_{\ell}$, where ℓ is the distance between the two.

(b) If the product of S_i and S_j is 1, activate the bond, if it is not already activated.

3. Flip each cluster with a probability $1/2$.

In one of the following chapters, we have used this cluster MC method to equilibrate systems in a fast and efficient way.

1.4.2 Molecular Dynamics Simulation

In this method, Newton's equations of motion are solved by calculating forces on each particle [32, 40]. Positions and velocities of the particles at time $t + \Delta t$ are calculated from the knowledge of the values at time t . There exist many different algorithms to solve the equations of motion. Verlet velocity algorithm [32, 40] is one of those. In this method, position and velocity of a particle i are updated as

$$\begin{aligned} x_i(t + \Delta t) &= x_i(t) + \Delta t v_i^x(t) + \frac{\Delta t^2}{2m} f_i^x \\ \text{and} \\ v_i^x(t + \Delta t) &= v_i^x(t) + \frac{\Delta t}{2m} [f_i^x(t) + f_i^x(t + \Delta t)], \end{aligned} \tag{1.18}$$

where, x_i , v_i^x and f_i^x are x components of the position (\vec{r}_i), velocity (\vec{v}_i) and force (\vec{f}_i). The force \vec{f}_i on particle i can be calculated from the potential U_i as

$$\vec{f}_i = -\vec{\nabla} U_i. \tag{1.19}$$

This algorithm enables us to calculate kinetic and potential energies at each time of the simulation runs simultaneously. In addition there is better energy conservation that makes it a widely used algorithm in molecular dynamics simulations.

To perform an MD simulation with constant temperature, a thermostat is needed. The essence is to couple the system with a heat bath. There exist several techniques to achieve this. Some of these preserve the hydrodynamics in the system, and some do not. A very commonly used hydrodynamics preserving thermostat is the Nosé-Hoover thermostat [32, 41]. We will discuss it below in brief. Apart from the Nosé-Hoover thermostat, Langevin Thermostat [40] is also widely used, though it is stochastic in nature.

Nosé-Hoover Thermostat: MD at constant temperature

In this method an extra degree of freedom, to mimic the effect of the reservoir, is introduced. In the formalism proposed by Nosé [41], the interaction of this (external) parameter s , with the physical system, is expressed via scaling of velocities of the

particles as

$$\vec{v}_i = s\dot{\vec{r}}_i. \quad (1.20)$$

Here \vec{v}_i is the effective velocity of the i^{th} particle as a result of the interaction with the heat bath. The parameter s , because of its presence in Eq. (1.20), appears also in the equations of motion. A potential energy term of the form $(n+1)k_B T \ln s$, where n is the total degrees of freedom, is also included to ascertain that the canonical ensemble averages are recovered. The extended Hamiltonian is written as [32]

$$\mathcal{H} = \sum_{i=1}^N \frac{\vec{p}_i^2}{2m_i s^2} + U(\vec{r}) + \frac{\vec{p}_s^2}{2Q} + (n+1)k_B T \ln s, \quad (1.21)$$

where $U(\vec{r})$ is the potential at coordinate \vec{r} , p_s is the momentum conjugate of the extra degree s , and Q can be thought of as the inertia related to s . With the introduction of a new quantity ξ' , defined as $\xi' = Q\dot{s}$, an effective friction parameter, the following equations of motion can be written [32]:

$$\frac{d\vec{r}_i}{dt} = \vec{v}_i, \quad (1.22)$$

$$\frac{d\vec{v}_i}{dt} = -\frac{1}{m_i} \frac{\partial U(\vec{r})}{\partial \vec{r}} - \xi' \vec{v}_i, \quad (1.23)$$

$$\frac{d\xi'}{dt} = \frac{\sum_{i=1}^N m_i \vec{v}_i^2 - n k_B T}{Q}, \quad (1.24)$$

$$\frac{d \ln s}{dt} = \xi', \quad (1.25)$$

for which the modified Hamiltonian does not contain the factor s in the first term on the right hand side. For a complete picture, see the extended Lagrangian formulation in Ref. [32].

From the above equations, it is clear that the deviation from the desired temperature is resisted by the friction parameter ξ' , which in turn can be tuned by the factor Q . The update equations for the x -component of the positions and velocities of the particles can be written as [32], using the velocity Verlet algorithm,

$$x_i(t + \Delta t) = x_i(t) + v_i^x(t)\Delta t + \frac{\Delta t^2}{2} [f_i^x(t) - \xi'(t)v_i^x(t)], \quad (1.26)$$

and

$$\begin{aligned}
v_i^x(t + \Delta t) = & v_i^x(t) + \frac{\Delta t}{2} [f_i^x(t) + f_i^x(t + \Delta t) - 2\xi'(t)v_i^x(t)] \\
& - \frac{\Delta t^2}{2} \left[\frac{\xi'(t)}{2} (f_i^x(t) + f_i^x(t + \Delta t) - 2\xi'(t)v_i^x(t)) \right. \\
& \left. + v_i^x(t) \left(\sum_{j=1}^N v_j^x(t)^2 - nk_B T \right) / Q \right]. \tag{1.27}
\end{aligned}$$

Similarly, y and z components of the positions and velocities can also be calculated. To arrive at Eqs. (1.26) and (1.27), the following procedure was followed: Following the Nosé-Hoover equations (Eqs. (1.22)-(1.25)), one can write the Verlet scheme for the i^{th} particle as (in 1D)

$$r_i(t + \Delta t) = r_i(t) + v_i(t)\Delta t + \left[\frac{f_i(t)}{m_i} - \xi'(t)v_i(t) \right] \frac{\Delta t^2}{2}, \tag{1.28}$$

and

$$v_i(t + \Delta t) = v_i(t) + \left[\frac{f_i(t + \Delta t)}{m_i} - \xi'(t + \Delta t)v_i(t + \Delta t) + \frac{f_i(t)}{m_i} - \xi'(t)v_i(t) \right] \frac{\Delta t}{2}. \tag{1.29}$$

Eq. (1.28) can be computed without difficulties and is the same as Eq. (1.26). On the other hand, Eq. (1.29) needs approximation as $\xi(t + \Delta t)$ and $v_i(t + \Delta t)$ are not known. We write

$$v_i(t + \Delta t) \simeq v_i(t) + \left[\frac{f_i(t + \Delta t)}{m_i} - \xi'(t)v_i(t) + \frac{f_i(t)}{m_i} - \xi'(t)v_i(t) \right] \frac{\Delta t}{2}. \tag{1.30}$$

This approximation leads to an error

$$c \simeq -\frac{\Delta t^2}{2} \left[\xi'(t) \frac{dv_i}{dt} + v_i \frac{d\xi'}{dt} \right], \tag{1.31}$$

where

$$\frac{dv_i}{dt} = \frac{v_i(t + \Delta t) - v_i(t)}{\Delta t} \simeq \frac{\left[\frac{f_i(t + \Delta t)}{m_i} - \xi'(t)v_i(t) + \frac{f_i(t)}{m_i} - \xi'(t)v_i(t) \right]}{2}. \tag{1.32}$$

Combining Eqs. (1.32), (1.31) and (1.30), one obtains Eq. (1.27).

Nosé-Hoover Barostat: MD at Constant Pressure

Most experiments are performed under constant pressure conditions. To mimic such a real-world scenario on a computer, barostating is required. Analogous to the extended constraint method used for thermostats, Andersen proposed [42] a method to perform constant pressure Molecular Dynamics. The proposed method consists of coupling the volume V with the Hamiltonian to mimic the effect of a piston in real systems. The kinetic and potential energies associated with the coupling are [32, 43]

$$K_V = \frac{1}{2}Q'\dot{V}^2, \quad (1.33)$$

and

$$\phi_V = P_{\text{ext}}V \quad (1.34)$$

respectively, where Q' is a parameter that can be thought of as an effective mass and P_{ext} is the desired pressure. A scaling variable \vec{s}' for this method is defined as

$$\vec{r} = V^{1/3}\vec{s}', \quad (1.35)$$

$$\vec{v} = V^{1/3}\dot{\vec{s}}'. \quad (1.36)$$

With this, the equations of motion can be obtained as

$$\begin{aligned} \ddot{\vec{s}}' &= \frac{\vec{f}}{mV^{1/3}} - \frac{2}{3}\dot{\vec{s}}'\dot{V}/V, \\ \ddot{V} &= \frac{P - P_{\text{ext}}}{Q'}, \end{aligned} \quad (1.37)$$

where, the force and the pressure are calculated from unscaled coordinates of the particles. Eq. (1.37) leads to a trajectory that is isobaric and isoenthalpic. We have mostly used the LAMMPS [44] package for constant pressure simulations to achieve faster computation.

1.4.3 Handling Long-range Forces

When the force or the potential, falls off very rapidly in space, a cut-off radius r_c can be defined, often without compromising with the basic aspects of physics, so that the force is neglected outside r_c . Examples of such situations are Lennard-Jones (LJ) potential, nearest-neighbour Ising Model, etc. These are referred to as

short-range forces [45, 46]. For such short-range forces, the cut-off radius can be very small compared to the size of the simulation box and potential at any given point is calculated directly by considering all the particles present only within the cut-off radius r_c .

However, we often encounter forces that are truly not of short-range variety. For them, the interaction spatially decays as r^{-m} , m being a reasonably small positive exponent. An example of such a potential is the electrostatic interaction between two charges. For such systems, the above-mentioned cut-off method may lead to results which are even qualitatively wrong.

There exist effective ways to tackle the systems with long-range interactions. For a lattice system, the Generalized Ewald summation [22, 40] technique is the most suitable one. For off-lattice systems, reaction field technique [40] and Particle-Particle Particle-Mesh (PPPM) [47] are two commonly used methods.

Generalized Ewald Summation

For systems with long-range interactions, the effect of mirror images of the actual systems across the periodic boundaries needed to be considered. The potential can be written in the form

$$U_m(i, j) = \sum_{\vec{\nu}} \frac{1}{r^m}, \quad (1.38)$$

where $\vec{\nu} [= (\nu_1, \nu_2, \dots, \nu_d)]$ with $\nu_\alpha = 0, \pm 1, \pm 2, \dots$, stands for the indices of the image boxes in α direction of the d dimensional hypercube. $\vec{L} [= (L_1, L_1, \dots, L_d)]$ denote the size of the simulation box. Then, $r = |\vec{r}(\vec{\nu}, \vec{r}_i, \vec{r}_j)| \equiv \vec{L} \cdot \vec{\nu} + |\vec{r}_i - \vec{r}_j|$ is the distance between two particles i and j , where the particles can be either inside the simulation box or in the imaginary boxes considered to implement the periodic boundary condition (PBC). Eq. (1.38) is equivalent to

$$\begin{aligned} U_m(i, j) &= \sum_{\vec{\nu}} \frac{1}{\Gamma(m/2)} \int_0^\infty \frac{1}{r^m} t^{\frac{m}{2}-1} e^{-t} dt \\ &= \sum_{\vec{\nu}} \left[\frac{1}{\Gamma(m/2)} \int_{(\kappa r)^2}^\infty \frac{1}{r^m} t^{\frac{m}{2}-1} e^{-t} dt \right. \\ &\quad \left. + \frac{2}{\Gamma(m/2)} \int_0^\kappa \rho^{m-1} e^{-r^2 \rho^2} d\rho \right] \\ &= U_m^1(i, j) + U_m^2(i, j), \end{aligned} \quad (1.39)$$

where $\Gamma(x)$ stands for the Gamma Function defined as

$$\Gamma(x) = \int_0^\infty t^{x-1} e^{-t} dt, \quad (1.40)$$

and κ is an arbitrary positive number. Here, $U_m(i, j)$ is divided into two parts:

$$U_m^1(i, j) = \sum_{\vec{\nu}} \frac{1}{\Gamma(m/2)} \frac{1}{r^m} \int_{(\kappa r)^2}^\infty t^{\frac{m}{2}-1} e^{-t} dt, \quad (1.41)$$

a short-range part and

$$U_m^2(i, j) = \sum_{\vec{\nu}} \frac{2}{\Gamma(m/2)} \int_0^\kappa \rho^{m-1} e^{-\rho^2 r^2} d\rho, \quad (1.42)$$

a long-range part, where integration variable t is replaced by $\rho^2 r^2$. Eq. (1.42) is then transformed from integration in real space to that into reciprocal space. Next the value of the dimension d is set to 2, so that $L = (L_x, L_y)$, $\nu = (\nu_x, \nu_y)$ and $r_i = (r_{ix}, r_{iy})$. After using a few clever tricks, Eq. (1.42) can be written as

$$\begin{aligned} U_m^2(i, j) &= \frac{2\pi^{d/2}}{\Gamma(m/2)V} \sum_{\vec{k}} \cos[2\pi\vec{k} \cdot ((\vec{r})_i - \vec{r}_j)] \\ &\times \frac{1}{2} (\pi k)^{m-d} \int_{\frac{\pi^2 k^2}{\kappa^2}}^\infty t^{-\frac{1}{2}(m-d)-1} e^{-t} dt, \end{aligned} \quad (1.43)$$

where $V = \prod_{\alpha=1}^d L_\alpha$ is the volume of the hyperspace. Eq. (1.43) and Eq. (1.41) add up to give the complete Ewald summation for any random positive value of σ . These two equations contain incomplete gamma functions, defined as,

$$\Gamma(s, x) = \int_x^\infty t^{s-1} e^{-t} dt \quad (1.44)$$

and they can be computed numerically. For the simulations of the Ising model, we have used a value $\kappa = 2/L$ as in Ref. [22].

Ideally, Ewald summation can be used for all values of m if the potential falls off as r^{-m} , r being the spatial distance between the particles. In reality, if $m \gg d$, where d is the system dimension, using a suitable cut-off one can make the simulation faster without losing much generality, especially when we study universality with respect to critical behavior. In the case of the Coulomb interaction, the potential falls as $1/r$, in $d = 3$, meaning $m < d$. In this case, it is even qualitatively wrong to

set a cutoff.

For Coulomb potential we have used the particle-particle particle-mesh or the PPPM method. For that a cutoff is used. Pair-wise interactions are used to calculate forces for particles inside the cutoff distance. For particles that are outside the cutoff, the system is mapped onto a regular mesh or grid, and then a fast Fourier transform (FFT) is used to calculate forces in reciprocal space, like in the Ewald case. In the Ewald summation the force calculation is done in two parts, short-range and long-range, by solving the equations in direct and reciprocal space, respectively. In PPPM, the continuous system is mapped onto grids to make it more efficient. In our Ewald case, the system is already defined on a lattice.

1.5 Finite Size Scaling

Computer simulation is a brilliant tool for studying properties of physical systems, but there exist limitations. One such limitation is related to the finite size effects [48–50]. A mole of any system has $\simeq 10^{24}$ number of particles. It is not practically possible to handle such a large number of particles in any computer simulation. Periodic boundary condition is a way to minimize the effects of finiteness by discarding the boundaries present, but there still exist deficiencies. A situation where the finite-size effects are very important is related to the critical point where various thermodynamic quantities, X , exhibit singularities [51],

$$X = X_0 \epsilon^{-x}, \quad (1.45)$$

where $\epsilon = |(T - T_c)/T_c|$. Here, T is the temperature of the system and T_c is the critical temperature. E.g., the correlation length, ξ , diverges as [51]

$$\xi \sim \epsilon^{-\nu}. \quad (1.46)$$

Combining Eq. (1.45) and Eq. (1.46), we can write [51]

$$X \sim \xi^{x/\nu}. \quad (1.47)$$

But, in computer simulations, ξ cannot grow indefinitely. It can take a maximum value equal to the system size L . As $T \rightarrow T_c$, then

$$X = A_0 L^{x/\nu}. \quad (1.48)$$

Then, away from T_c , Eq. (1.45) is modified to be written as [48, 51]

$$X = L^{x/\nu} Y(y), \quad (1.49)$$

where $Y(y)$ is a system-size independent scaling function, y being a dimensionless scaling variable. An appropriate choice for y is $(L/\xi)^{1/\nu}$. With this choice of y , and assuming $Y(y) = A_0$, at $T = T_c$, one should expect

$$Y(y) \sim y^{-x}, \quad (1.50)$$

for $T \gg T_c$. In one of the following work chapters, we have used this finite-size scaling analysis to obtain the growth exponent α .

1.6 Overview of the Thesis

In line with the synopsis here we provide a brief overview of the thesis. We have studied structure and dynamics related to phase transitions in systems of different types. We have considered phase separation in binary mixtures, a para-to-ferromagnetic transition, and Ice formation in a model of water from various fluid phases. Each of these systems is described by long-range interparticle/inter-spin interactions. For two of the systems, we have shown that a hotter system equilibrates faster to a new state belonging to a low temperature region. This is related to the surprising Mpemba effect, a topic of much current interest. The other aspect was related to quantifying universalities of structure, growth, and aging based on the range of interaction.

Bibliography

- [1] A. J. Bray, *Adv. Phys.* **51**, 481 (2002).
- [2] H. E. Stanley, *Introduction to Phase Transitions and Critical Phenomena* (Oxford Science Publications, 1971).
- [3] A. Onuki, *Phase Transition Dynamics* (Cambridge University Press, 2002).
- [4] N. D. Goldenfeld, *Lectures On Phase Transitions And The Renormalization Group* (Westview Press, 1992).
- [5] G. Jarger, *Arch. Hist. Exact Sci.* **53**, 5 (1998).
- [6] M. E. Fisher, *Reports on Progress in Physics* **30**(2), 615 (1967).
- [7] T. C. B. McLeish, M. E. Cates, J. S. Higgins, P. D. Olmsted, and A. J. Bray, *Phil. Trans. R. Soc. Lond. A* **361**(1805), 781 (2003).
- [8] K. Binder, *Phys. Rev. B* **15**, 4425 (1977).
- [9] E. D. Siggia, *Phys. Rev. A* **20**, 595 (1979).
- [10] K. Binder and D. Stauffer, *Phys. Rev. Lett.* **33**, 1006 (1974).
- [11] H. Furukawa, *Phys. Rev. A* **31**, 1103 (1985).
- [12] A. J. Bray, *Phys. Rev. E* **47**, 3191 (1993).
- [13] C. Yeung, *Phys. Rev. Lett.* **61**, 1135 (1988).
- [14] D. S. Fisher and D. A. Huse, *Phys. Rev. B* **38**, 373 (1988).
- [15] C. Yeung, M. Rao, and R. C. Desai, *Phys. Rev. E* **53**, 3073 (1996).
- [16] S. Ghosh and S. K. Das, *Phys. Rev. E* **109**, L052102 (2024).

-
- [17] H. Christiansen, S. Majumder, and W. Janke, Phys. Rev. E **99**, 011301 (2019).
 - [18] H. Christiansen, S. Majumder, M. Henkel, and W. Janke, Phys. Rev. Lett. **125**, 180601 (2020).
 - [19] F. Corberi, E. Lippiello, and P. Politi, J. Stat. Phys. **176**, 510 (2019).
 - [20] H. Christiansen, S. Majumder, and W. Janke, Phys. Rev. E **103**, 052122 (2021).
 - [21] F. Müller, H. Christiansen, and W. Janke, Phys. Rev. Lett. **129**, 240601 (2022).
 - [22] T. Horita, H. Suwa, and S. Todo, Phys. Rev. E **95**, 012143 (2017).
 - [23] M. E. Fisher, S. keng Ma, and B. G. Nickel, Phys. Rev. Lett. **29**, 917 (1972).
 - [24] J. Sak, Phys. Rev. B **8**, 281 (1973), <https://link.aps.org/doi/10.1103/PhysRevB.8.281>.
 - [25] T. C. Hansen, Nature Comm. **12**(2041-1723), 3161 (2021).
 - [26] J. Carrasco, A. Michaelides, M. Forster, S. Haq, R. Raval, and A. Hodgson, Nat. Mater. **8**, 427 (2009).
 - [27] E. B. Moore, E. de la Llave, K. Welke, D. A. Scherlis, and V. Molinero, Phys. Chem. Chem. Phys. **12**, 4124 (2010).
 - [28] M. Matsumoto, S. Saito, and I. Ohmine, Nature **416**, 409 (2002).
 - [29] J. L. F. Abascal, E. Sanz, R. García Fernández, and C. Vega, The Journal of Chemical Physics **122**(23), 234511 (2005).
 - [30] Z. Tang, W. Huang, Y. Zhang, Y. Liu, and L. Zhao, InfoMat **5**(2), e12352 (2023).
 - [31] L. P. F. Burridge, Henry C., Scientific Reports **6**, 2045 (2016).
 - [32] D. Frenkel and B. Smit, *Understanding Molecular Simulation* (Academic Press, 2002).
 - [33] D. P. Landau and K. Binder, *A Guide to Monte Carlo Simulations in Statistical Physics* (Cambridge University Press, 2005).
 - [34] R. J. Glauber, Journal of Mathematical Physics **4**(2), 294 (1963).

-
- [35] I. S. Aranson and L. S. Tsimring, *Rev. Mod. Phys.* **78**, 641 (2006).
- [36] M. E. Fisher, in M. S. Green, ed., *Critical phenomena* (Academic Press, New York, 1971).
- [37] R. H. Swendsen and J.-S. Wang, *Phys. Rev. Lett.* **58**, 86 (1987).
- [38] K. Fukui and S. Todo, *Journal of Computational Physics* **228**(7), 2629 (2009).
- [39] A. J. Walker, *ACM Trans. Math. Softw.* **3**(3), 253–256 (1977).
- [40] M. P. Allen and D. J. Tildesley, *Computer Simulation of Liquids* (Oxford University Press, 1991).
- [41] S. Nose, *J. Phys. Condens. Matter* **2**, SA115 (1990).
- [42] H. C. Andersen, *The J. Chem. Phys.* **72**(4), 2384 (1980).
- [43] G. J. Martyna, D. J. Tobias, and M. L. Klein, *J. Chem. Phys.* **101**(5), 4177 (1994).
- [44] A. P. Thompson, H. M. Aktulga, R. Berger, D. S. Bolintineanu, W. M. Brown, P. S. Crozier, P. J. in 't Veld, A. Kohlmeyer, S. G. Moore, T. D. Nguyen, *et al.*, *Comp. Phys. Comm.* **271**, 108171 (2022).
- [45] S. Majumder and S. K. Das, *Europhys. Lett.* **95**(4), 46002 (jul 2011).
- [46] J. Midya and S. K. Das, *Phys. Rev. Lett.* **118**, 165701 (2017).
- [47] R. W. Hockney and J. W. Eastwood, *Computer Simulation Using Particles* (CRC Press, 1988).
- [48] S. Majumder and S. K. Das, *Phys. Rev. E* **81**, 050102 (2010).
- [49] M. E. Fisher and M. N. Barber, *Phys. Rev. Lett.* **28**, 1516 (1972).
- [50] D. W. Heermann, L. Yixue, and K. Binder, *Physica A: Statistical Mechanics and its Applications* **230**(1), 132 (1996).
- [51] S. K. Das, S. Roy, S. Majumder, and S. Ahmad, *Europhys. Lett.* **97**(6), 66006 (2012).

Chapter 2

Kinetics of Phase Separation in Systems with Long-range Interaction: Study of Domain Structure and Growth

2.1 Introduction

Certain key questions concerning the kinetics of phase transitions connect to the aspect of universality in far-from-equilibrium dynamics [1]. An objective there [1] is to understand relaxation within a system following its quench from a homogeneous or disordered region to an ordered or a phase-separated region of a phase diagram. During this process, interesting patterns, consisting of domains rich or poor in specific components, form, and their average size, ℓ , grows with time (t) as [1]

$$\ell(t) \sim t^\alpha. \quad (2.1)$$

Alongside the order-parameter conservation, the range of the inter-particle interactions present in the system can also play a major role in deciding the value of the exponent α , and thus, the universality. For systems where only short-range interactions are present, the phenomena concerning coarsening is extensively studied, over the years, and the value of the growth exponent(s) is well established. In this case, $\alpha = 1/2$ for non-conserved order-parameter [1], whereas, for conserved order-parameter dynamics the value of α is $1/3$ [1], in absence of hydrodynamics.

On the other hand, systems having long-range interactions are not probed so

extensively, although such systems are also of experimental relevance. Even for the Ising model (IM), despite the simplicity, there exist serious computational challenges for the long-range (LRIM) variety [2–7]. The situation is particularly unsatisfactory for the case of *conserved order-parameter* dynamics, due to slower dynamics.

For systems with interactions falling off with radial distance r as $r^{-(d+\sigma)}$, there exist theoretical predictions [8] for the domain growth [8]:

$$\ell(t) \propto \begin{cases} t^{\frac{1}{2+\sigma}} & \sigma < 1 \\ t^{\frac{1}{3}} & \sigma > 1, \end{cases} \quad (2.2)$$

suggesting that the boundary between short- and long-range universality is at $\sigma = 1$. Only two computational studies [4, 9], including a recent one [4], to the best of our knowledge, investigated the conserved case, reporting results *only* on the domain growth. The structure of the domains formed during the phase separation is yet to be studied carefully.

A key aspect of an ordering or phase-separating dynamics is related to the self-similar structure of the domains and corresponding scaling properties. A typical investigation of the structure of the domains considers the calculation of two-point equal-time correlation function, $C(r, t)$, defined as [1]

$$C(r, t) = \langle \psi(r, t) \psi(0, t) \rangle - \langle \psi(r, t) \rangle \langle \psi(0, t) \rangle. \quad (2.3)$$

At late times, $C(r, t)$, in standard situations, satisfies a scaling form [1]

$$C(r, t) \equiv \tilde{C}(r/\ell(t)), \quad (2.4)$$

that reflects self-similarity. Another important quantity with more experimental relevance is the structure factor, $S(k, t)$, which is the Fourier transform of $C(r, t)$, k being the wave number. $S(k, t)$ follows the scaling form [1]

$$S(k, t) \equiv \ell^d \tilde{S}(k\ell), \quad (2.5)$$

where d is the dimension of the system. In Eq. (2.4) and (2.5), \tilde{C} and \tilde{S} are master functions which are independent of time.

In $k \rightarrow \infty$ limit, $S(k, t)$ scales as k^{-3} , for Ising-like scalar order-parameter systems, referred to as the Porod law [1]. This behavior is related to a short-distance

singularity in $C(r, t)$ due to the presence of (sharp) domain boundaries. The theoretically predicted exponent value 3, however, is only true if the final quench temperature is zero. If the system is quenched to a non-zero final temperature, the domain boundaries are not sharp, and there we get the exponent value somewhat less than 3. The small k behavior is also interesting to study and we will be discussing it in the next chapter.

In this chapter, we will discuss the results on the domain growth and the structure that we have obtained from the analyses of Monte Carlo (MC) [10] simulations of the LRIM in space dimension $d = 2$. We will compare the results from either sides of the boundary between short- and long-range regimes. We will also discuss a structural anomaly that is present on the long-range side, fading away as one approaches the above mentioned boundary.

2.2 Model and Methods

We have carried out MC simulations of Ising systems where spins are sitting on a $L \times L$ square lattice with lattice constant of unity. To mimic the conserved order-parameter dynamics, Kawasaki spin exchange moves are chosen. The Hamiltonian of the model system is

$$H = -\frac{1}{2} \sum_i \sum_{j \neq i} J_{ij}(r) S_i S_j, \quad (2.6)$$

where, i and j stand for i^{th} and j^{th} lattice sites, S_i (S_j) represents the value of the spin, either $+1$ or -1 , at lattice point i (j) and J_{ij} is the coupling term that has the form [8]

$$J_{ij} = \frac{J}{r^{d+\sigma}}. \quad (2.7)$$

Here r is the scalar distance between the points i and j , d ($= 2$) is the space dimension and σ is the parameter that determines how fast or slow the interaction strength falls off with the increase in distance when d is fixed. We have varied the parameter σ and have tried to find out the dependence of structure and growth on it. We have also considered systems with different sizes to understand and eliminate the roles of the finite-size effects. For most part, however, we stuck to $L = 256$. In the case of the LRIM, the critical temperature T_c is highly sensitive [11] to the change in the value of σ . For all our simulations, while varying σ , we have quenched systems to a final temperature, which is a fixed fraction of T_c corresponding to that particular value of σ , viz., $T = 0.6T_c$, starting configurations being random. E.g., for

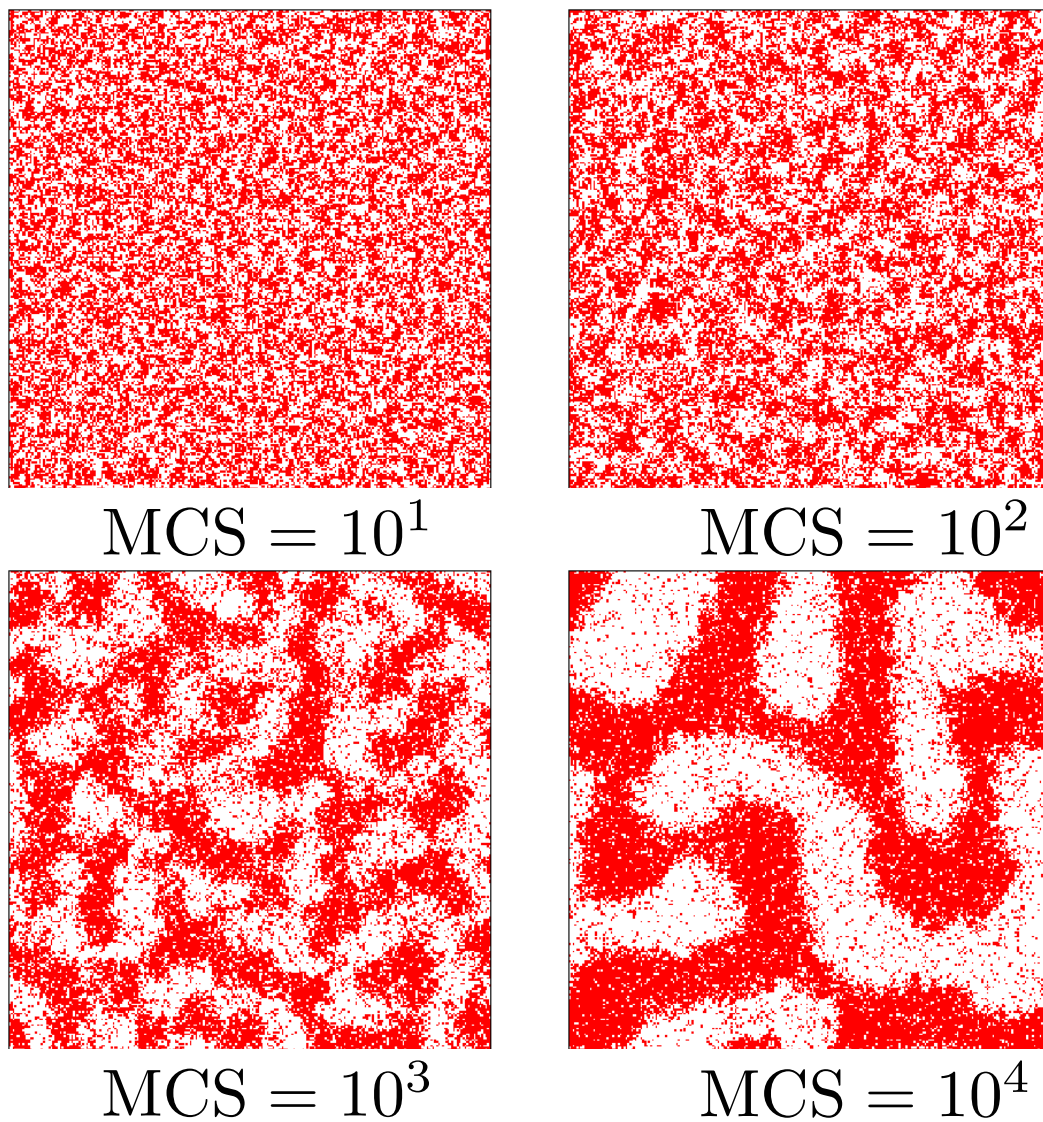


Figure 2.1: Snapshots at different MC steps for an evolution with $\sigma = 0.6$, following quench of a random initial configuration to a temperature $T = 0.6T_c$. Locations of the particles are marked. These results are for $L = 256$.

$\sigma = 0.6$, we have considered $T_c \simeq 12.555$ (in reduced units) and mainly $L = 256$ [11].

We have used the periodic boundary condition (PBC) for our simulations. In every direction, we have added five image boxes. One needs to calculate the change in energy due to the spin exchange and then accept or reject the move depending on certain criteria. For this energy calculation part, we have used the Ewald summation technique [11], where the inter-spin interactions are divided into two parts - short- and long-range and calculated in real and Fourier spaces, respectively. For details, including value of relevant parameter, see section 1.4.3.

In Fig. 2.1, we have pictorially depicted the evolution of a system from a completely homogeneous state to a phase-separated state. The size of the domains formed inside the system is calculated by scanning the system along different cartesian coordinate axes and measuring the distance between two successive interfaces. The results that we will be presenting in this chapter are obtained after averaging over a large number of runs with independent initial configurations.

We must mention here that the average domain size can also be calculated via other methods, e.g., from the decay of two-point equal time correlation function and from the location of the maximum of the corresponding structure factor. However, results from these different methods differ only by prefactors. Since our interest is in the estimation of growth exponents we stick to only one method.

2.3 Results

A careful observation of the snapshots in Fig. 2.1 suggests the presence of significant noise. This is because of a choice of a reasonably high temperature. We needed to remove the noise [12] in order to calculate the length of the domains appropriately. In Fig. 2.2 domain lengths from systems with two different σ values are plotted, against time, in a log-log scale. Recall that time in our simulations is measured in units of MC steps (MCS), one MCS being equivalent to L^2 trial moves. For each value of σ , the presented data have been obtained after averaging over 175 independent MC runs for system size $L = 256$. From this figure it appears that the growth, at later times, is faster for smaller σ , i.e., longer range of interaction. In the remaining part of the chapter, we will quantify this and other aspects.

In Fig. 2.3(a), we plot the two-point equal-time correlation function, from three different t , as a function of the scalar distance r , for $\sigma = 0.6$. In part (b) of the same figure, we have scaled the abscissa by domain length ℓ to get a collapse of the data. The observed nice collapse implies that the structures are self-similar in the

relevant time regimes of the growth, as will be clearer later.

To quantify the growths by estimating the correct growth exponents, we calculate the instantaneous exponent α_i , defined as [12]

$$\alpha_i = \frac{d \ln \ell(t)}{d \ln t}. \quad (2.8)$$

As $t \rightarrow \infty$, the value of α_i should give us the correct value of α . In Fig. 2.4 we plot the quantity $1/\alpha_i$ as a function of $1/t$. To ascertain the absence of any finite size effects, in part (a) of Fig. 2.4, for $\sigma = 0.6$, we show results from three different system sizes. All of them show convergence to the same value. In part (b), we have shown the same plot for $\sigma = 0.95$, but this time only for one system size, viz., $L = 256$, after being confident of the absence of finite-size effects, in this time regime, from the exercise in part (a). Note that the growth for $\sigma = 0.95$ is slower than that for $\sigma = 0.6$. So, it is expected that the finite-size effects will appear later. For both the values of σ , values of α are estimated via appropriate extrapolations to the asymptotic limit. In Fig. 2.5 we plot our estimates as a function of σ . In the same graph, we have also plotted the theoretical predictions [8]. Note that such a general simulation study on growth was not carried out earlier.

As the results, particularly the trend, are in good agreement with the theoretical predictions [8], we turn our attention to the structural aspect. We show in Fig. 2.6(a) the structure factor $S(k, t)$ from two different σ values. Data from the simulations of systems with $\sigma = 0.6$ are presented with ‘circles’, whereas the dashed line is used for $\sigma = 0.8$. The solid lines represent certain expected power-law(s). For visual clarity, the abscissa of the data collected from the systems with $\sigma = 0.8$ are artificially shifted, and this operation does not alter our observations or conclusions. We observe a structural anomaly, in terms of deviation from the Porod tail [1]. Recall that the k^{-3} (Porod law) behavior here is related to a “short distance” singularity arising from discontinuity in the spatial order, due to the appearances of domain boundaries. Interestingly, in both the cases, this behavior appears in two places separated by a ‘knee’ – see the bending between two power-law regimes. We have marked them by putting a rectangular box around. This feature is completely absent in the short-range case [13]. By the naked eye, it is clear that the anomaly is stronger for smaller σ . In part (b) of Fig. 2.6, we have plotted the structure factor $S(k, t)$ against wave number k , only for $\sigma = 0.6$, for three different system sizes, viz., $L = 256, 512$ and 1024 . This is to show that the anomaly is there for each value of L and is not an artifact of any finite-size effects.

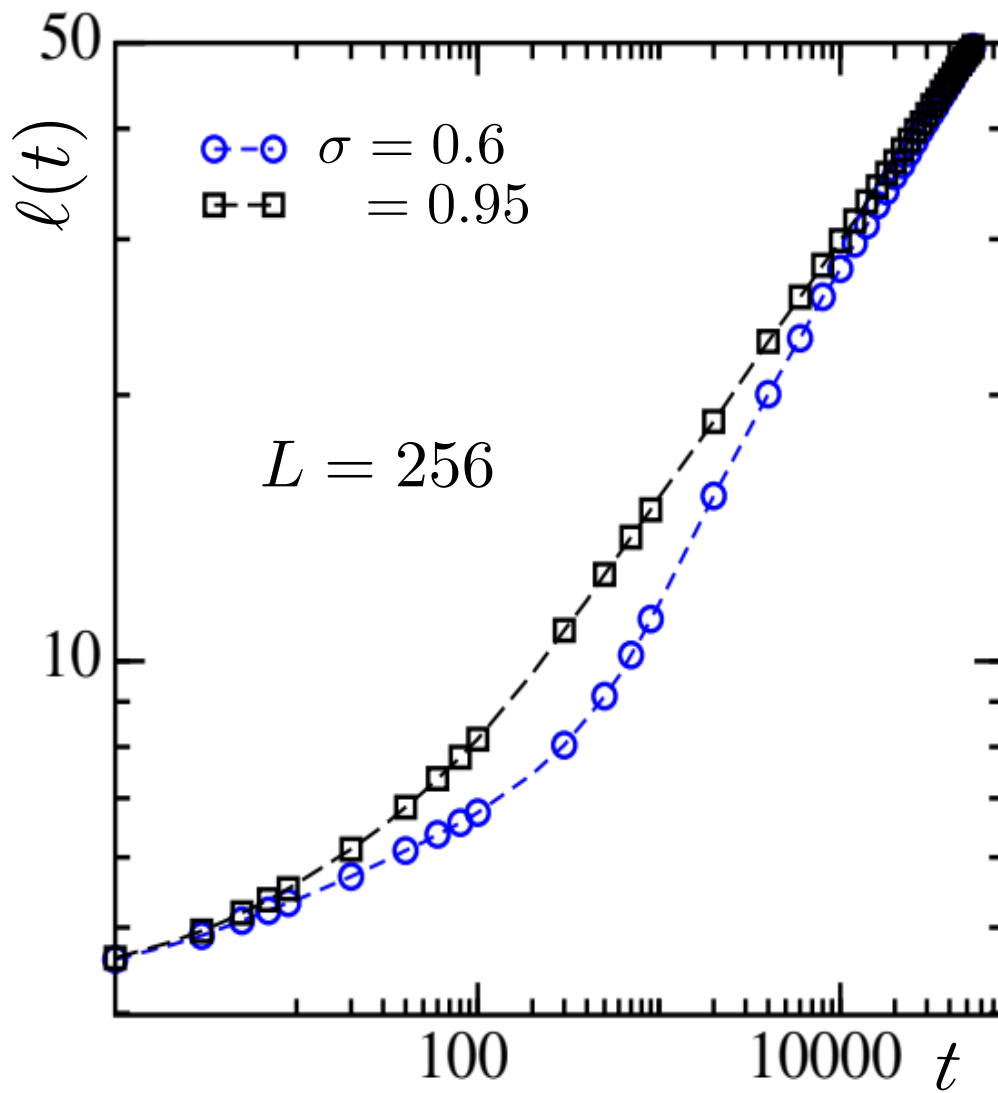


Figure 2.2: Average domain length, ℓ , is plotted versus time t . We have included results for systems with $\sigma = 0.6$ and 0.95 .

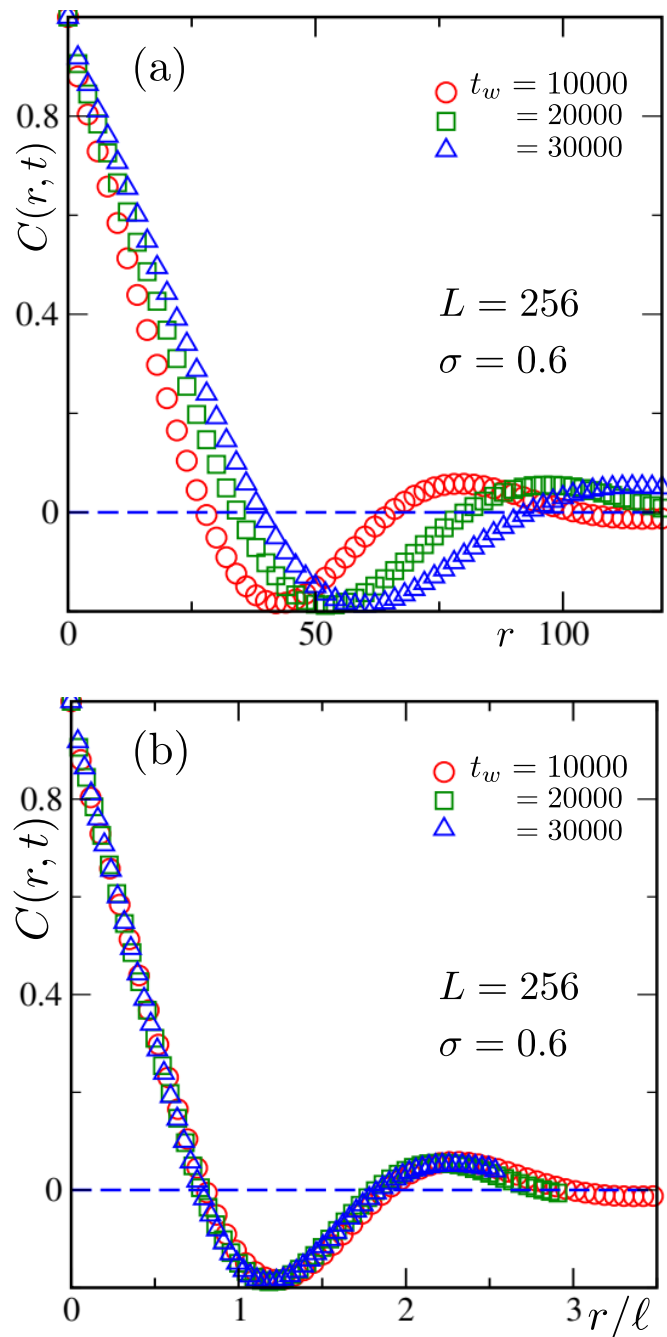


Figure 2.3: (a) Correlation functions, $C(r, t)$, from three different times, are plotted versus the distance r , for $\sigma = 0.6$. In (b), distance r is scaled by the domain lengths ℓ at corresponding times to obtain a collapse of the data.

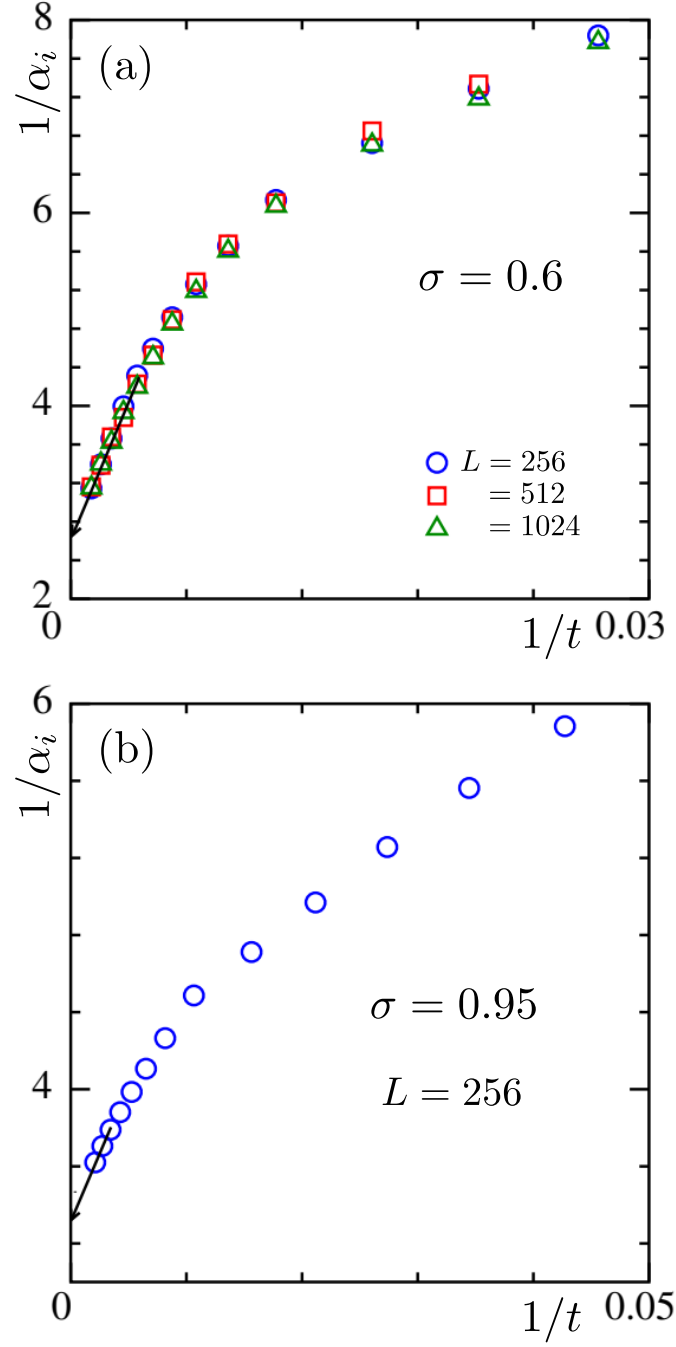


Figure 2.4: (a) The inverse of the instantaneous exponent, α_i , for $\sigma = 0.6$ and different values of L , are plotted versus $1/t$. The solid line is a guide to the eyes, showing possible convergence of the data in the $t \rightarrow \infty$ limit. We have discarded some noisy data points at a very late time for a better visualization. (b) Same as in (a), but here the results are for $\sigma = 0.95$ and only one system size, viz., $L = 256$.

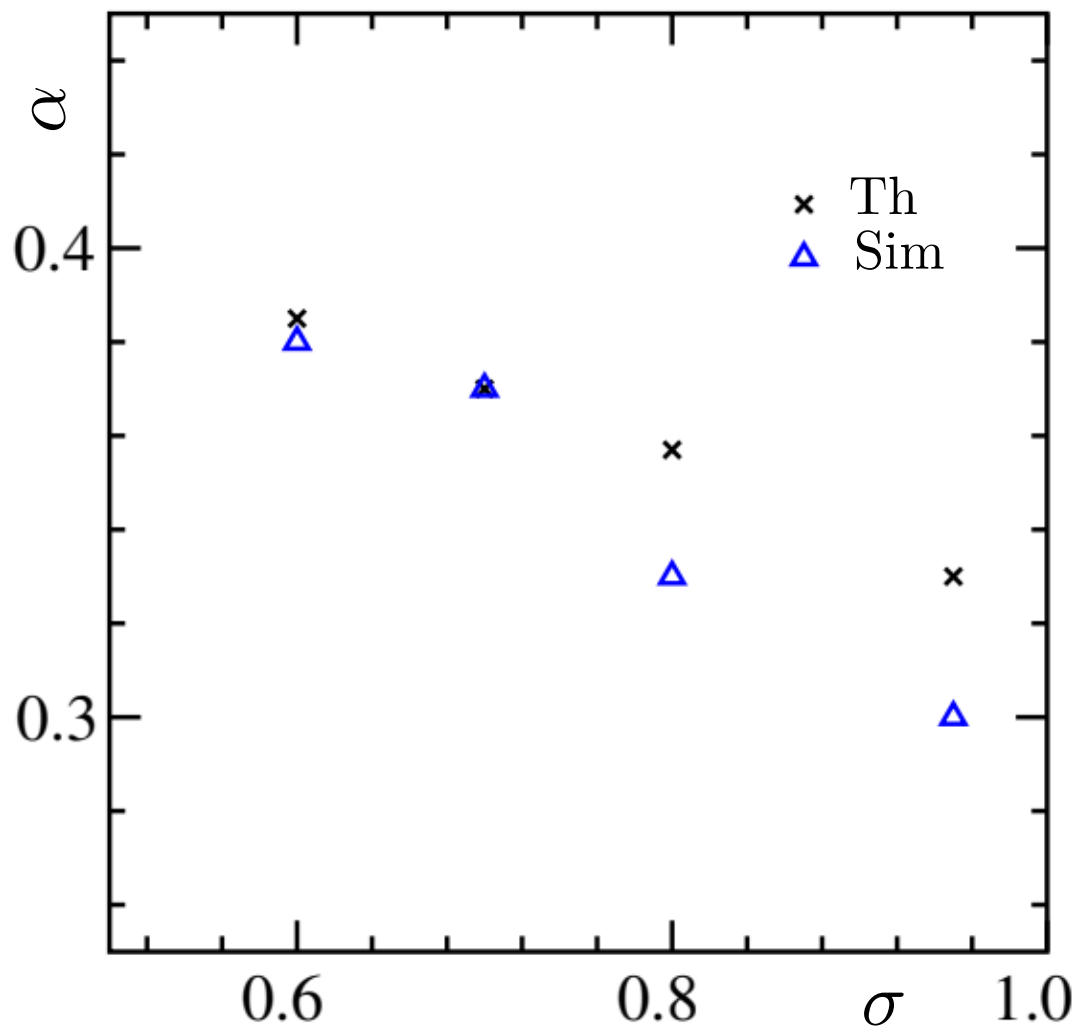


Figure 2.5: Plot of α as a function of σ . Results from both Theory (Th) and Simulations (Sim) are included.

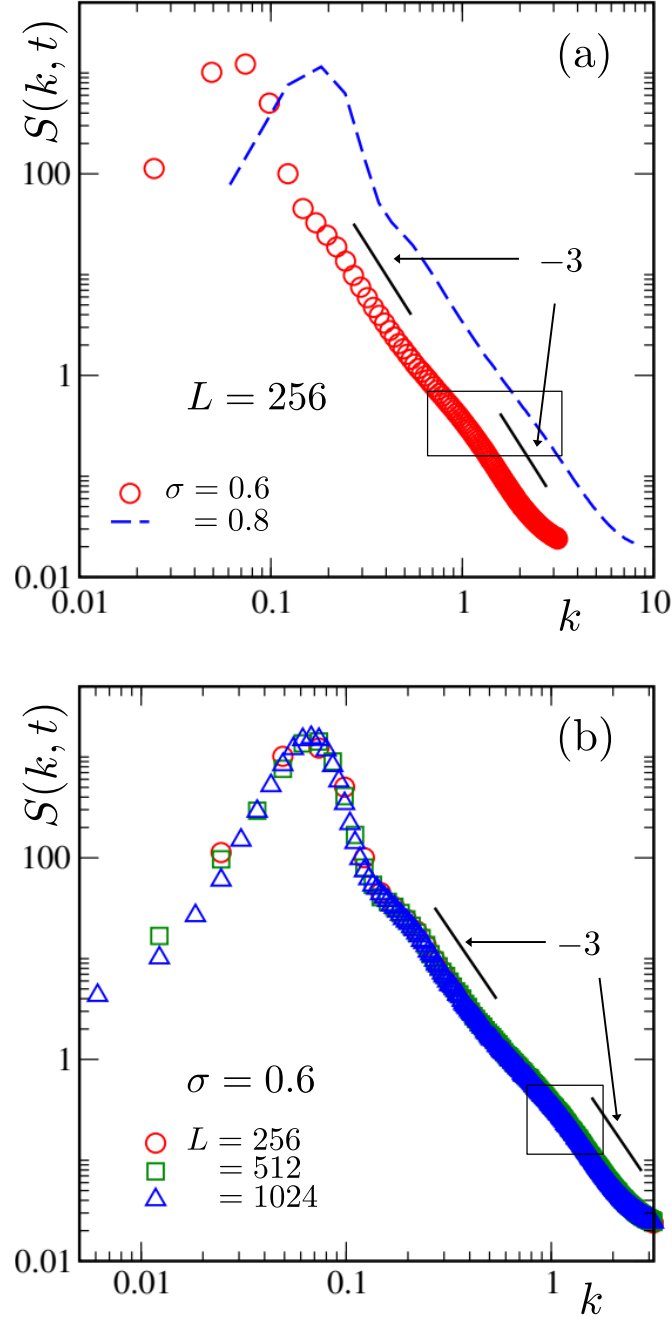


Figure 2.6: (a) Structure factor, $S(k, t)$, from systems with two different σ values, viz., $\sigma = 0.6$ and 0.8 , are plotted against wave number k . The abscissa of the data from $\sigma = 0.8$ is shifted by hand for a clear view. Solid lines represent the expected power-law behavior. The rectangular box is drawn to capture the anomalous regions present. (b) Same plots as in (a), for systems with only $\sigma = 0.6$ and three different values of L .

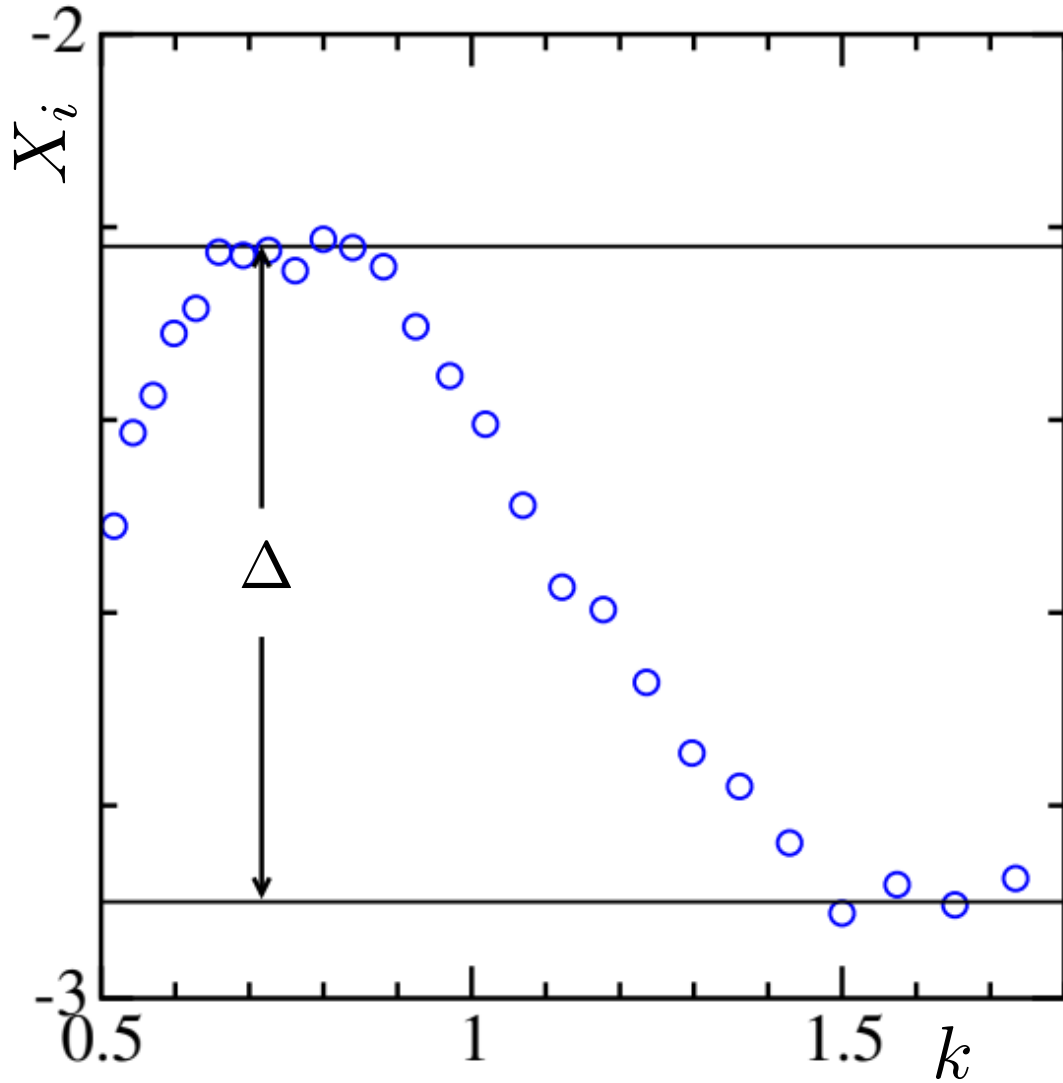


Figure 2.7: We plot X_i , for $\sigma = 0.6$, versus wave-number k , with $L = 256$. The upper horizontal line shows the maximum corresponding to a knee shown in Fig. 2.6. The lower one estimates the Porod exponent. The difference between these two is identified as Δ .

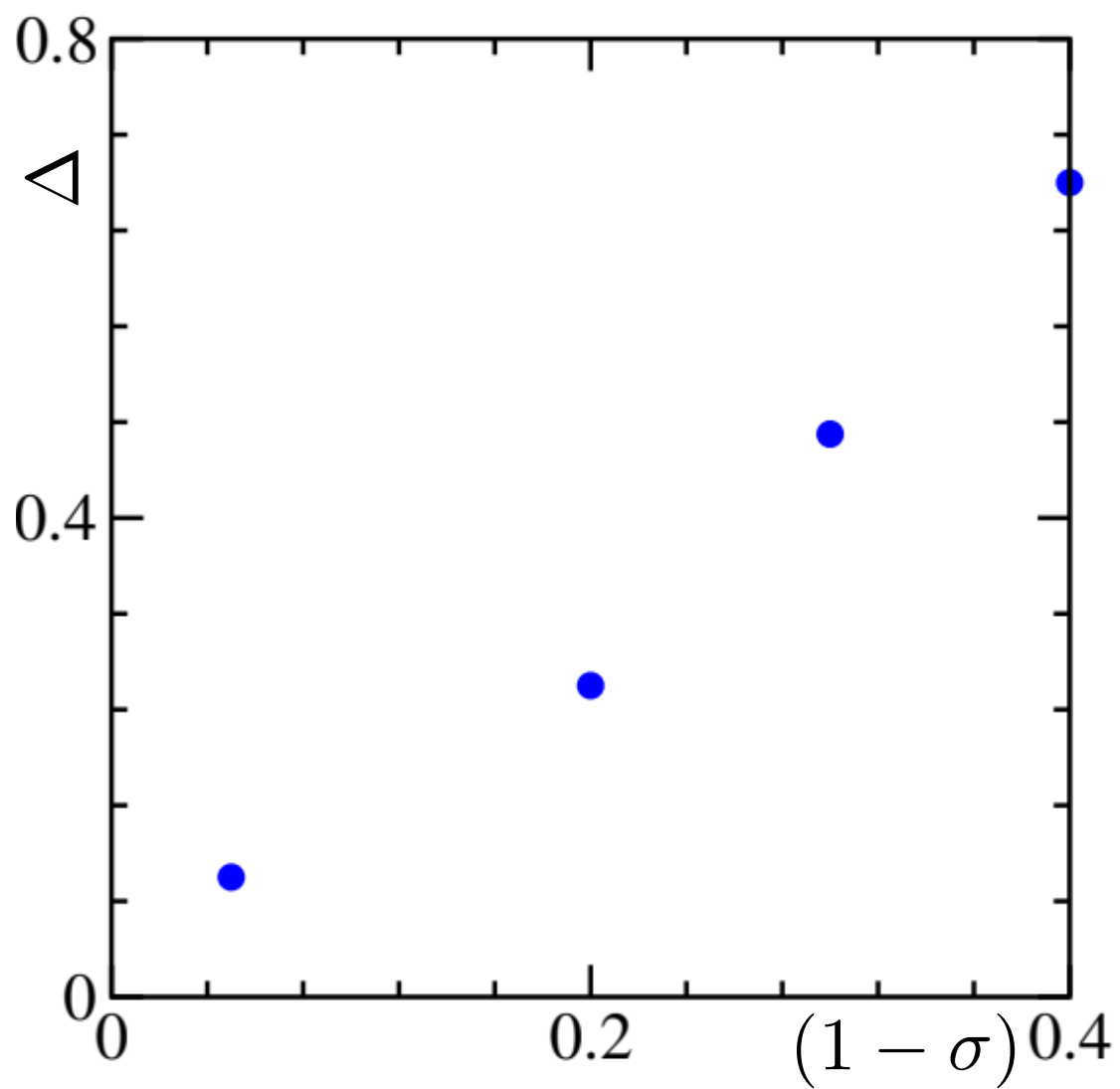


Figure 2.8: Plot of Δ as a function of $(1 - \sigma)$.

To quantify this irregularity in systems with long-range interactions, we define a quantity

$$X_i = \frac{d \ln S(k, t)}{d \ln k}, \quad (2.9)$$

as it is a useful practice to calculate such instantaneous exponents rather than estimating the power-law from the log-log plots [14]. When X_i is plotted against k , the so-called knee should result in a maximum at an intermediate value of k , before finally acquiring a value close to -3 , again, for very large k . In Fig. 3.5, we demonstrate this for $\sigma = 0.6$. The difference between the maximum value of X_i and the estimated value of Porod exponent, we refer to as Δ . In Fig. 2.8, we have plotted Δ against $(1 - \sigma)$. From the plot, it appears that the Δ has a strong dependence on σ which tends to disappear as $\sigma \rightarrow 1$, the theoretically expected transition point for short- and long-range regimes.

2.4 Conclusion

In this chapter, we have investigated the phenomenon of domain coarsening during phase separation in systems with long-range interaction. We also have analyzed the structure during the evolution process.

We have carried out MC simulations [15] of the long-range Ising model [8, 14, 16], using Kawasaki spin-exchange [15] mechanism, in space dimension $d = 2$. Systems prepared at very high temperatures are quenched to a final temperature $T = 0.6T_c$, for several values as σ , the parameter that controls the interaction range.

The growth exponents, α , are extracted via the calculations and analyses of the instantaneous exponent. We have found a dependence of α on the value of σ for $\sigma < 1$. These results are in good agreement with the existing theoretical predictions [8]. We again refer the reader to Fig. 2.5. There our simulation results indicate increasing rate of growth with the decrease of σ , i.e., the increase of range of interaction. The corresponding theoretical calculations by Bray suggest $\alpha = 1/(2 + \sigma)$. The trend of the simulation data are quite consistent with this expectation. For no σ the deviation from the expectation is larger than 10%. In space dimension $d = 3$ also we expect a similar trend. This is by taking lessons from the understanding with nearest neighbor Ising model. For the latter, the rate of growth is independent of space dimension.

On the aspect of pattern, we have noticed an anomaly that appears as a knee in the large- k decay of the structure factor, $S(k, t)$. We have shown that the anomaly

disappears as $\sigma \rightarrow 1$, the theoretically expected boundary between long and short-range interactions.

It will be interesting to consider even lower values of σ . However, given that the expectation is to encounter faster growth with the increase of range of interaction, finite-size effects will be hit earlier. Thus, to probe data even over a minimally reasonable duration of time, larger sizes of systems will be needed. This we will leave out for future.

Copyright and Permission

The results from this chapter are now published as:

Soumik Ghosh and Subir K. Das, “Nonuniversal aging during phase separation with long-range interaction”, Physical Review E **109**, L052102 (2024)

We have reproduced the results here following the policy of the American Physical Society. The article can be found online with the link below:

<https://link.aps.org/doi/10.1103/PhysRevE.109.L052102>

Bibliography

- [1] A. J. Bray, Adv. Phys. **51**, 481 (2002).
- [2] R. Agrawal, F. Corberi, F. Insalata, and S. Puri, Phys. Rev. E **105**, 034131 (2022).
- [3] F. Corberi, E. Lippiello, and P. Politi, J. Stat. Phys. **176**, 510 (2019).
- [4] F. Müller, H. Christiansen, and W. Janke, Phys. Rev. Lett. **129**, 240601 (2022).
- [5] H. Christiansen, S. Majumder, and W. Janke, Phys. Rev. E **99**, 011301 (2019).
- [6] H. Christiansen, S. Majumder, M. Henkel, and W. Janke, Phys. Rev. Lett. **125**, 180601 (2020).
- [7] J. C. Halimeh, M. Punk, and F. Piazza, Phys. Rev. B **98**, 045111 (2018).
- [8] A. J. Bray, Phys. Rev. E **47**, 3191 (1993).
- [9] T. Ishihara and H. Hayakawa, Phys. Rev. E **50**, 1629 (1994).
- [10] D. P. Landau and K. Binder, *A Guide to Monte Carlo Simulations in Statistical Physics* (Cambridge University Press, 2005).
- [11] T. Horita, H. Suwa, and S. Todo, Phys. Rev. E **95**, 012143 (2017).
- [12] S. Majumder and S. K. Das, Phys. Rev. E **81**, 050102 (2010).
- [13] J. F. Marko and G. T. Barkema, Phys. Rev. E **52**, 2522 (1995).
- [14] S. Ghosh and S. K. Das, Phys. Rev. E **109**, L052102 (2024).
- [15] D. Frenkel and B. Smit, *Understanding Molecular Simulation* (Academic Press, 2002).
- [16] H. Christiansen, S. Majumder, and W. Janke, Phys. Rev. E **103**, 052122 (2021).

Chapter 3

Kinetics of Phase Separation in Systems with Long-range Interaction: Study of Aging

3.1 Introduction

An important task, for understanding out-of-equilibrium systems, is to quantify relaxations starting from different ages, following certain perturbation [1]. Such aging phenomena is often studied via the autocorrelation function [1–11],

$$C_{ag}(t, t_w) = \langle \psi(\vec{r}, t) \psi(\vec{r}, t_w) \rangle - \langle \psi(\vec{r}, t) \rangle \langle \psi(\vec{r}, t_w) \rangle. \quad (3.1)$$

Here ψ is a space (\vec{r}) and time-dependent order parameter, t_w ($\leq t$) representing the waiting time, also referred to as the age of the system. The decay of C_{ag} is typically slower for an older system than a younger one, which reflects aging with passing time. This fact violates the time-translation invariance and implies that in an “away-from-steady-state” situation, there is no scaling collapse of data for C_{ag} when results for different t_w are plotted versus $t - t_w$. This is unlike the steady-state or equilibrium situation. However, collapse is interestingly observed [1] when the data are plotted versus ℓ/ℓ_w ($= x$), where ℓ is the characteristic length of the system at time t and ℓ_w is the value of ℓ at $t = t_w$. In the limit $x \rightarrow \infty$, one then discusses the scaling behaviour [1]

$$C_{ag}(t, t_w) \sim (\ell/\ell_w)^{-\lambda}, \quad (3.2)$$

λ being referred to as the aging exponent. As

$$\ell(t) \sim t^\alpha, \quad (3.3)$$

Eq. (3.2) can also be written as

$$C_{ag}(t, t_w) \sim (t/t_w)^{-\lambda'}, \quad (3.4)$$

with $\lambda' = \alpha\lambda$. The values of α and λ take part in characterizing universality in kinetics of phase transitions [1, 6, 9, 12].

A key difference between the computational studies of domain growth and aging is that the latter requires much superior statistics for significantly longer runs than the former. E.g., for a similar quality of data on the instantaneous exponents for aging, one requires statistics, as well as run lengths, improved by a factor more than 10 compared to the case of domain growth. This makes the consideration of bigger systems difficult for aging. Thus, despite being an important aspect, progress on the understanding of aging is significantly inferior to that of domain growth.

In the static critical phenomena, alongside a few other details, the range of the interaction decides classes of universality [13]. It is expected, though there will be two classes, above and below a certain cut-off for the range of interaction, in each of these the critical exponents will have values independent of further micro-variations of the interaction range. Investigation of such features are of much fundamental and practical importance for nonequilibrium dynamics as well [11, 14–19]. Question arises, if, within the same model framework, the above-mentioned universality picture remains unchanged, i.e., whether the interaction-range boundary between the two dynamic classes is the same as in the static case, and unique sets of exponents define growth and aging phenomena on the two sides, irrespective of the distance from the boundary. However, unlike the case of critical phenomena, progress in the case of evolution dynamics with the variation of the range of interaction is limited. This is despite the fact that long-range interactions are omnipresent in phase transitions, irrespective of the scales of the systems and the constituents.

In the previous chapter, we have discussed about the domain growth. There we have seen deviations from the static picture. In this chapter, we present results on the *aging phenomena*, to extract λ , for the conserved LRIM, covering a wide variation in the interaction range. It appears that λ also has an interesting dependence on the range of interaction. This overall picture is strikingly different from the static

case, in terms of universality as well as shifting of the above-mentioned boundary. The values of λ are discussed against a theoretical bound [3], to facilitate which we analyze the structural properties. Furthermore, we report an important scaling law combining growth and aging.

3.2 Model and Methods

We have used the same model system as used in the previous chapter, with the Hamiltonian [11, 18, 20]

$$H = -\frac{1}{2} \sum_i \sum_{j \neq i} J_{ij}(r) S_i S_j, \quad S_i = \pm 1, \quad (3.5)$$

with i and j standing for i^{th} and j^{th} points on a 2D square lattice. Recall that J_{ij} is interaction strength with a power-law form

$$J_{ij} = \frac{J}{r^{d+\sigma}}, \quad (3.6)$$

r being the distance between the points i and j . The space dimension d has a fixed value 2. So σ is the parameter that actually controls the rate of decay of the interaction strength.

We start with 50 : 50 mixtures of up and down spins (or A and B particles) placed randomly on a $L \times L$ square lattice. This corresponds to a system with infinite temperature. We quench these systems to a final temperature, T_f , inside the coexistence curve. We have performed this exercise for several different values of σ . It is important to remind here that the critical temperature T_c depends on the value of σ [21] and, as usual, also on the system sizes [21]. For our simulations, we have always quenched our systems to $T_f = 0.6T_c$ for every value of σ and have chosen the corresponding T_c values appropriately. We have performed Monte Carlo (MC) simulations with Kawasaki Spin Exchange dynamics. In this method, two spins at the nearest sites are chosen randomly and exchanged. The exponential of the energy change is then calculated and compared to a random number. For a detailed description, we refer the reader to section 1.4.1. We have used periodic boundary condition (PBC) throughout. Eq. (3.5) suggests that for every spin, we need to sum over all the lattice points along with periodic images. To deal with this, we have used a technique called generalized Ewald Summation [21], which is an effective way to make such calculations faster. In this method, the potential energy term is

divided into two parts - short and long-range term. While the short-range part is solved in real space, the long part is solved in Fourier space. For further details, see section 1.4.3.

Whenever important, we have carried out simulations of systems with different system sizes, viz., $L = 256, 512$ and 1024 . Quantitative results will be presented after averaging over 175 uncorrelated runs for systems with $L = 256$. For $L = 512$ and 1024 , the averaging is done over 100 and 8 configurations respectively. Both MPI and OpenMP parallelization are implemented in our codes to carry out the simulations faster.

3.3 Results

To begin with, we plot the autocorrelation function $C_{ag}(t, t_w)$ for $\sigma = 0.6$, from different values of waiting time t_w in Fig. 3.1, in a log-log scale. In part (a), we have presented the data as it is. There we can see a discontinuous jump which has a connection with the equilibration of domain magnetization. In part (b) of the same figure, we have discarded the jumps, keeping data concerning the growth of the domains. We have also multiplied the data with a suitable constant pre-factor so that they converge to unity as $t/t_w \rightarrow 1$. This operation does not alter the character of the decay, and thus, the outcome of our further analysis. The solid line in Fig. 3.1(b) is the power law behavior with the exponent value written next to it. For situations where the slope is continuously changing, predicting the exponent from a log-log plot is not appropriate. A better way is to calculate the instantaneous exponent.

Here, we introduce a quantity λ_i defined as [8]

$$\lambda_i = -\frac{d \ln C_{ag}(t, t_w)}{d \ln \ell / \ell_w}. \quad (3.7)$$

This quantity, when plotted against t/t_w , shows a nice linear trend. Thus, from simple extrapolation, the value of λ can be obtained from λ_i . In Fig. 3.2, we have plotted λ_i from two different σ , viz., 0.6 and 0.95 , versus t_w/t . For $\sigma = 0.6$, we have shown results from simulations with three different system sizes. All the data sets are in good agreement. In the case of $\sigma = 0.95$, thus, we have presented data from only $L = 256$. This is because of the fact that the growth in this case is slower and so the finite-size effects are expected to be weaker than those for $\sigma = 0.6$. The solid

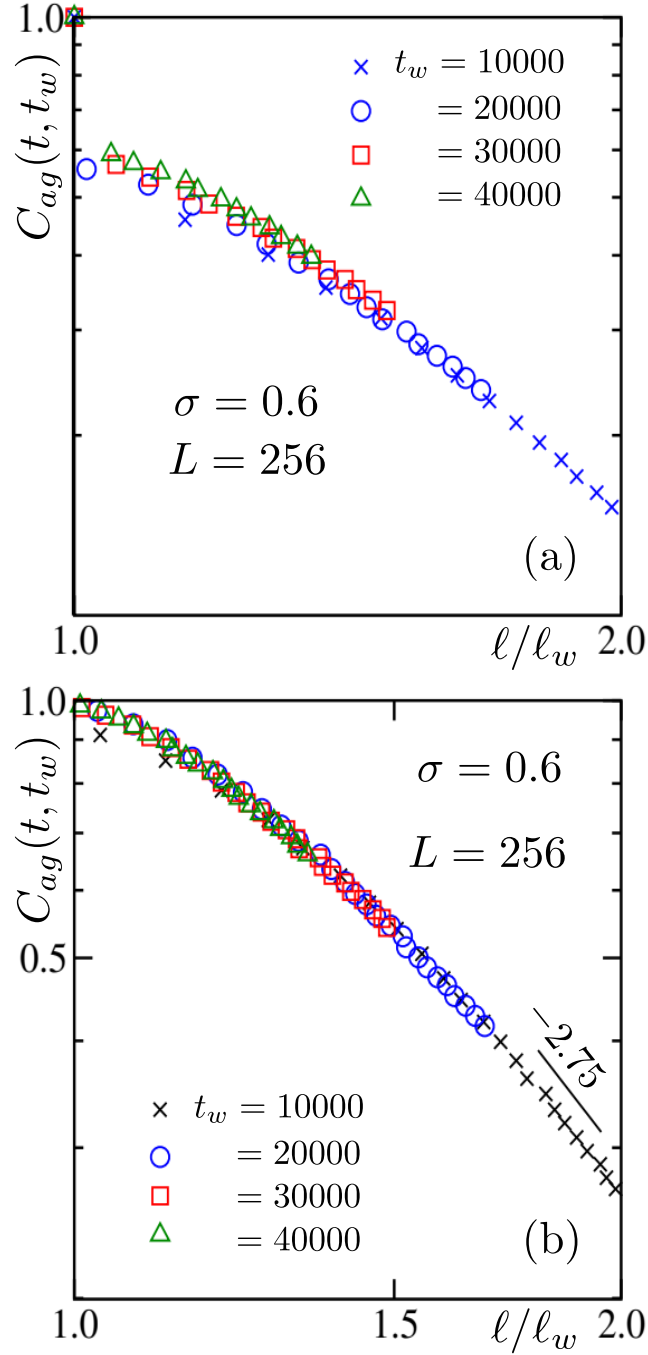


Figure 3.1: Plots of the autocorrelation function, $C_{ag}(t, t_w)$, as a function of ℓ/ℓ_w , for the LRIM, with $\sigma = 0.6$. Results for several different ages have been included. (a) shows the original data with a jump that corresponds to the equilibration of domain magnetization. Results in (b) are scaled by a pre-factor, after discarding the jumps, such that C_{ag} smoothly approaches 1, as $\ell/\ell_w \rightarrow 1$, for most of the t_w values. Such a transformation does not affect the decay exponent. The solid line represents a power-law decay with the mentioned value of the exponent. The presented results are for $L = 256$, the unit being the lattice constant.

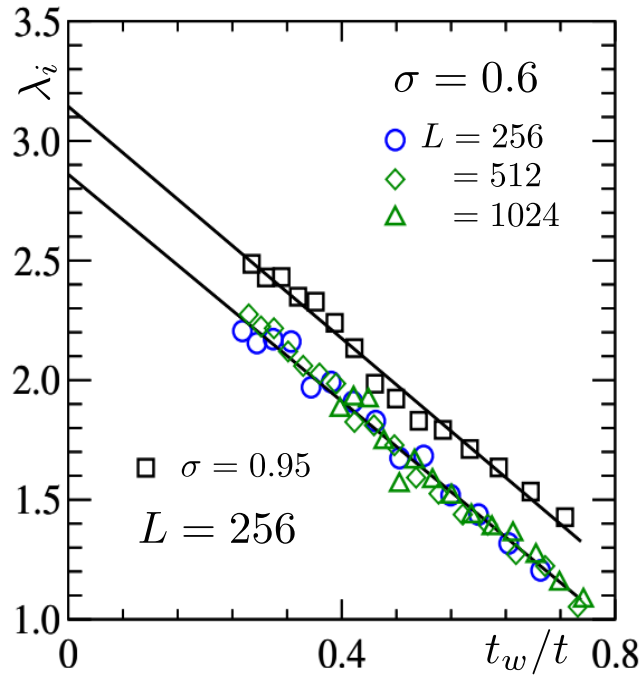


Figure 3.2: Instantaneous exponent, λ_i , are plotted versus t_w/t , for different σ and system sizes. Solid lines are the linear fits to the data sets from $L = 256$. Since λ_i is a noisy quantity, running averaging was carried out for data smoothening.

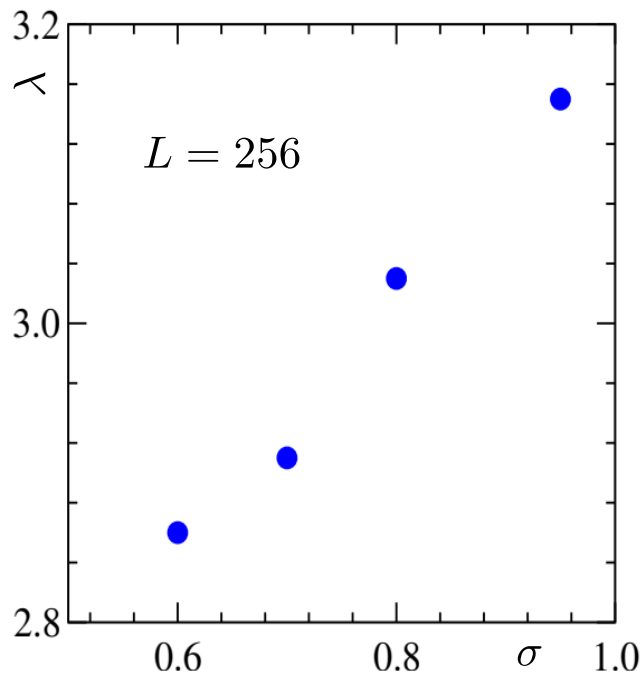


Figure 3.3: The estimated values of the aging exponent, λ , from the fits in Fig. 3.2, are shown against σ . These are calculated by considering t_w values from the scaling regimes.

lines are the fits to simulation data, gathered for $L = 256$ system, to the form

$$\lambda_i = \lambda + a \frac{t_w}{t}, \quad (3.8)$$

a being a constant. From there, we get different values of λ for different σ , implying the fact that the aging exponents are *nonuniversal*, like α , having a dependence on the range of interaction. In Fig. 3.3, we have plotted λ , that we have obtained using Eq. 3.8, for four different σ values, for $\sigma < 1$.

We will come back to this and verify these results later in this chapter again. Before that, we recall certain lower bounds on λ , provided by Yeung, Rao and Desai (YRD) [3]:

$$\lambda \geq \frac{d + \beta}{2}, \quad (3.9)$$

where β is defined via small wavenumber power-law character of the structure factor as

$$S(k, t) \sim k^\beta. \quad (3.10)$$

For systems with short-range interaction and conserved order-parameter dynamics, one has $\beta = 4$ in $d = 2$ [22]. In that case, for the bound to remain valid, λ should have a value greater than 3, which is clearly not the case. This can be appreciated from Fig. 3.3. So, we take a closer look at the structure factor, especially, the small k behaviour of it. Portions of the structure factors, $S(k, t)$, are plotted against k in a log-log scale in Fig. 3.4, for $\sigma = 0.6$ and 0.95 . The slopes of the plots in $k \rightarrow 0$ limit provide the values of the exponent β . The dashed line is a power-law with an exponent 4, the desired value of β for the short-range case. It is quite evident from the figure that the values of β , for $\sigma < 1$, are smaller than 4. We repeat, to quantify a power-law behavior, the right choice is to calculate the instantaneous exponent. Here, we define it as

$$X_i = \frac{d \ln S(k, t)}{d \ln k}. \quad (3.11)$$

In Fig 3.5 we have plotted X_i as a function of k . Even if we take the maxima of X_i , from these plots, as choices of β , no violation of the YRD bound can be ascertained. With this conclusion, we return to our topic of original interest, i.e., the dependence of growth and aging on σ .

Now we extract the quantity λ' , from the simulation results for λ and existing theoretical predictions of α [14, 16], as $\lambda' = \lambda\alpha$. In Fig. 3.6, we plot λ' as a function of σ . Within a small fluctuation, $\lambda \simeq 1.1$, irrespective of the value of σ . This result

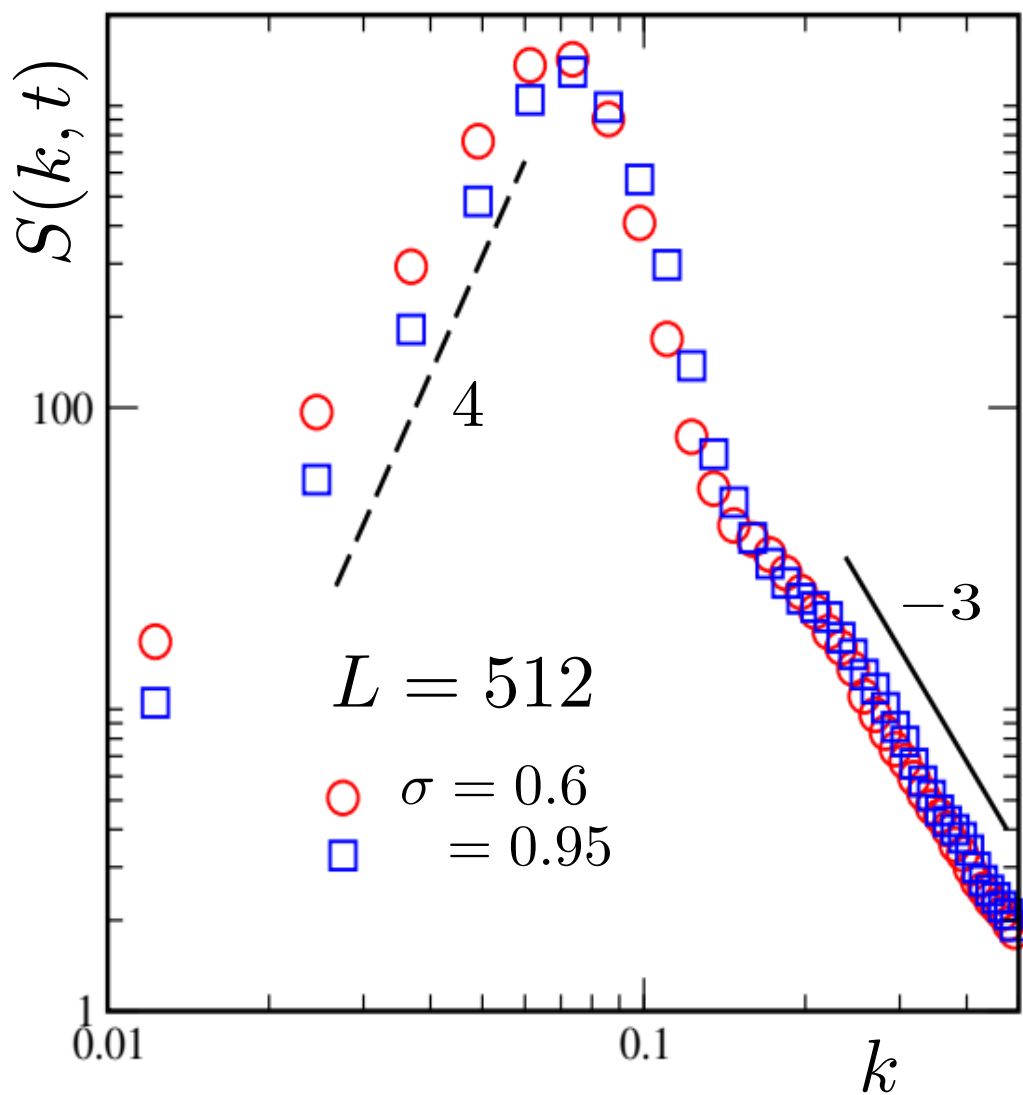


Figure 3.4: Equal-time structure factors, $S(k, t)$, are plotted versus wave number k . The dashed and the solid lines are power-laws. System size, values of σ and exponents are mentioned in appropriate places inside the frame.

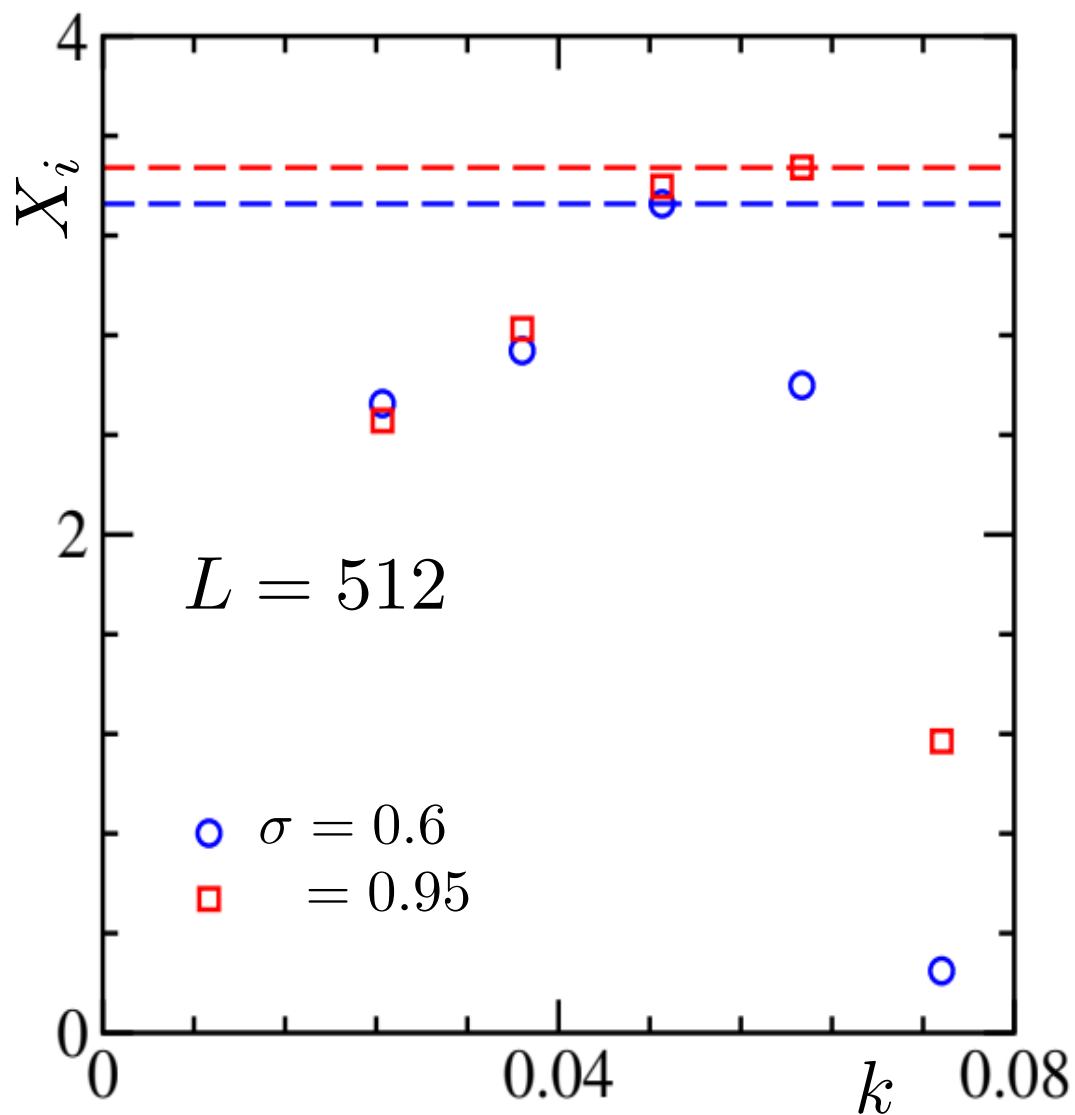


Figure 3.5: The quantity X_i is plotted versus k , for $\sigma = 0.6$ and 0.95 . Here, we have shown a small portion of the ordinate that is important for verifying the YRD bound. The horizontal dashed lines define the ceiling for the instantaneous exponent. The line colors are matched with the symbols to clearly identify the maxima for different values of σ .

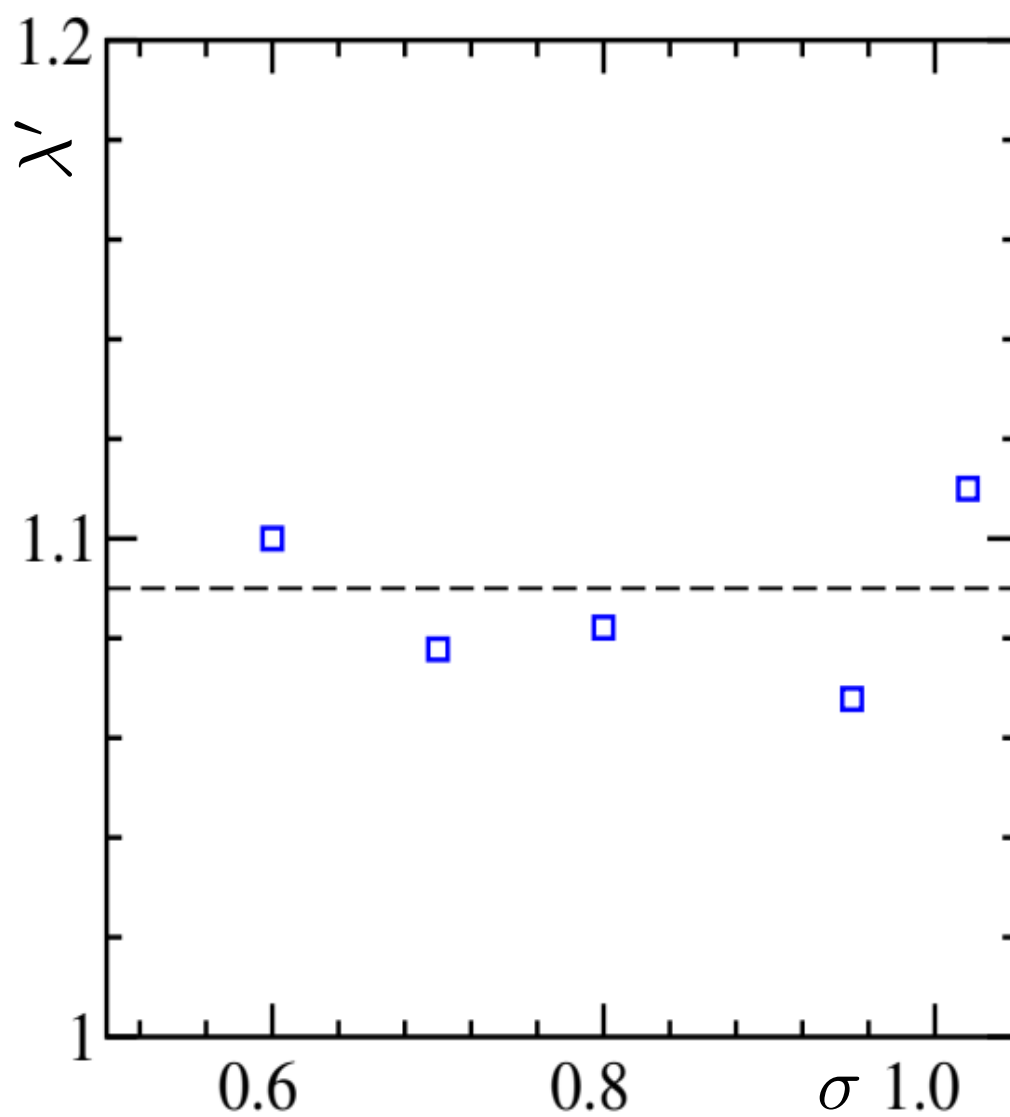


Figure 3.6: The quantity λ' , obtained from the calculated values of λ and theoretical predictions for α , is plotted versus σ .

is quite interesting, to confirm which we carry out further analysis by including the case of short-range interaction (nearest neighbor) as well.

In Fig. 3.7, we plot $C_{ag} \times y^{\lambda'}$, where $y = t/t_w$, as a function of y . When λ' is chosen correctly, the ordinate should take a constant value for $y \rightarrow \infty$. Data from $\sigma = 0.6$ and the nearest neighbor (NN) Ising model are presented, for $L = 512$, with the choice $\lambda' = 1.1$. The observation certainly confirms our previous conclusion on universality of the product. A and B are two constants introduced for the purpose of better visualization only.

3.4 Conclusion

In this chapter, we have studied aging in a long-range Ising model with conserved order-parameter dynamics. For this purpose, we have quenched systems to a state point well inside the coexistence curve with random initial configurations. The interaction that we have chosen between the spin sites, varies as $1/r^{d+\sigma}$ [13, 23, 24]. We have chosen a set of σ values in such a way that the system under consideration belongs to the long-range universality class and noted the effect of σ on aging. The autocorrelation function, calculated for different waiting times shows a nice collapse when initial jumps, related to equilibration of domain magnetization, are discarded.

We have observed an interesting dependence of the aging exponent λ on σ . For $\sigma < 1$, λ increases with the decrease of the interaction range. We have also confirmed the validity of the YRD bound [3]. To do so, we have looked at the structural properties of the systems.

We have combined the growth exponent α with the aging exponent λ , to define a quantity $\lambda' = \alpha\lambda$. We find $\lambda' \simeq 1.1$, for all $\sigma < 1$, despite the fact that both α and λ vary with σ . Furthermore, we have revisited the nearest-neighbor (NN) Ising model. In this case also the above mentioned universal value of λ' is observed.

While our observation here is the nonuniversality in λ , we intend to confirm it and arrive at much accurate estimations of the corresponding values via simulations of much bigger systems over significantly longer times. We also intend to study aging phenomena with this model in higher dimensions. Even though growth exponent may not change with such variation of space dimension, our experience with nearest neighbor Ising model suggest that there might be differences in the aging exponent.

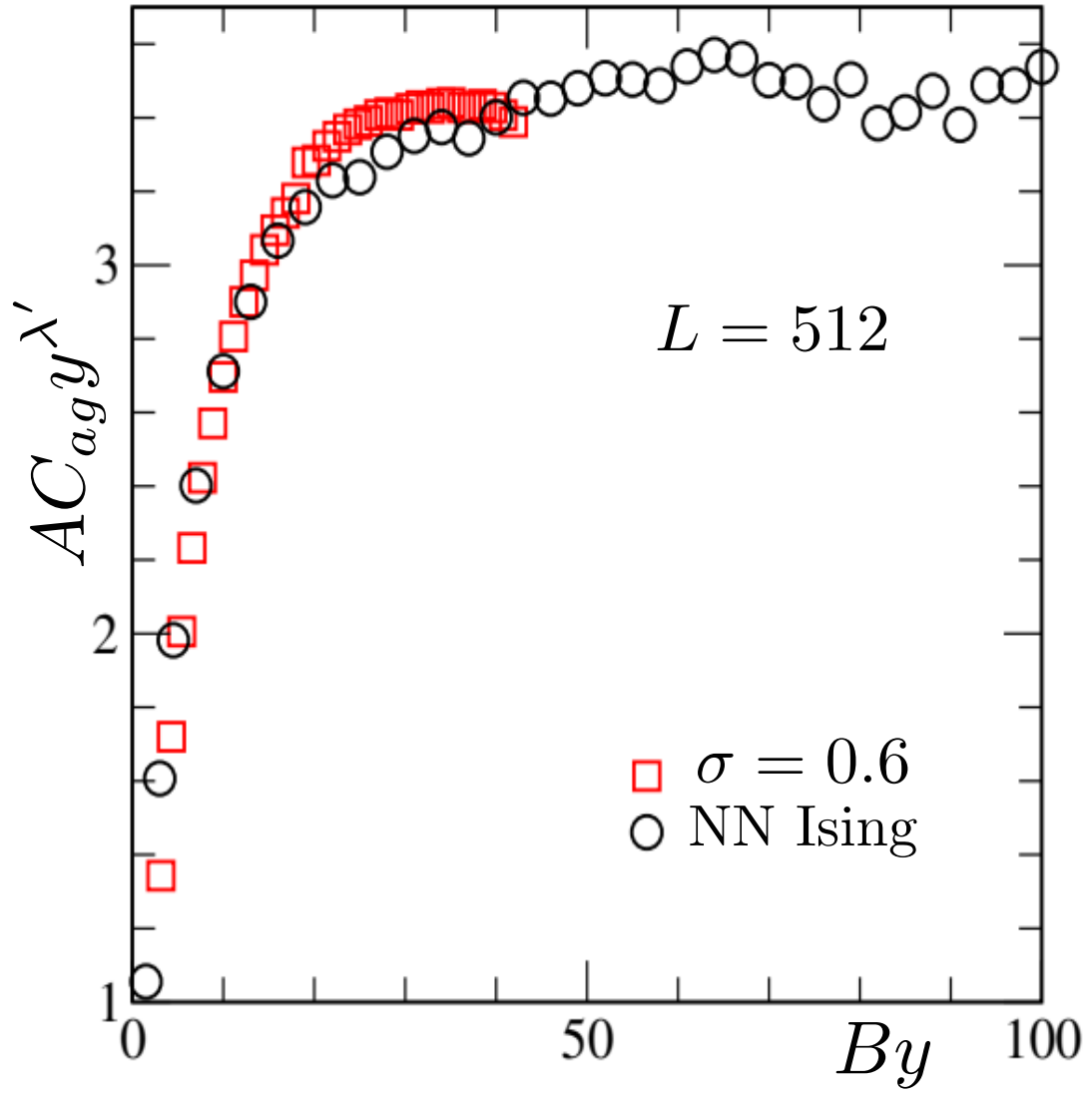


Figure 3.7: $C_{ag}(t, t_w) \times y^{\lambda'}$ is plotted versus y for $\sigma = 0.6$ and the nearest neighbor (NN) Ising model, with $L = 512$. The constant prefactors, A and B are introduced only for visual convenience. We have chosen $\lambda' = 1.1$ for both the cases.

The results from this chapter are now published as:

Soumik Ghosh and Subir K. Das, “Nonuniversal aging during phase separation with long-range interaction”, Physical Review E **109**, L052102 (2024)

We have reproduced the results here following the policy of the American Physical Society. The article can be found online with the link below:

<https://link.aps.org/doi/10.1103/PhysRevE.109.L052102>

Bibliography

- [1] D. S. Fisher and D. A. Huse, Phys. Rev. B **38**, 373 (1988).
- [2] F. Liu and G. F. Mazenko, Phys. Rev. B **44**, 9185 (1991).
- [3] C. Yeung, M. Rao, and R. C. Desai, Phys. Rev. E **53**, 3073 (1996).
- [4] M. Henkel, A. Picone, and M. Pleimling, Europhys. Lett. (EPL) **68**, 191 (2004).
- [5] E. Lorenz and W. Janke, Europhys. Lett. (EPL) **77**, 10003 (2007).
- [6] M. Zanetti, in S. Puri and V. Wadhawan, eds., *Kinetics of Phase Transitions* (Boca Raton: CRC Press, 2009).
- [7] J. Midya, S. Majumder, and S. K. Das, J. Phys. Condens. Matter **26**, 452202 (2014).
- [8] J. Midya, S. Majumder, and S. K. Das, Phys. Rev. E **92**, 022124 (2015).
- [9] N. Vadakkayil, S. Chakraborty, and S. K. Das, J. Chem. Phys. **150**(5), 054702 (2019).
- [10] N. Vadakkayil, S. K. Singha, and S. K. Das, Phys. Rev. E **105**, 044142 (2022).
- [11] H. Christiansen, S. Majumder, M. Henkel, and W. Janke, Phys. Rev. Lett. **125**, 180601 (2020).
- [12] A. J. Bray, Adv. Phys. **51**, 481 (2002).
- [13] M. E. Fisher, S. keng Ma, and B. G. Nickel, Phys. Rev. Lett. **29**, 917 (1972).
- [14] A. J. Bray, Phys. Rev. E **47**, 3191 (1993).
- [15] A. J. Bray and A. D. Rutenberg, Phys. Rev. E **49**, R27 (1994).
- [16] F. Müller, H. Christiansen, and W. Janke, Phys. Rev. Lett. **129**, 240601 (2022).

-
- [17] R. Agrawal, F. Corberi, F. Insalata, and S. Puri, Phys. Rev. E **105**, 034131 (2022).
 - [18] F. Corberi, E. Lippiello, and P. Politi, J. Stat. Phys. **176**, 510 (2019).
 - [19] H. Christiansen, S. Majumder, and W. Janke, Phys. Rev. E **99**, 011301 (2019).
 - [20] S. Ghosh and S. K. Das, Phys. Rev. E **109**, L052102 (2024).
 - [21] T. Horita, H. Suwa, and S. Todo, Phys. Rev. E **95**, 012143 (2017).
 - [22] C. Yeung, Phys. Rev. Lett. **61**, 1135 (1988).
 - [23] J. Sak, Phys. Rev. B **8**, 281 (1973), <https://link.aps.org/doi/10.1103/PhysRevB.8.281>.
 - [24] N. Defenu, A. Trombettoni, and A. Codello, Phys. Rev. E **92**, 052113 (2015), <https://link.aps.org/doi/10.1103/PhysRevE.92.052113>.

Chapter 4

Coarsening in the Long-range Ising Model with Conserved Dynamics

4.1 Introduction

When quenched inside a miscibility gap, from a high-temperature homogeneous phase, a system, comprising of multiple components, undergoes phase transition [1–6]. It tries to reach a new equilibrium, having regions of different components coexisting with each other, via the formation of small domains that are rich in like particles. Given the fundamental and technological significance, understanding of the growth of these domains received significant importance [2–4, 6–23] in material science and statistical physics communities. Usually, the related length scale (ℓ), i.e., the average size of the domains, grows with time in power-law fashion. For systems having only short-range interactions, the growth behavior is vastly studied and well understood. In such situations, for conserved order-parameter case, in the absence of hydrodynamics, mimicking phase separation, say, in solid mixtures, one expects [2–4, 6, 7]

$$\ell(t) \sim t^\alpha, \text{ with } \alpha = \frac{1}{3}. \quad (4.1)$$

This is confirmed via computational studies [8–10, 24] with spin models such as the nearest neighbor Ising model (NNIM) [10] and the Potts model [6]. The expectation in Eq. (4.1) appears valid for equal as well as unequal proportions of the components in mixtures.

The long-range counterpart [25, 26], e.g., of the Ising model, in d space dimensions, where the interaction falls off with distance r as $r^{-(d+\sigma)}$, has become a topic of much recent interest [27–32]. In this case, for conserved order-parameter dynamics, a theory suggests [26]

$$\alpha = \frac{1}{2 + \sigma}, \text{ for } \sigma < 1. \quad (4.2)$$

However, for $\sigma > 1$, long-range interaction has been stated to have no role in deciding the domain growth exponent and thus [26], $\alpha = 1/3$, which is the same as the NNIM case. While this general fact may differ from our knowledge of boundary of interaction range, as well as understanding of universality, obtained from studies of equilibrium critical phenomena [33, 34], computer simulations showed consistency [31, 32]. It is worth mentioning here that a theoretical expectation for the nonconserved order-parameter dynamics is [25, 26]

$$\alpha = \frac{1}{1 + \sigma}, \text{ for } \sigma < 1, \quad (4.3)$$

which also was found to be consistent with simulation studies [27, 29]. In this case, $\alpha = 1/2$, for $\sigma > 1$, same as the nonconserved dynamics for the NNIM [2].

Here we revisit the case of long-range conserved dynamics. The objective, primarily, is to quantify the early-time behavior. For this purpose, we carry out Monte Carlo (MC) simulations [6] with the long-range Ising model (LRIM) [26], with equal proportion of mixture components. We analyze the obtained results via advanced methods, including a finite-size scaling (FSS) technique. The outcomes reveal the following. For σ somewhat less than unity, at early times we find the exponent α to be as high as even the theoretical expectation for the nonconserved dynamics. This is despite the fact that the imposed dynamics in our simulations is the conserved one. At late times, however, we find $\alpha \simeq 1/(2 + \sigma)$, expectation recorded in Eq. (4.2) for the conserved dynamics. For $\sigma > 1$, we find the growth to be consistent with $\alpha = 1/3$, from rather early times. Our results on such crossover are surprising and, to the best of our knowledge, were never reported before. Although the presence of two distinct growth regimes is a completely new observation in the context of the Ising model, the microcanonical microscopic dynamics of the ϕ^4 model [35], in the presence of long-range interaction, give rise to two different growth exponents in early and late times in $d = 1$ [36].

The rest of the chapter is organized as follows. Section 4.2 contains the descriptions of the model and the basic methods. Results, along with the discussions of the

techniques of analysis, are presented in Section 4.3. Finally, Section 4.4 concludes the chapter with a brief summary.

4.2 Model and Methods

We have studied the LRIM in $d = 2$. The model has the Hamiltonian [25, 26, 29, 32]

$$H = -\frac{1}{2} \sum_i \sum_{j \neq i} J(r) S_i S_j, \quad J(r) = \frac{1}{r^{d+\sigma}}. \quad (4.4)$$

Here $J(r)$ is the interaction strength for a separation r between two spins S_i and S_j at sites i and j that can take values $+1$ or -1 , corresponding to, say, A and B types of particles in a $A + B$ binary mixture. For fixed d , σ decides the range of interaction, for which we consider a wide variation.

We start with random initial configurations, with 50 : 50 up and down spins sitting on 2D periodic $L \times L$ square lattices, mimicking a very high temperature (T) scenario. These configurations are instantaneously quenched to final temperatures $T_f = 0.6T_c$, where T_c represents a critical temperature [37]. It should be noted that the value of T_c depends upon σ , as well as on the system size L [37].

We implement Kawasaki spin-exchange dynamics [2] in our MC simulations [6, 38]. A trial move in this method is made of the following steps. First, a lattice site is randomly chosen. Spin (or a particle) at that site is then interchanged with that at a randomly chosen nearest neighbor site. This conserves the order parameter. Such a move is accepted according to the standard Metropolis criterion [6]. An MC step (MCS), the unit of our simulation time, is made of L^2 such moves.

Given that our primary goal is to probe early time behavior, we have studied certain small system sizes, viz., $L = 16, 24$ and 32 . To identify the crossovers, we have also considered systems as large as $L = 256$. Given the difficulty with the simulations of systems possessing long-range interactions, reaching adequately long time and getting good statistics is already difficult for the latter system size. This is despite the fact that we have used Ewald summation [37] and parallelized our code. For the details on Ewald summation and related parameter, please see section 1.4.3.

The lengths from the evolution snapshots were calculated as the first moments of the domain-size distribution functions, there the size of a domain being the separation between two consecutive domain boundaries along any given Cartesian direction [10]. For final temperatures that are reasonably above zero, there can be

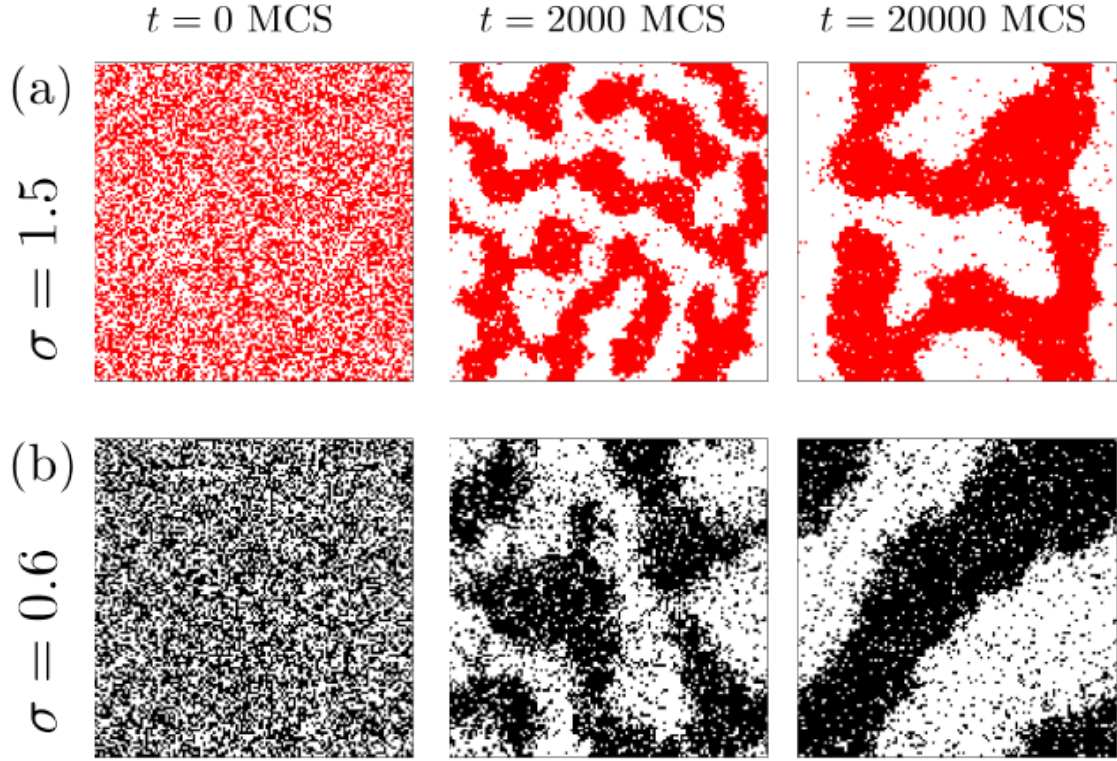


Figure 4.1: Evolution snapshots of the 2D systems, with $L = 128$, when quenched to $0.6T_c$, from high temperature, are shown for (a) $\sigma = 1.5$ and (b) $\sigma = 0.6$. The locations of the particles are marked. For each σ value, in addition to the initial configuration, two well-grown configurations are displayed.

significant noise in the snapshots. This may introduce errors in the calculations of ℓ . To avoid such inaccuracy we have eliminated this noise, via the application of a majority spin rule [10].

All quantitative results are presented after averaging over data from runs with many different independent initial configurations. The numbers fall in the range between 175 and 192, for L lying between 256 and 16.

4.3 Results

In parts (a) and (b) of Fig. 4.1, we have shown evolution snapshots of systems with two different σ values, viz., $\sigma = 1.5$ and $\sigma = 0.6$, the former belonging to the short-range side of the interaction and the latter falling on the long-range side [26]. In each of the cases starting composition was a random arrangement of A and B

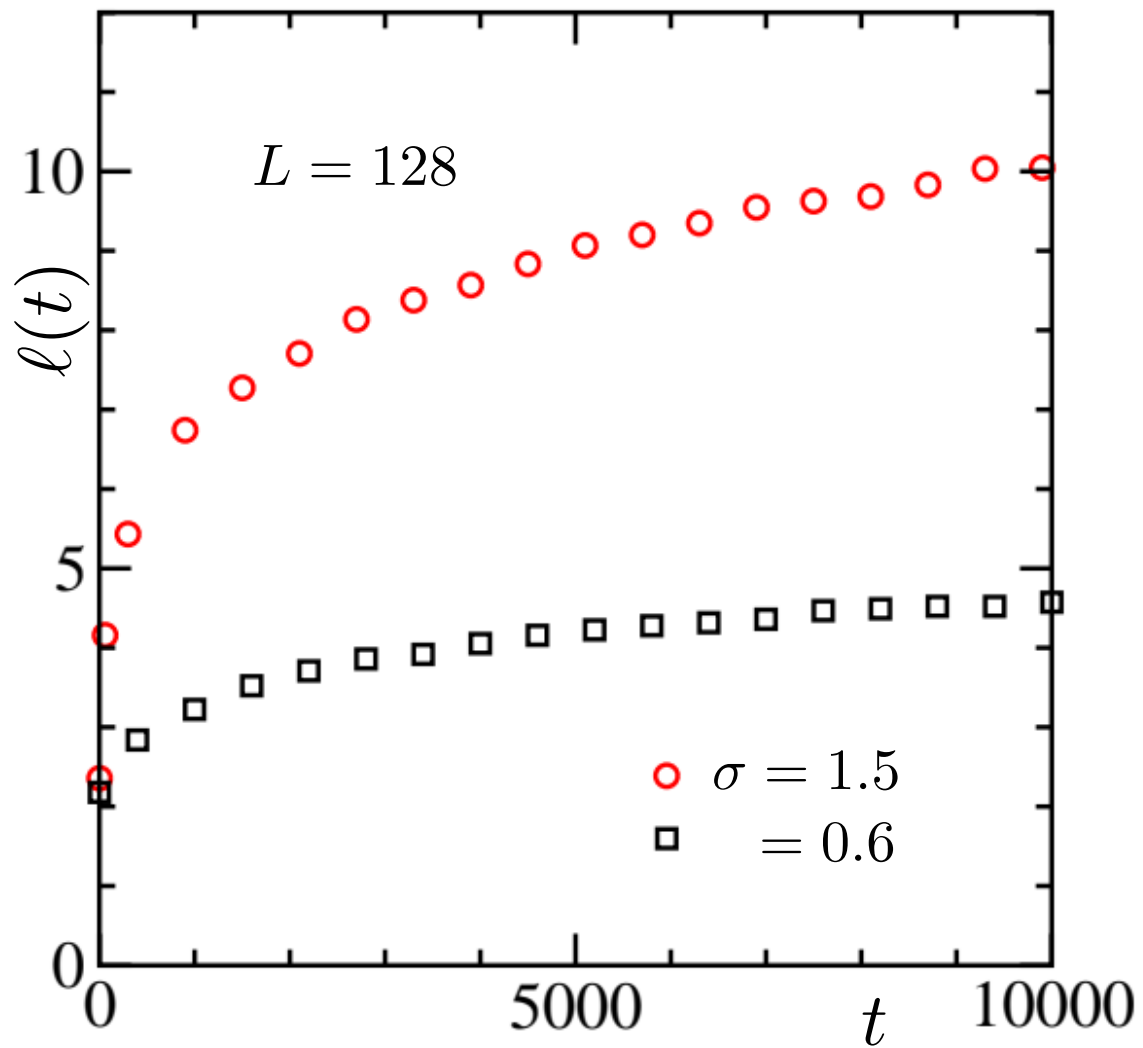


Figure 4.2: Domain length, $\ell(t)$, of systems with different σ values, are plotted against time t . The system size is mentioned inside the frame.

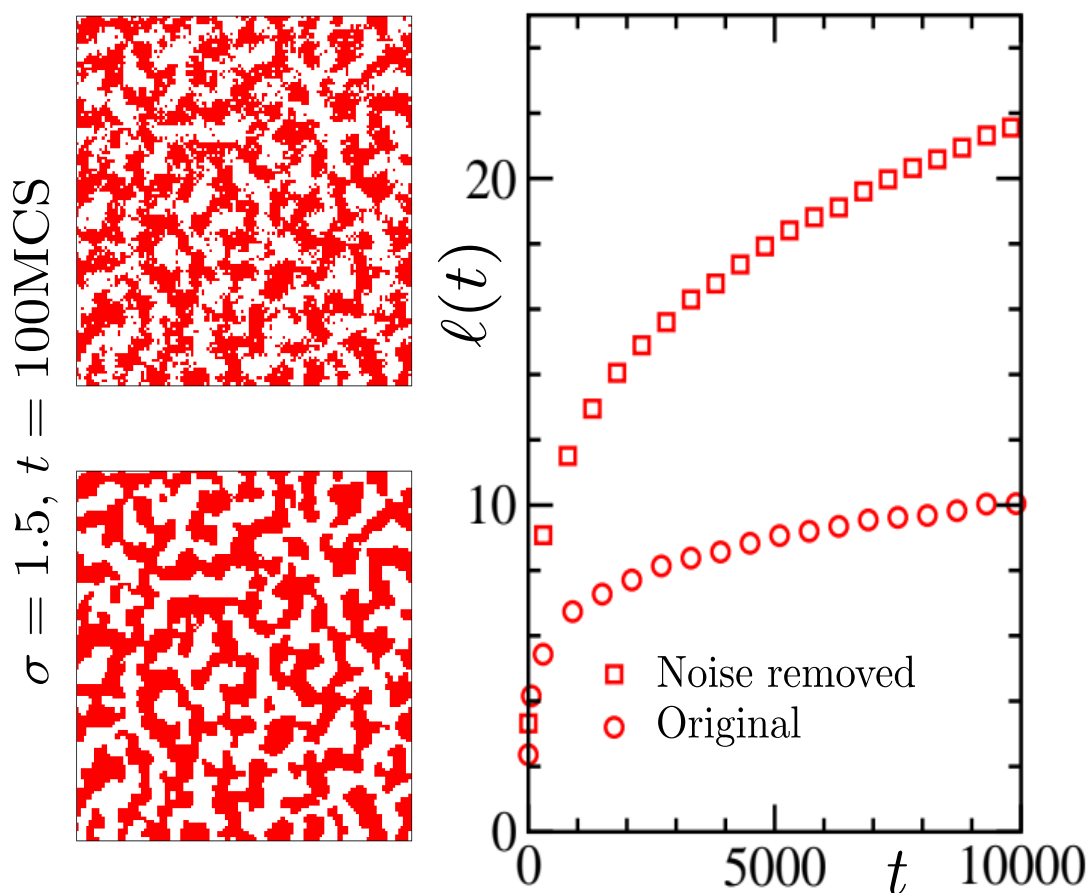


Figure 4.3: The upper left frame shows a snapshot taken during the evolution of a system with $\sigma = 1.5$. The lower left frame contains the same snapshot after removing the noise. See the text for discussion and reference related to the removal of noise. The right frame shows a comparison between domain lengths calculated by using snapshots with and without noise. These results are for $L = 128$.

particles. Clearly, for the longer range case the growth is faster. However, this cannot be concluded from Fig. 4.2 where we have shown plots of $\ell(t)$, versus t , for the same two values of σ . This unexpected quantitative feature is due to the fact that the snapshots for $\sigma = 0.6$ contain significantly more noise than those for $\sigma = 1.5$. In fact, for both the cases there exist much noise, the averages of which are time dependent till the corresponding length scales reach the values of equilibrium correlation lengths at the considered final temperatures. This fact on competing growth, between lengths related to noise and real coarsening, can lead to inappropriate conclusions on the rate of domain growth, that we are interested in, if the actual snapshots are used for the calculation of the latter. In Fig. 4.3 we demonstrate how a noise removal exercise, mentioned earlier, picks up the actual domain morphology by discarding (noisy) fluctuations. See the two left frames and their descriptions in the caption. In the right frame, we plot $\ell(t)$, versus t , calculated by using snapshots with and without noise. Clearly, in the plot obtained by using the original snapshots, values of $\ell(t)$ are hugely underestimated! In the remaining part, thus, we have used the noise removed snapshots to calculate ℓ . Our goal is to quantify the growths, for a large range of σ , the primary focus, as stated above, being on early times.

We calculate the instantaneous exponent, α_i , defined as [8–10]

$$\alpha_i = \frac{d(\ln \ell(t))}{d(\ln t)}. \quad (4.5)$$

Value of α_i , when $\ell \rightarrow \infty$, is the expectation for α in the long-time limit. In Fig. 4.4(a), we have plotted this quantity as a function of $1/\ell$, for $\sigma = 0.6$ and 0.9 . It appears that there exist two distinct regimes, for each σ . Extrapolations of the trends exhibited by these two different regimes, to $\ell \rightarrow \infty$, i.e., $1/\ell \rightarrow 0$, lead to two drastically different values of α . If we accept the late time trend, corresponding extrapolations are consistent with the theoretical predictions for conserved order-parameter dynamics [26], see Eq. (4.2). On the other hand, extrapolations of the early time trends provide much higher values for α !

In the main frame of Fig. 4.4(b), we have displayed a similar plot for the NNIM. In this case, the late time behavior is a continuation of rather early time trend [8–10]. The same feature is true for the LRIM with $\sigma = 1.5$ that already is on the short-range side of the interaction [26]. See the inset for the latter plot. This hints towards the fact that the rates of growth, for the long-range variety, with $\sigma < 1$, during early parts are different from the asymptotic values. Furthermore, careful observations

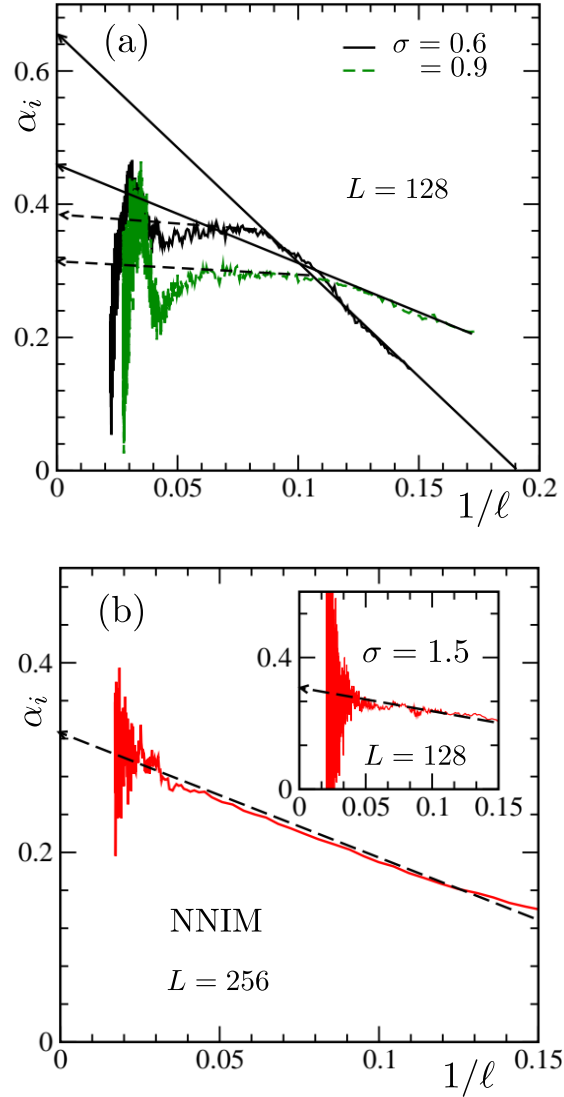


Figure 4.4: (a) Instantaneous exponent, α_i , for different σ values, viz., $\sigma = 0.6$ and 0.9 , are plotted against $1/\ell$. (b) Same as (a), but here the results are for the nearest neighbor Ising model (NNIM). Inset shows the same plot for the LRIM with $\sigma = 1.5$. Various arrow-headed lines are guides to the eyes. All the data are presented after running averaging. Data earlier than the presented ones suffer from noise removal exercise. See text for a discussion on the latter fact.

suggest that the longevity of the early part keeps shortening before disappearing at a certain value of σ , possibly unity. In the following, we aim to confirm these early-time exponents via certain FSS analysis [10, 39, 40].

When a homogeneous system is quenched inside the coexistence regime, it takes a while to fall unstable and then reach a scaling regime of growth that may be considered free from any significant correction. If we denote this waiting time as t_0 , and the corresponding length as ℓ_0 , $\ell(t)$ can be expressed as [9, 10]

$$\ell(t) = \ell_0 + At'^{\alpha}, \quad (4.6)$$

with $t' = t - t_0$. In simulations, due to the finiteness of the systems (and also due to certain freezing phenomenon [41]), domains can grow only up to a certain value, say, ℓ_{\max} . In such situations, Eq. (4.6) should be modified as, following a finite-size scaling [10, 39, 42] ansatz,

$$\ell(t) - \ell_0 = Y(y)(\ell_{\max} - \ell_0). \quad (4.7)$$

In Eq. (4.7), $Y(y)$ is a system-size independent (finite-size) scaling function and y is a dimensionless scaling variable. A suitable choice for y is [10]

$$y = \frac{(\ell_{\max} - \ell_0)^{\frac{1}{\alpha}}}{t'}. \quad (4.8)$$

If we plot $Y(y)$ as a function of y , for the correct choices of ℓ_0 and α , data from different system sizes should collapse to form a master curve. In the limit $y \rightarrow \infty$, i.e., for the finite-size unaffected regime, a power-law behavior,

$$Y \sim y^{-\alpha}, \quad (4.9)$$

should emerge, to comply with Eq. (4.6). However, if there exists a crossover between two different growth regimes, data collapse cannot be expected. Thus, to probe the early time behavior, study should be restricted to smaller system sizes. For this reason, for the FSS analysis, to identify early time growth exponent, we choose $L = 16, 24$ and 32 , for which the finite-size effects enter before the crossover, for the considered σ value, viz., $\sigma = 0.6$, that we use to demonstrate the exercise.

In Fig. 4.5, for $\sigma = 0.6$, we have shown $\ell(t)$, as a function of t , for the above three system sizes. It is clear from the plots that for different system sizes finite-size effects appear at different times. In Fig. 4.6, we have shown the finite-size

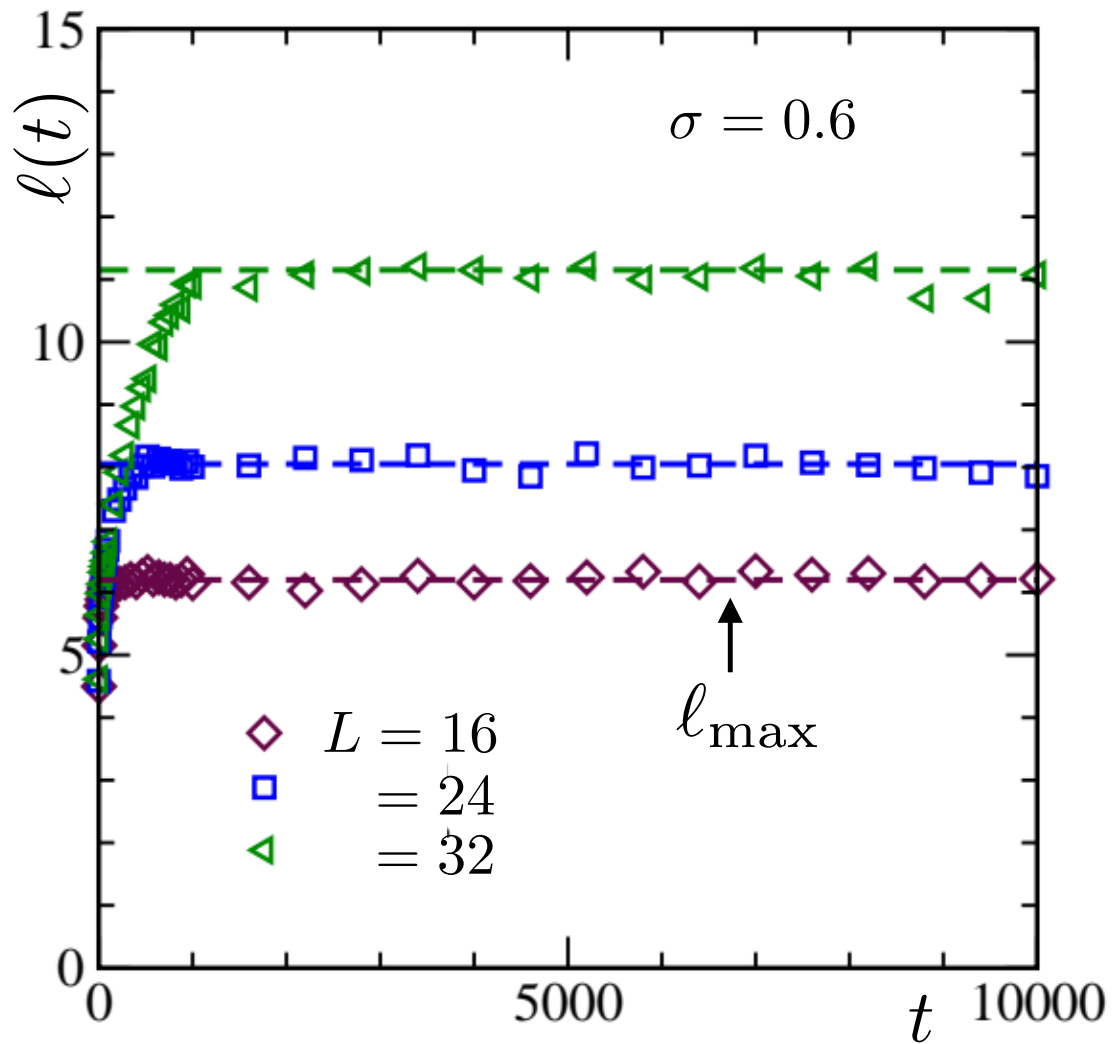


Figure 4.5: (a) Plots of $\ell(t)$, versus t , for $\sigma = 0.6$, from three different system sizes. The dashed horizontal lines are our estimates for ℓ_{\max} . See text for the definition of the latter.

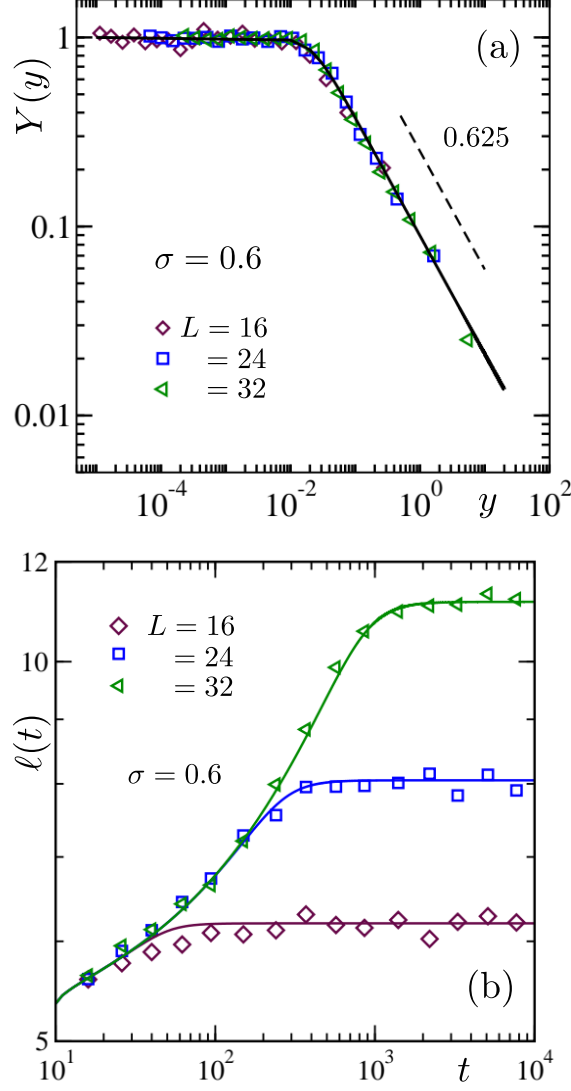


Figure 4.6: (a) Double-log plots of the finite-size scaling function, $Y(y)$, against the scaling variable y , for $\sigma = 0.6$. Data for a few different system sizes, viz., $L = 16, 24$, and 32 , are included. The dashed line represents Eq. (4.9) with $\alpha = 0.625$. The solid line is a fit of the simulation data to Eq. (4.11). See text for the best fit values of relevant parameters. (b) Eq. (4.12) (see the solid lines) is compared with direct growth data for $L = 16, 24$ and 32 . For the purpose of clear visualization, of comparison between simulation data and the analytical lines, we have thinned down the data sets in both parts (a) and (b).

scaling exercise, on a log-log scale, using the same set of system sizes. A very good collapse of data is achieved for the choices $\alpha \simeq 0.625$ and $\ell_0 = 5.35$. This value of α is the theoretically predicted exponent for the nonconserved dynamics with long-range interaction [26, 29], viz., $\alpha = 1/(1 + \sigma)!$ For large y , the collapsed data are consistent with Eq. (4.9), for $\alpha = 0.625$, an expectation for the validity of the FSS analysis.

For $\sigma = 0.6$, the observed value of α , from the FSS, should be compared with $\simeq 0.65$, the number that emerges from the extrapolation of early time trend in Fig. 4.4(a). The agreement is reasonably close. Here it should be noted that for the NNIM the linear behavior of α_i was shown to have a connection with α and ℓ_0 as [9, 10]

$$\alpha_i = \alpha \left[1 - \frac{\ell_0}{\ell} \right]. \quad (4.10)$$

By considering the FSS numbers, viz., $\alpha = 0.625$ and $\ell_0 = 5.35$, we obtain $-\alpha\ell_0$, the slope of α_i vs $1/\ell$ plot, to be $\simeq -3.34$. This is quite close to -3.42 , the measured slope from Fig. 4.4(a), deviating from each other by less than even 3%.

We have used an analytical form for the scaling function $Y(y)$, given in Ref. [43]:

$$Y(y) = Y_0 \left(b + \frac{y^\theta}{\alpha} \right)^{-\alpha/\theta}, \quad (4.11)$$

where Y_0 , b , and θ are positive constants. Here the value of θ should determine the finite-size universality class. While obtained for a somewhat different purpose, usefulness of this function for phase transitions in finite systems was recently demonstrated in Refs. [44, 45]. This function describes the scaled data in Fig. 4.6(a), with $\theta \simeq 2.6$, quite nicely, while $\alpha = 0.625$.

From Eq. (4.11), via a back transformation, one can write [45]

$$\ell(t) = \ell_0 + Y_0(\ell_{\max} - \ell_0) \left[b + \frac{(\ell_{\max} - \ell_0)^{\theta/\alpha}}{\alpha(t - t_0)^\theta} \right]^{-\alpha/\theta}. \quad (4.12)$$

The analytical form in Eq.(4.12) can be used to describe direct data for growth in finite systems of arbitrary sizes. This usefulness is demonstrated in Fig. 4.6(b).

Covering a wide range of σ , we intent to draw a complete picture, depicting two different growth regimes, before and after the crossover. For this purpose, we need bigger systems. In Fig. 4.7(a), for $\sigma = 0.6$, we have plotted ℓ' ($= \ell(t) - \ell_0$) as a function of t' , for relatively larger system sizes: $L = 128, 192$ and 256 . As expected,

on a log-log scale, we observe two distinct linear-looking regimes with a crossover, suggesting that the exponent changes from quite a high value to a lower one. In part (b) of this figure, we have presented similar plots, but here for $\sigma = 0.8$, and observed a similar crossover.

From these exercises, we conclude that for $\sigma < 1$ initially one observes very rapid growth, which crosses over, at late times, to $1/(2+\sigma)$. To check if structural scaling exists in both the regimes, in Fig. 4.8 we show data collapse for

$$C(r, t) = \langle S_i(t)S_j(t) \rangle - \langle S_i(t) \rangle \langle S_j(t) \rangle, \quad (4.13)$$

the two-point equal-time correlation function [2] for separation r between lattice sites i and j , when $\sigma = 0.6$. Part (a) is for early period and part (b) contains data from late times. Nice collapse can be appreciated throughout. Here it should be noted that the observed scaling of the form [2]

$$C(r, t) \equiv C(r/\ell(t)) \quad (4.14)$$

implies self-similar growth. Furthermore, the validity of the scaling confirms that the comparison of ℓ at different times is meaningful.

Next, we visit the finite-size scaling again, this time for $\sigma > 1$. Double-log plots of scaling function $Y(y)$, obtained by using different system sizes, are plotted in Fig. 4.9(a), against the scaling variable y , for $\sigma = 1.5$. An excellent collapse is realized when $\alpha = 0.32$, for small as well as large system sizes. The dashed line is a power-law with exponent -0.32 . This is consistent with the conclusion from the exercise in the inset of Fig. 4.4(b). The solid line in Fig. 4.9(a) represents a fit to the Eq. (4.11). Given that here we have used larger systems, it is, thus, clear that the domain growth exponent α remains constant throughout with a value $\alpha \simeq 1/3$ for $\sigma > 1$ [26]. Here also, in part (b), we demonstrate, how the direct data, for different system sizes, can be described by Eq. (4.12).

Recalling the objective of drawing a comprehensive picture, we return to $\sigma < 1$. Given the fact that as σ approaches unity, the crossover occurs earlier and at a smaller length scale, it becomes a necessity to restrict simulations with even smaller systems for a FSS. In that case, however, FSS will suffer from significant corrections to scaling. This can already be appreciated from Fig. 4.6(b). Clearly there exists a deviation between the analytical function [see Eq. (4.12)] and the simulation data for the smallest system size, whereas the agreement is nearly perfect for the

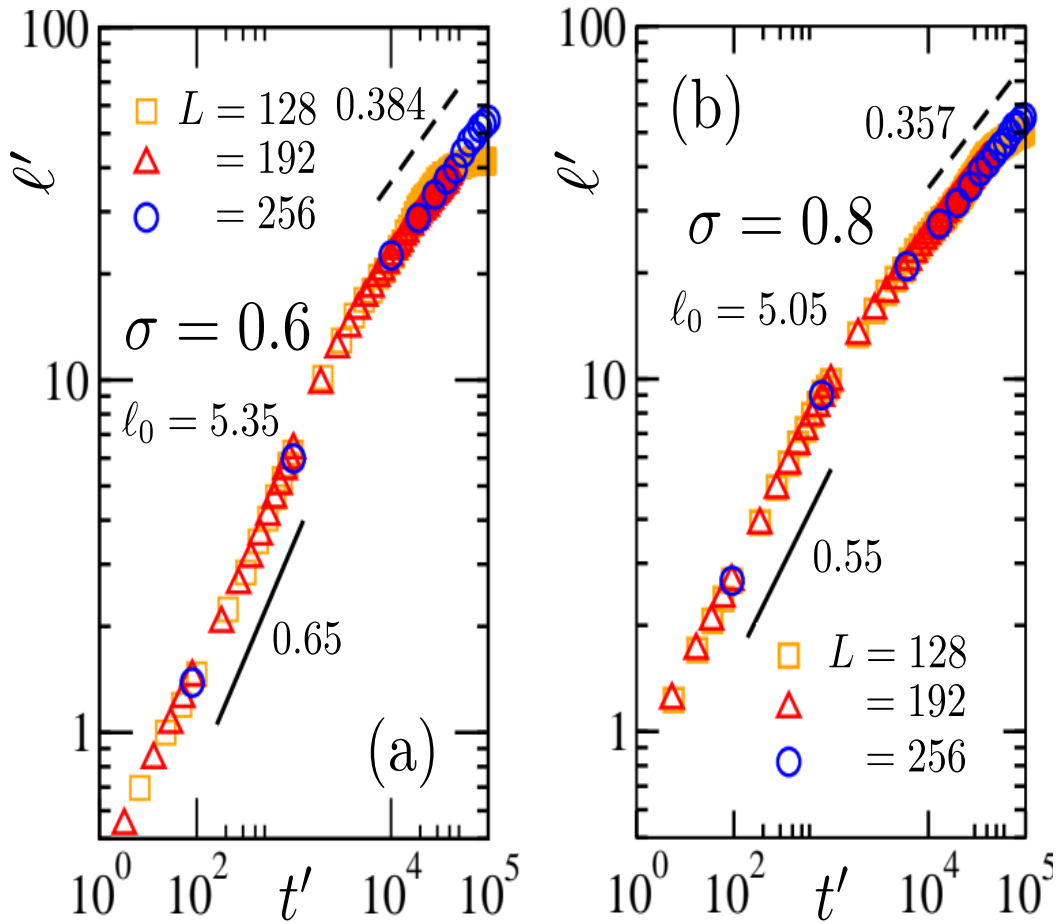


Figure 4.7: Plots of $\ell'(t)$ ($= \ell - \ell_0$), as a function of t' ($= t - t_0$), on a log-log scale, for (a) $\sigma = 0.6$ and (b) $\sigma = 0.8$. In each of the cases data from three different system sizes have been included. This is to show that the post-crossover bending is not due to finite-size effects. Solid lines are for the initial behavior of the growth and the dashed lines denote the later time, $\alpha = 1/(2 + \sigma)$, growth.

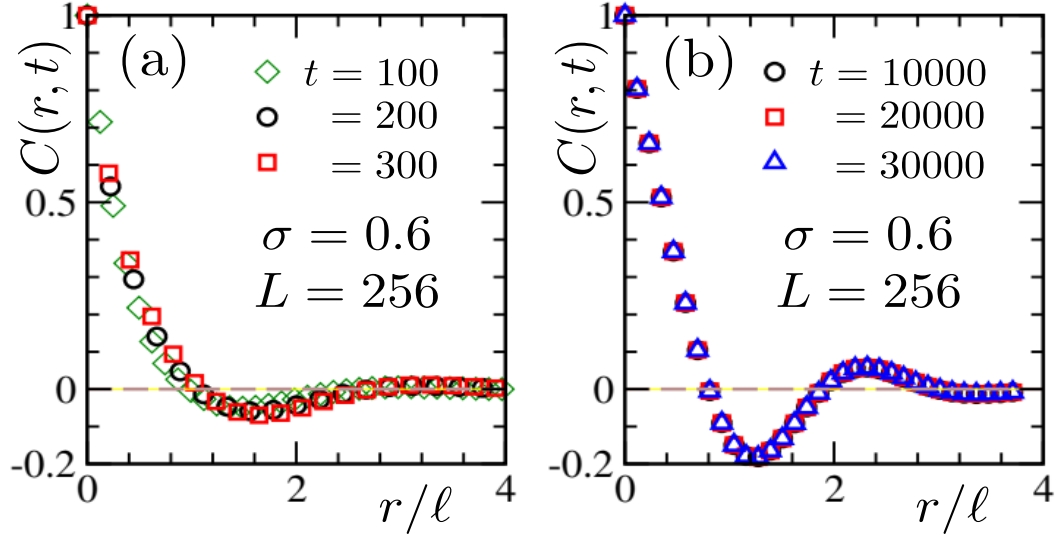


Figure 4.8: Scaling plot of $C(r, t)$, for $\sigma = 0.6$ and $L = 256$, using data from (a) early and (b) late times.

larger systems. In such a situation, appreciating the fact that the FSS and the instantaneous exponent approaches provide values of α that are close to each other, we stick to the estimates from the latter method.

In Fig. 4.10, we provide a detailed picture of growth covering both long and short-range regimes of σ . It appears, as $\sigma \rightarrow 1$, the early time exponent tends to merge with the late time values at $\alpha \simeq 1/3$. For σ reasonably small, interestingly, these values of α are quite consistent with the corresponding numbers for the nonconserved order-parameter dynamics.

4.4 Conclusion

Although the problem of domain coarsening in different model systems, following quenches to state points inside the coexistence curve, received much importance, studies with long-range interactions have been carried out relatively rarely. Nevertheless, there exist theoretical predictions [25, 26] for the latter variety, though only a handful of studies considered confirming these predictions via simulations [27–32].

In this work, we have carefully studied the domain coarsening in 2D long-range Ising model, via computer simulations. We have performed Monte Carlo simulations with the Kawasaki spin-exchange mechanism. Systems prepared at very high temperature were quenched to final temperatures $T = 0.6T_c$, for various different

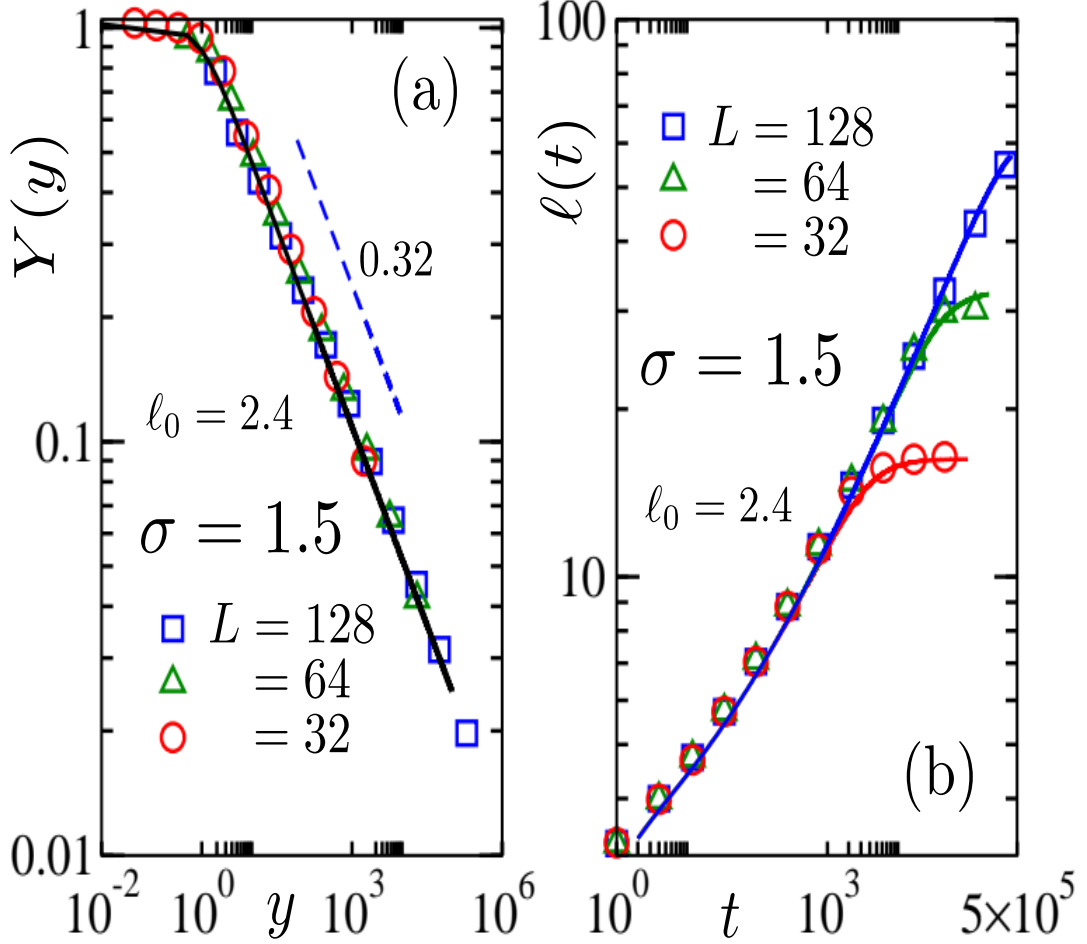


Figure 4.9: (a) Finite-size scaling exercise for $\sigma = 1.5$, using $\ell(t)$ data from different system sizes. The dashed line represents Eq. (4.9) with $\alpha = 0.32$ and the solid line is a fit of the simulation data to the analytical form in Eq. (4.11). (b) Same as Fig. 4.6(b) but here the demonstration is for $\sigma = 1.5$. The considered values of ℓ_{\max} for $L = 32, 64$ and 128 are $16, 32$ and 64 , respectively. Like in Fig. 4.6 here also we have thinned down the data sets, for visual clarity.

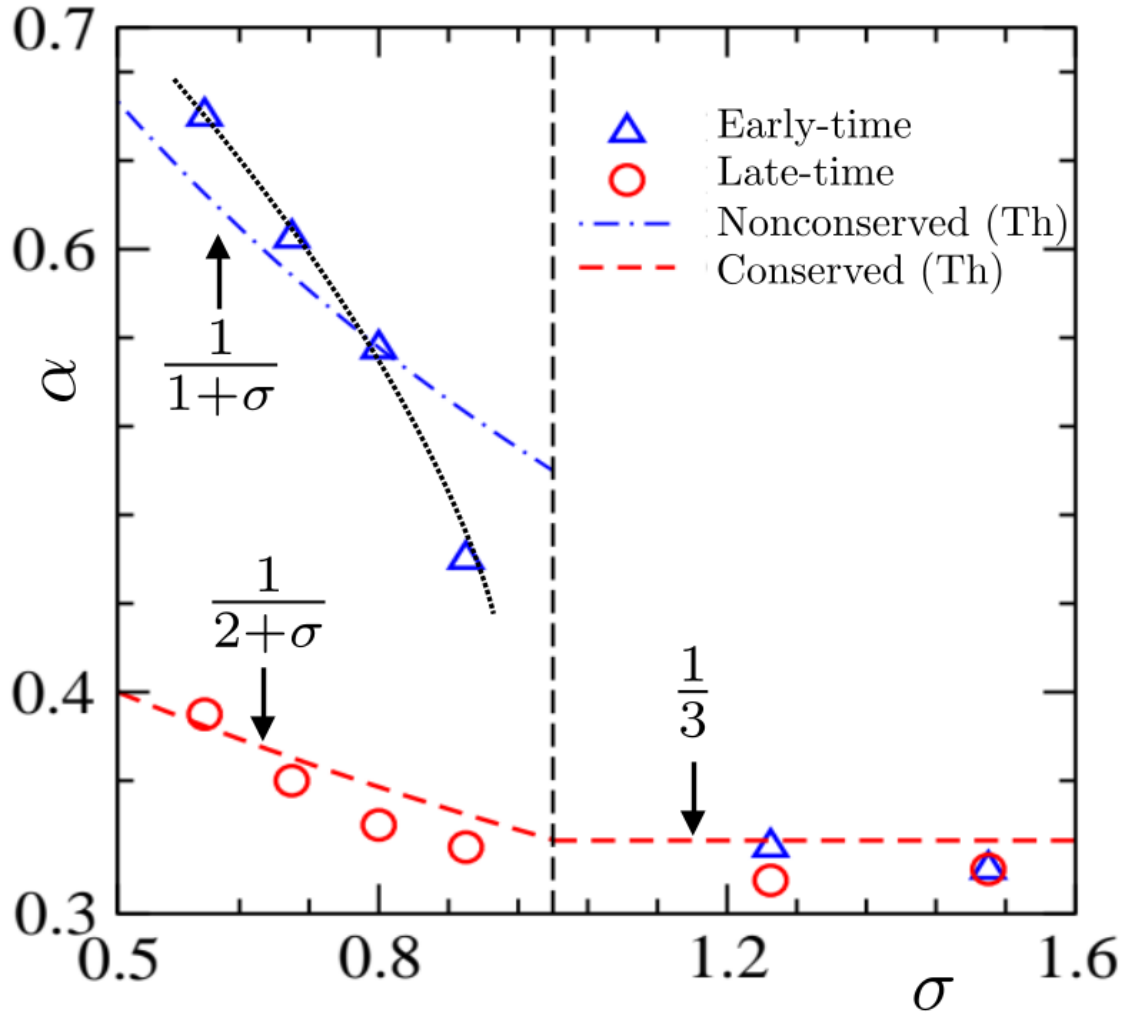


Figure 4.10: Both early-time and late-time values of the growth exponent α are plotted against σ . Simulation results are shown with symbols, whereas the relevant theoretical predictions (Th) are shown by dashed and dashed-dotted lines. The continuous line is a guide to the eye. The values of the late time exponents for $\sigma < 1$ are taken from Ref. [32]. For $\sigma > 1$, it was difficult to choose regions of data sets to estimate early and late time values of α . The overlapping numbers provide testimony to this fact.

values of σ , that dictate the range of interaction. From the analyses of the obtained simulation results, using finite-size scaling and other advanced techniques, we have come to the conclusion that for $\sigma < 1$, there exist two distinct regimes of growth. Initially, domains grow much faster with exponents being close to $1/(1 + \sigma)$, a prediction for nonconserved dynamics. Then, a “crossover” takes place, and α picks up the theoretically predicted value, $1/(2 + \sigma)$, for the conserved order parameter. The early time exponent, however, tends to $1/3$ as σ increases. For $\sigma > 1$, from reasonably early times, the growth exponent picks up the theoretical number [26] $1/3$, irrespective of the value of σ .

It may be recalled that we have removed the noise in the snapshots before calculating the average sizes of domains. Given that at early times the noise is relatively less, it may be a valid question to ask, whether the exceptionally fast growths at early times, for small values of σ , are due to the removal of the noise. Note that when the domains are small in size, this exercise may lead to artificial merger of these, leading to inappropriate conclusions. Keeping this in mind, we have analyzed the data for early periods without removing the noise as well. Our conclusions remain essentially unchanged. E.g., for $\sigma = 0.6$, we get pre-crossover exponent to be $\simeq 0.6$. On the other hand, if the noise is not removed, post-crossover exponent for this σ value appears much smaller than the expectation!

While the asymptotic growth exponents may remain same in $d = 3$ as well, as seen in the case of nearest neighbor Ising model, the early time behavior may have dimension dependence. However, this speculation requires verification.

The primary results from this chapter are now available in an article submitted to arXiv. The link is given below:

<https://doi.org/10.48550/arXiv.2410.13447>

Bibliography

- [1] M. E. Fisher, Rep. Prog. Phys. **30**, 615 (1967).
- [2] A. J. Bray, Adv. Phys. **51**, 481 (2002).
- [3] S. Puri, V. Wadhawan, and (ed.), *Kinetics of Phase Transitions* (Boca Raton: CRC Press, 2009).
- [4] A. Onuki, *Phase Transition Dynamics* (Cambridge University Press, 2002).
- [5] L. F. Cugliandolo, Comptes Rendus. Physique **16**(3), 257 (2015).
- [6] D. P. Landau and K. Binder, *A Guide to Monte Carlo Simulations in Statistical Physics* (Cambridge University Press, 2005).
- [7] I. Lifshitz and V. Slyozov, J. Phys. Chem. Solids **19**, 35 (1961).
- [8] D. A. Huse, Phys. Rev. B **34**, 7845 (1986).
- [9] J. G. Amar, F. E. Sullivan, and R. D. Mountain, Phys. Rev. B **37**, 196 (1988).
- [10] S. Majumder and S. K. Das, Phys. Rev. E **84**, 021110 (2011).
- [11] J. Midya and S. K. Das, Phys. Rev. Lett. **118**, 165701 (2017).
- [12] M. Laradji, S. Toxvaerd, and O. G. Mouritsen, Phys. Rev. Lett. **77**, 2253 (1996).
- [13] V. Testard, L. Berthier, and W. Kob, Phys. Rev. Lett. **106**, 125702 (2011).
- [14] A. K. S. Avinash Chauhan and A. Singh, Molecular Simulation **50**, 394 (2024).
- [15] S. Majumder, Phys. Rev. E **107**, 034130 (2023).
- [16] P. Mullick and P. Sen, Phys. Rev. E **95**, 052150 (2017).
- [17] F. Corberi, L. F. Cugliandolo, F. Insalata, and M. Picco, Phys. Rev. E **95**, 022101 (2017).

-
- [18] F. Perrot, P. Guenoun, T. Baumberger, D. Beysens, Y. Garrabos, and B. Le Neindre, Phys. Rev. Lett. **73**, 688 (1994).
 - [19] J. Van Lindt, A. Bratek-Skicki, P. N. Nguyen, D. Pakravan, L. F. Durán-Armenta, A. Tantos, R. Pancsa, L. Van Den Bosch, D. Maes, and P. Tompa, Commun. Biol. **4**, 77 (2021).
 - [20] E. Kiran and W. Zhuang, J. Supercrit. Fluids **7**, 1 (1994).
 - [21] A. E. Bailey and D. S. Cannell, Phys. Rev. Lett. **70**, 2110 (1993).
 - [22] H. Jiang, N. Dou, G. Fan, Z. Yang, and X. Zhang, J. Chem. Phys. **139**, 124903 (2013).
 - [23] T. Nose, in K. P. Ghiggino, ed., *Progress in Pacific Polymer Science 3* (Springer Berlin Heidelberg, 1994), pp. 1–11, ISBN 978-3-642-78759-1.
 - [24] S. K. Das and S. Puri, Phys. Rev. E **65**, 026141 (2002).
 - [25] A. J. Bray, Phys. Rev. B **41**, 6724 (1990).
 - [26] A. J. Bray, Phys. Rev. E **47**, 3191 (1993).
 - [27] H. Christiansen, S. Majumder, and W. Janke, Phys. Rev. E **99**, 011301 (2019).
 - [28] F. Corberi, E. Lippiello, and P. Politi, J. Stat. Phys. **176**, 510 (2019).
 - [29] H. Christiansen, S. Majumder, M. Henkel, and W. Janke, Phys. Rev. Lett. **125**, 180601 (2020).
 - [30] R. Agrawal, F. Corberi, F. Insalata, and S. Puri, Phys. Rev. E **105**, 034131 (2022).
 - [31] F. Müller, H. Christiansen, and W. Janke, Phys. Rev. Lett. **129**, 240601 (2022).
 - [32] S. Ghosh and S. K. Das, Phys. Rev. E **109**, L052102 (2024).
 - [33] M. E. Fisher, S. keng Ma, and B. G. Nickel, Phys. Rev. Lett. **29**, 917 (1972).
 - [34] J. Sak, Phys. Rev. B **8**, 281 (1973).
 - [35] R. C. Desai and R. Zwanzig, J. Stat. Phys. **19**, 1 (1978).

-
- [36] F. Staniscia, R. Bachelard, T. Dauxois, and G. D. Ninno, *Europhys. Lett.* **126**, 17001 (2019).
 - [37] T. Horita, H. Suwa, and S. Todo, *Phys. Rev. E* **95**, 012143 (2017).
 - [38] D. Frenkel and B. Smit, *Understanding Molecular Simulation* (Academic Press, 2002).
 - [39] D. W. Heermann, L. Yixue, and K. Binder, *Physica A: Statistical Mechanics and its Applications* **230**(1), 132 (1996).
 - [40] M. E. Fisher and M. N. Barber, *Phys. Rev. Lett.* **28**, 1516 (1972).
 - [41] N. Vadakkayil, S. Chakraborty, and S. K. Das, *J. Chem. Phys.* **150**(5), 054702 (2019).
 - [42] S. K. Das, S. Roy, S. Majumder, and S. Ahmad, *Europhys. Lett.* **97**(6), 66006 (2012).
 - [43] S. K. Das, *Proc. R. Soc. A* **477**, 20200689 (2021).
 - [44] S. K. Das, *Physica A: Statistical Mechanics and its Applications* **646**, 129871 (2024).
 - [45] T. Paul, N. Vadakkayil, and S. K. Das, *Phys. Rev. E* **109**, 064607 (2024).

Chapter 5

Mpemba Effect in WATER: A simulation study

5.1 Introduction

When cooled below its freezing temperature, liquid water goes through a phase transition and turns into solid *Ice*. Although many different crystalline structures of Ice have been found [1], hexagonal Ice (or Ih) is the most commonly observed structure. A phase diagram showing different forms of Ice at different temperatures and pressures is presented in Fig. 5.1. It shows experimental results, as well as results gathered from certain simulation studies.

In spite of the fact that often we encounter freezing of liquid Water or vapor into Ice, simulations of such fact is a difficult task. When bulk water is cooled down below the freezing point, instead of freezing immediately, it enters a ‘supercooled’ state that is less stable than the Ice. This metastable state may persist for a significantly long time, depending upon whether the nucleation is homogeneous or heterogeneous [2,3].

A hotter body of water freezes faster, than a colder one, when kept inside a refrigerator at a subzero temperature [4–7]. This counterintuitive fact is referred to as the Mpemba Effect (ME) [8] and is discussed since the time of Aristotle [9]. A demonstration of such anomalous behavior via computer simulations is nonexistent, though there are works by providing possible explanations if the effect really exists [10–12]. Such a status is perhaps due to the difficulty owing to the complex natures of Water molecules and related interactions that do not allow simulations of adequately large systems for long enough times. The long simulations are needed to counter, as mentioned above, the metastable features that may severely delay nucleation during

a transition from a fluid phase to Ice. An important question here is to ask: How the ME may be connected to the metastability – Should the longevity of the latter be a function of the initial temperature? Or, growth, following the nucleation, is the only contributor to the initial temperature dependence of the transformation? Questions have also been raised if the ME is a result of differences in times for reaching the final temperature from different starting temperatures [13, 14]. Interestingly, to the best of our knowledge, there exists no simulations reporting either the presence of the ME in any simple model or addressing all the above mentioned questions. The aim of this chapter is to demonstrate ME in a model water.

5.2 Model and Methods

We have chosen a reasonably realistic model of water [15]: **TIP4P/Ice**. From Fig. 5.1, we can appreciate the fact that the phase diagram generated for this model is very close to that we get from experiments. Especially, at low pressures, the agreement is very good. We have marked this region by a circle. As we have performed all our simulations near ($\simeq 4.5$ atm) ambient pressure, TIP4P/Ice model suits us perfectly. This is a four-point rigid water model with transferable intermolecular potential. There, in addition to the points related to the positions of one oxygen (O) atom and two hydrogen (H) atoms, an additional (negative) charge point M exists. This point, having a charge 1.1794, in the electronic unit, is placed at a fixed distance (0.1577\AA) from O along the bisector of the H-O-H angle, having experimentally measured value 104.52° [15]. Fixed O-H bond of distance 0.9572\AA and a constant H-O-H angle of 104.52° are constrained by implementing SHAKE algorithm [16]. The O atoms interact with each other via the LJ potential of the form [15, 17]

$$U = 4\epsilon \left[\left(\frac{\sigma}{r} \right)^{12} - \left(\frac{\sigma}{r} \right)^6 \right], \quad (5.1)$$

where ϵ is the interaction strength, σ is the particle diameter, r is the centre-to-centre distance between two particles. For this model, $\epsilon = 0.21084$ kcal/mole and $\sigma = 3.1668\text{\AA}$. A related schematic diagram is shown in Fig. 5.2. Each H-atom carries a positive charge of magnitude 0.5897. All charged points, expectedly, interact via the Coulombic potential [15]

$$E = \frac{Cq_1q_2}{\epsilon_k r}, \quad (5.2)$$

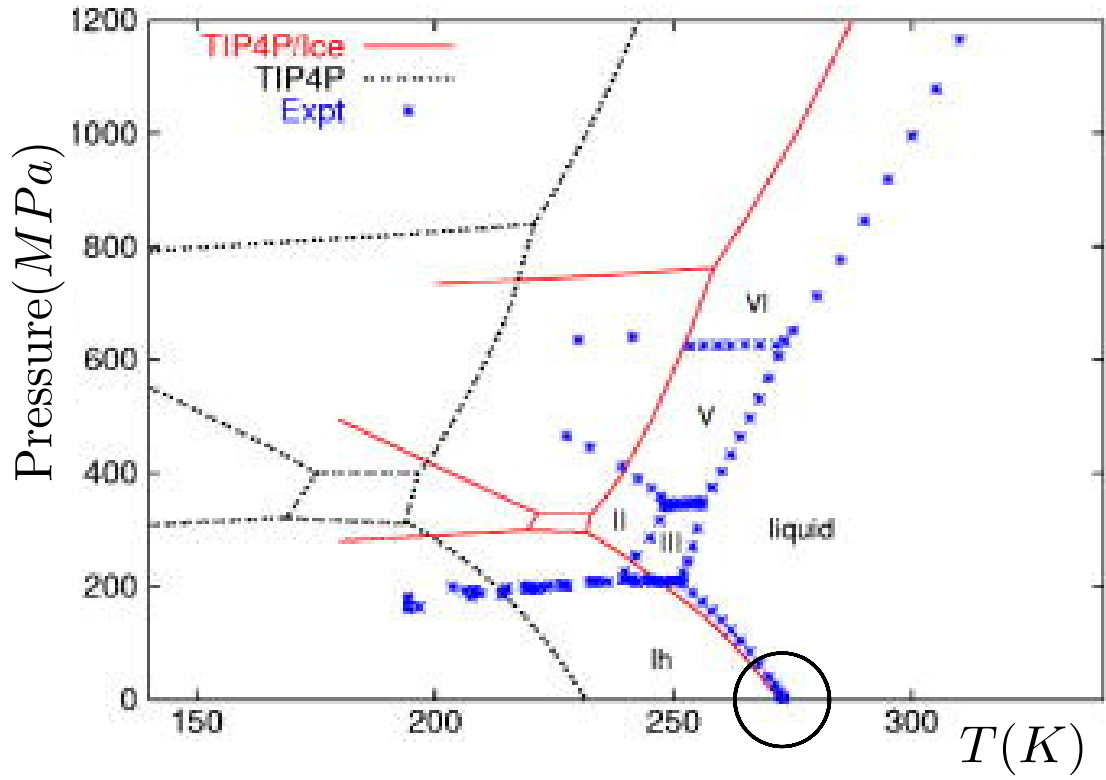


Figure 5.1: Comparisons of phase behavior [15], obtained from simulations of two different models of water, viz., TIP4P and TIP4P/Ice, as well as from experiments. The circle is to highlight the convergence of the phase diagrams obtained via simulations of TIP4P/Ice model and that from experiments.

where, q_1 and q_2 are the two charge values, C is a constant and ϵ_k is the permittivity constant. The masses of O and H atoms are set to be 15.9994 amu and 1.008 amu, respectively [15].

With this model, we carry out NPT MD simulations with 96 molecules [18–20], using LAMMPS [21], having Nosé-Hoover thermo- [22, 23] and barostats [24]. The timestep for all our simulations were kept fixed to 1-femtosecond.

We first equilibrate our systems at various different temperatures, T_s , above the freezing temperature which is $272.2K$, for the chosen model system. Then we pick up configurations from the equilibrated trajectories and quench them to a fixed final temperature $T_f = 230K$. A further intermediate protocol is described in the results section.

Here we have used particle-particle particle-mesh or the PPPM method, to handle the long range potential, instead of the Ewald summation. This is embedded in the LAMMPS simulation program. For details, see section 1.4.3.

5.3 Results

To start with, we have placed 96 water molecules in our simulation box, with centers arranged on a simple cubic lattice, as depicted in Fig. 5.3, to avoid any unnecessary overlap. From here, we equilibrate the system at various different starting temperatures (T_s). For all T_s values, we keep the pressure same. For a particular value of the starting temperature, $T_s = 400$, energy profile after equilibration is shown in Fig. 5.4(a). In part (b) of the same figures, we have shown a snapshot picked up from the trajectory in (a).

The equilibrated system is then quenched instantaneously to $T_f = 230K$. We have carried out the MD simulation, following this, for 500ns. The potential energy (PE) of the evolving system, for $T_s = 400K$, is shown in Fig. 5.5. In part (a), we have used a log scale for time to capture the initial decay in energy. Note that this behavior becomes invisible when plotted using a linear scale. At a very late time, we can see a jump in PE. For a better picture of this, in part (b) we have plotted the same quantity on a linear scale. Here, a jump in the PE is very clear. As we look at the structure, we find that there is an ordering in the system that creeps in after the jump and persists till the end of our simulation. Fig. 5.5(c) shows a snapshot of the system from the ordered time regime. From preliminary investigations, based on visual comparison of the structures, we conclude that following a quench, water finally turns into ice but the nucleation process is delayed due to the appearance of

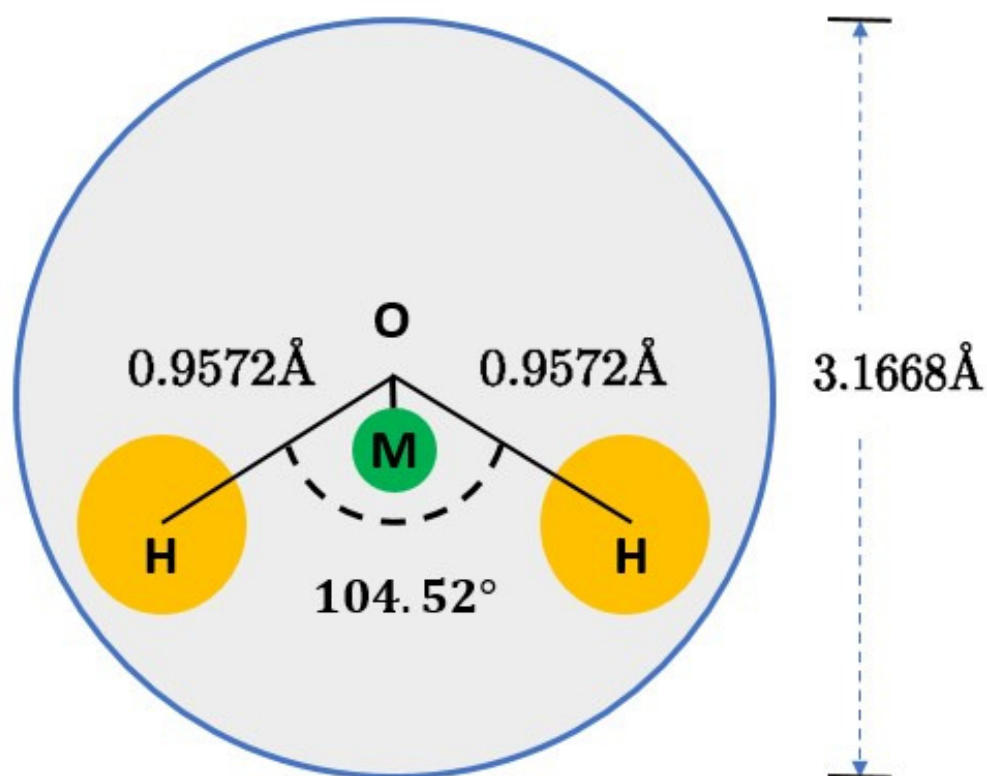


Figure 5.2: A schematic diagram of the TIP4P/Ice model of water. See text for the description.

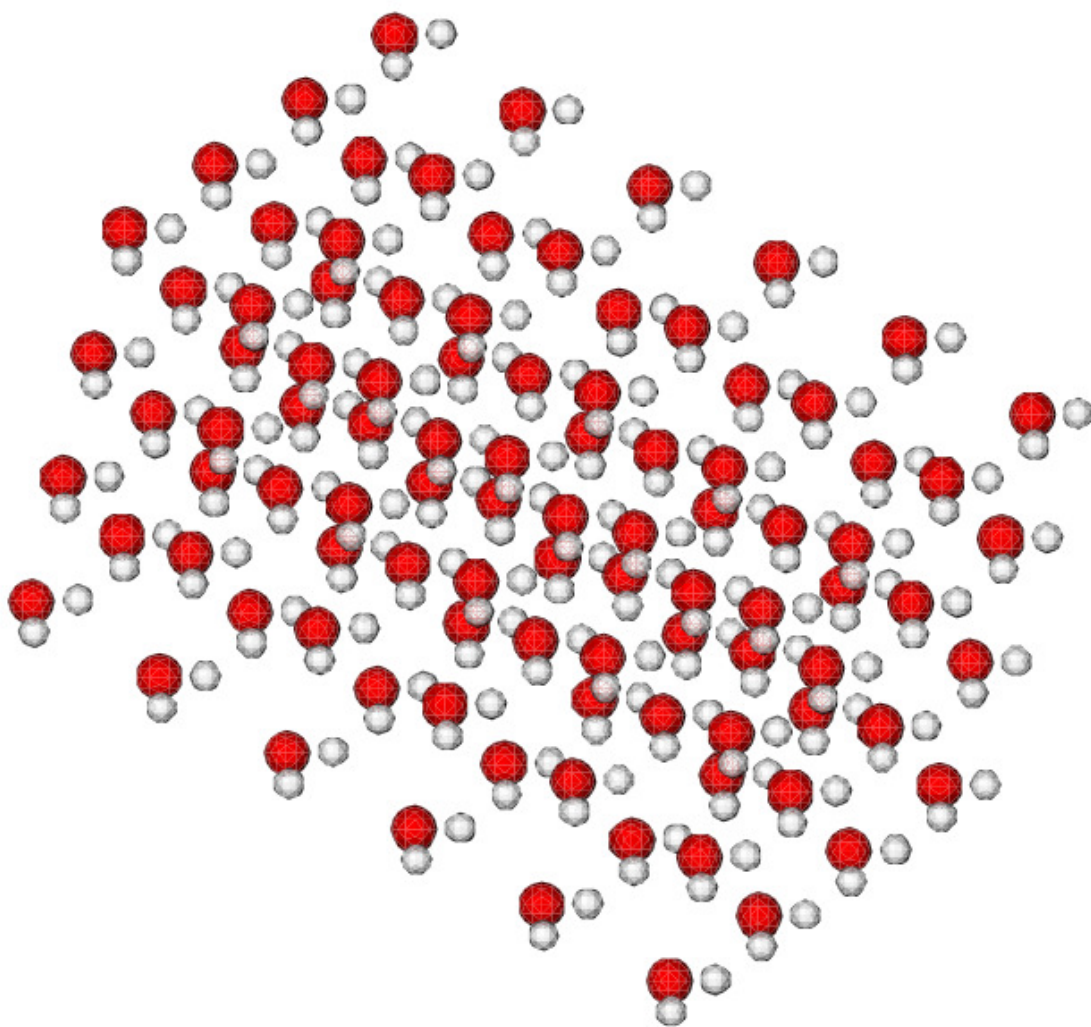


Figure 5.3: Water molecules are arranged on a simple cubic lattice. The bond lengths and orientations within a molecule were taken from GitHub [25], to provide inputs to the LAMMPS [21] simulations. Oxygen atoms are shown in red and Hydrogens in grey.

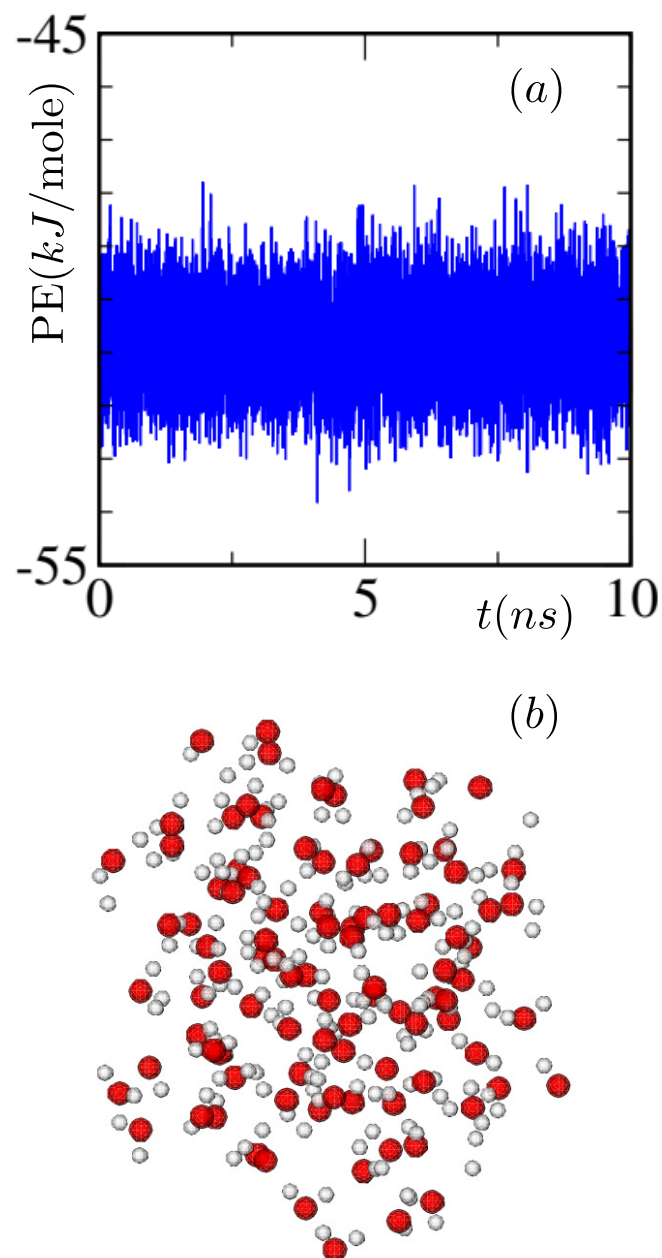


Figure 5.4: (a) Potential energy (PE), per molecule, is plotted for an equilibrium system at 400K . (b) A typical configuration is shown from the equilibrium regime shown in (a).

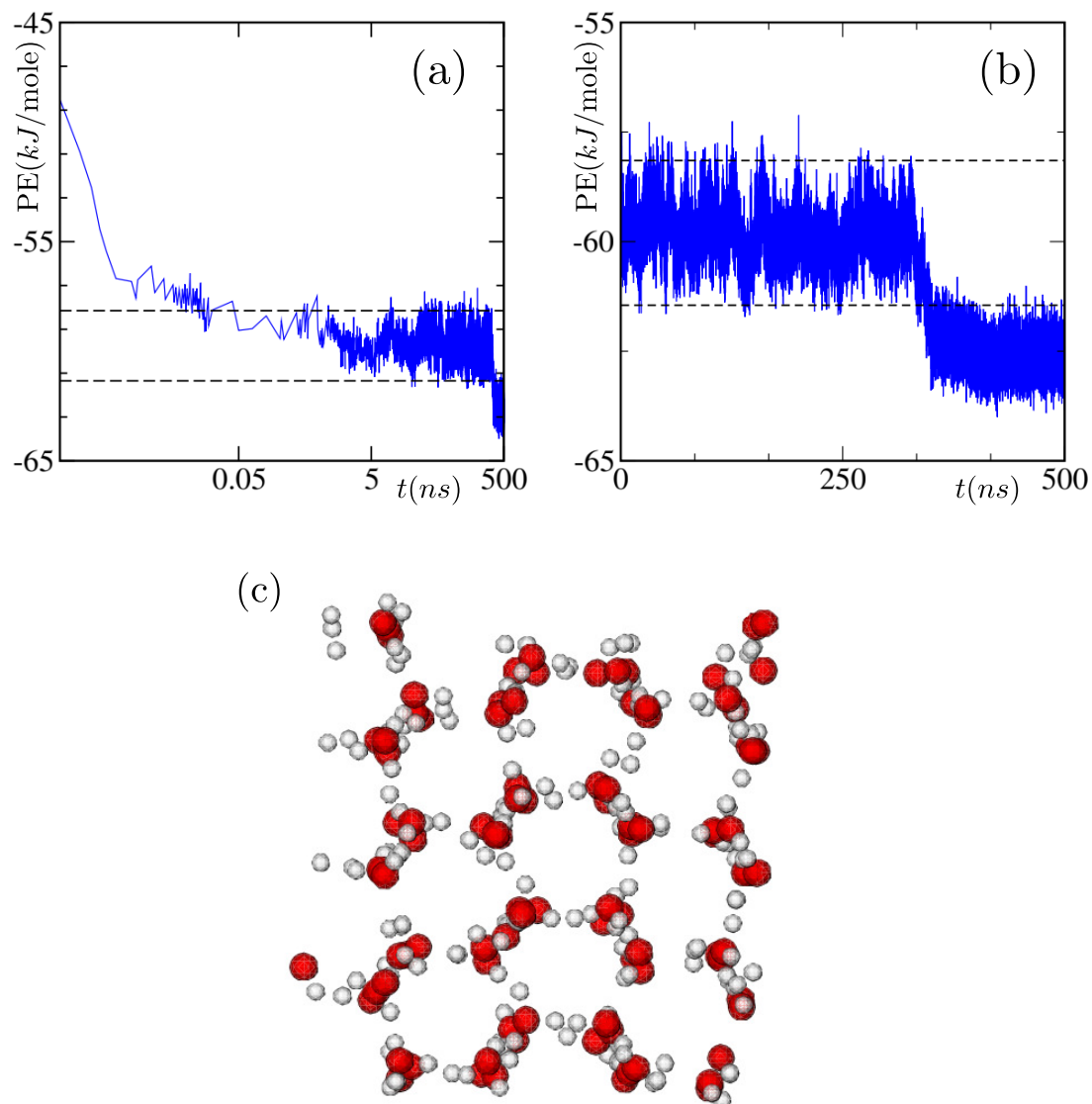


Figure 5.5: Potential energy corresponding to a simulation run, with initial configuration prepared at $400K$, is shown following a quench to $230K$. Log scale for time is used in (a) to capture the fast decay in energy at small time limit. In (b), the time scale is kept linear so that the jump in the potential energy can be clearly seen. (c) A snapshot taken from the Ice regime is shown. Red dots denote the positions of the O atoms, whereas, H atoms are shown in gray. The arrangement of the atoms suggest a hexagonal Ice structure.

a metastable state that persists for a reasonably long time.

We have performed the same exercise for many different T_s . It should be noted that like other simulation studies of water, only a small fraction of the runs lead to freezing. In Fig. 5.6, we have shown the temperature of the system as a function of time, t , for $T_s = 400K$. Clearly, the value of T_f is reached within a small fraction of a nanosecond.

To distinguish Ice structure from supercooled metastable water, we use a local bond order calculation method [26,27]. In the method that we have followed [28,29], structure in the system is identified by computing the coherence of the orientational order of an atom with that of its neighbors. For this purpose, we calculate a quantity \vec{q}_{lm} , for all atoms, connected to the spherical harmonics, $Y_{lm}(\theta, \phi)$, as

$$\vec{q}_{lm}(I) = \frac{1}{nnn(i)} \sum_{j=1}^{nnn(i)} Y_{lm}(\theta(\vec{r}_{ij}), \phi(\vec{r}_{ij})). \quad (5.3)$$

Here, $nnn(i)$ is the number of neighbors inside a cut-off radius of 3.2\AA , whereas, θ and ϕ are the azimuthal and polar angles, respectively, created by the bond \vec{r}_{ij} with the lab frame. Next, a $2l + 1$ component vector $\vec{q}_l \equiv [\vec{q}_{l,-l}, \vec{q}_{l,-l+1}, \dots, \vec{q}_{l,l}]$ is defined for each atom i . A quantity q_l is, then, calculated as [28]

$$q_l(i) = \frac{1}{nnn(i)} \sum_{j=1}^{nnn(i)} \frac{\vec{q}_l(i) \cdot \vec{q}_l^*(j)}{|\vec{q}_l(i)| |\vec{q}_l(j)|}. \quad (5.4)$$

The choice $l = 6$ is standard for distinguishing Ice from Water. In Fig. 5.7, the blue curve shows the probability distribution of q_6 after the jump in energy seen in Fig. 5.5(b). The same distribution is shown in red for a period before the jump, i.e., for supercooled water. The distribution plots not only prove the fact that the energy jump corresponds to the freezing of metastable liquid Water into Ice, but also provide information on the structure of the ice crystal. From the presence of a sharp peak around ~ 0.75 , the hexagonal structure of the Ice phase can be confirmed [28].

Our objective in this chapter is to study the role of initial temperature on freezing. For that purpose, we have prepared samples at various different starting temperatures T_s , ranging from $275K$ to $550K$, covering vapor as well as liquid phases of water. Systems from these T_s are then quenched to the above mentioned final temperature $T_f = 230K$. For each T_s , many simulation runs, up to 500ns, starting

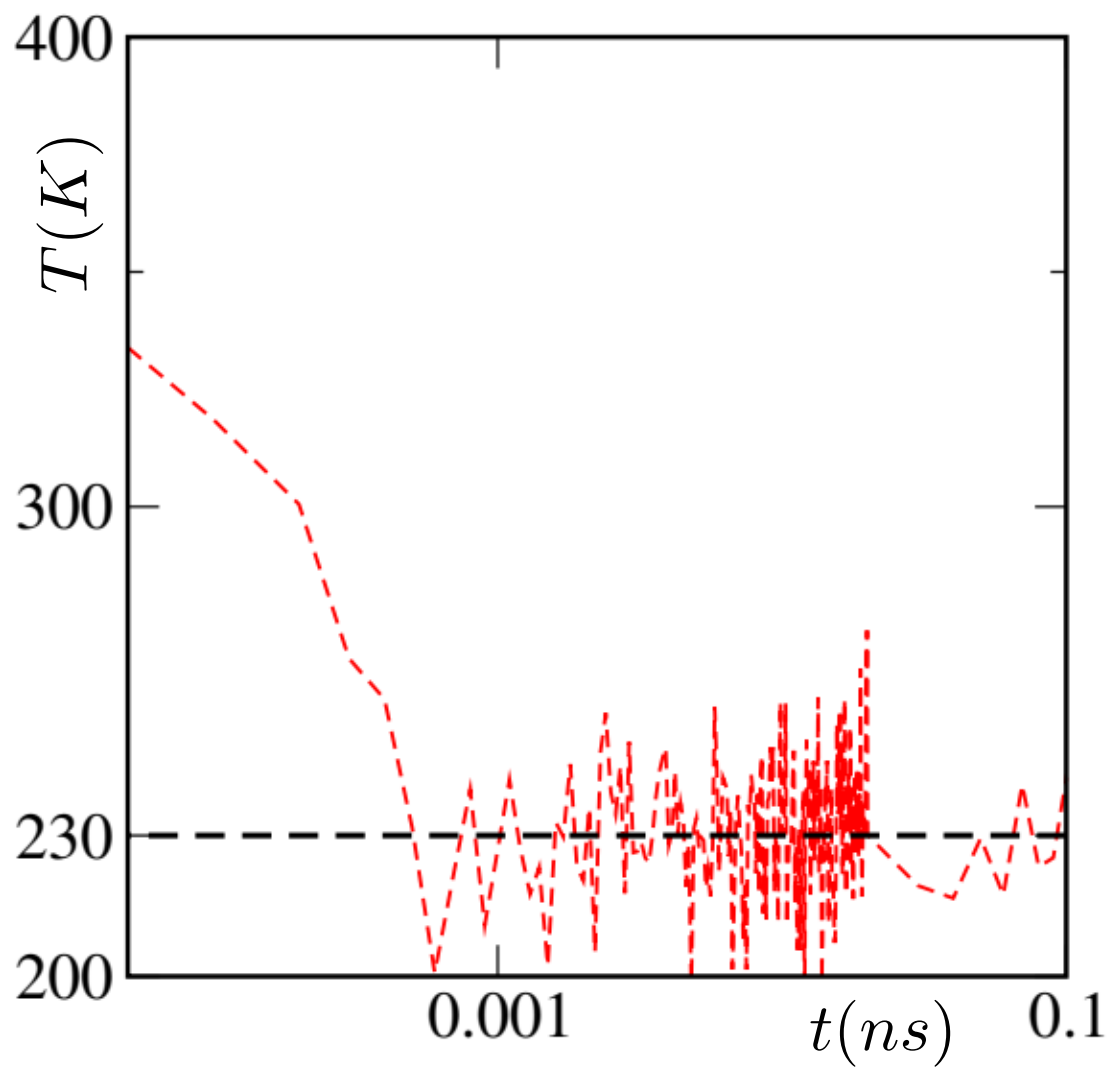


Figure 5.6: The temperature, T , of the system is plotted versus time, t , for the simulation in Fig. 5.5.

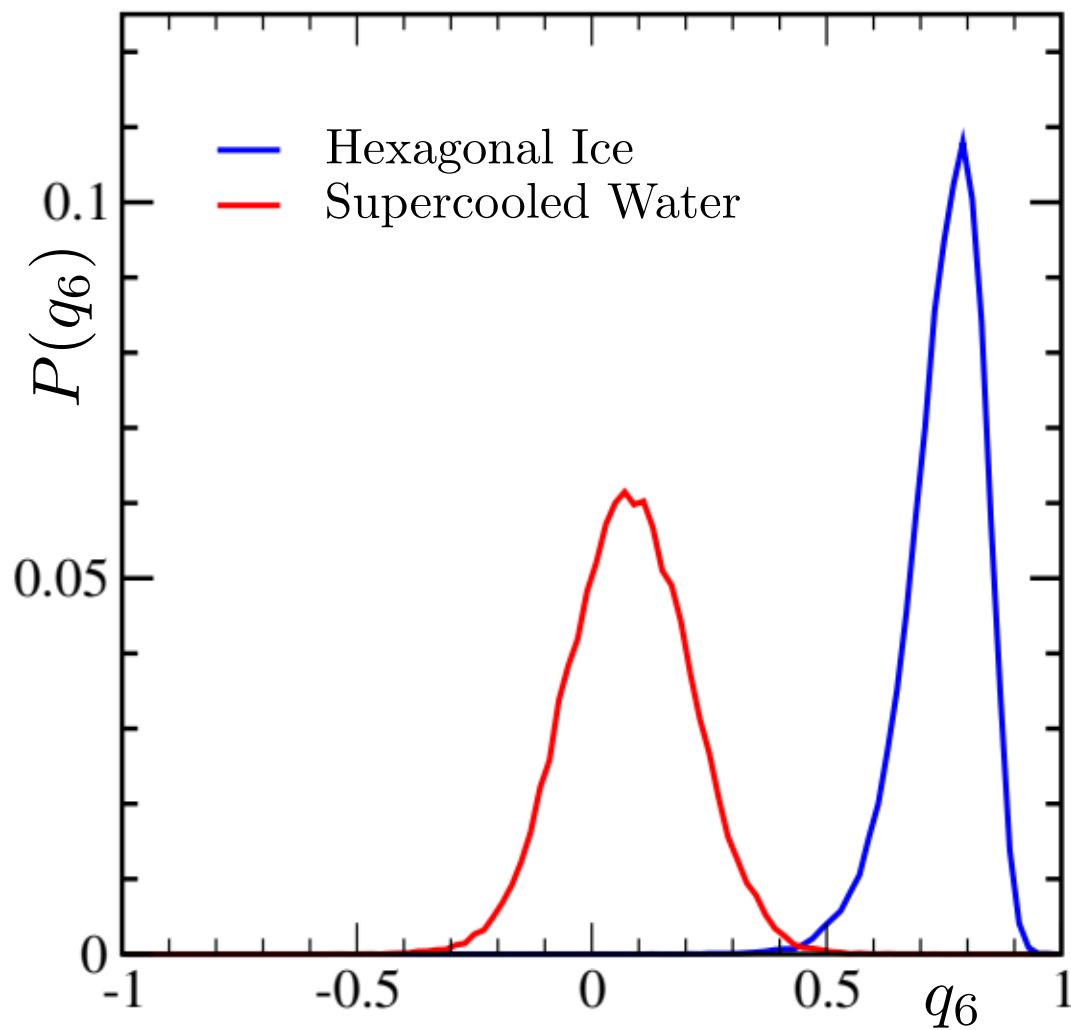


Figure 5.7: The probability distribution $P(q_6)$ of the sixth order local bond order q_6 is plotted. The blue curve corresponds to the periods after the energy jump seen in Fig. 5.5 (a) and (b). The location of the peak indicates a hexagonal Ice crystal. The red line is the same quantity but this is for supercooled/metastable water.

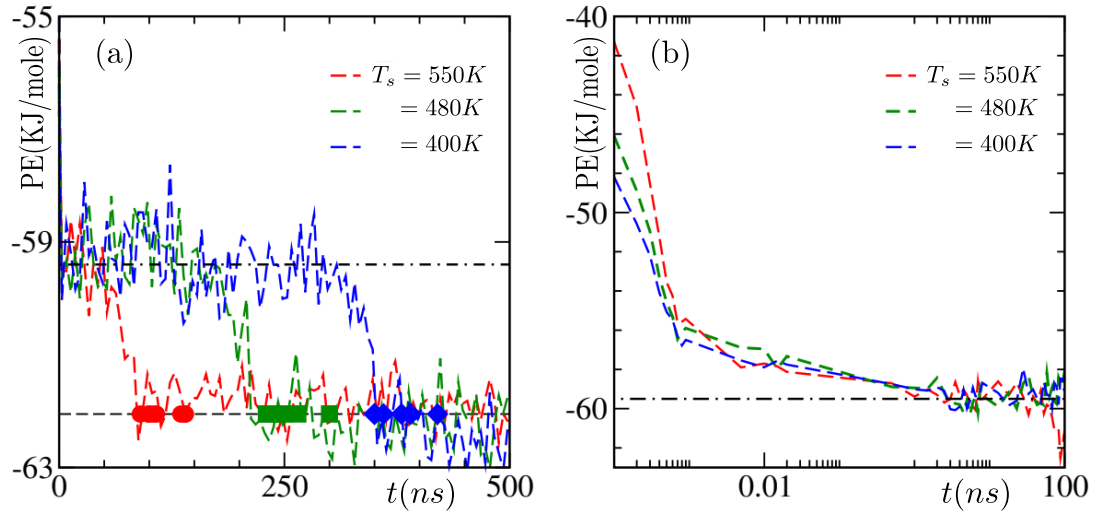


Figure 5.8: (a) Potential energy is plotted as a function of time for the TIP4P/Ice simulations. Results are shown for quenches to $T_f = 230\text{K}$, from a few starting temperatures, T_s . Data in each of the sets are thinned down for the sake of clarity. The symbols show the locations of jumps for simulation runs with certain other starting configurations. A unique color is used for a given T_s . The early parts of the energy decay are shown again in (b) by using a log scale for the abscissa. The horizontal lines stand for approximately the average values for intermediate metastable liquid and final Ice phase energies.

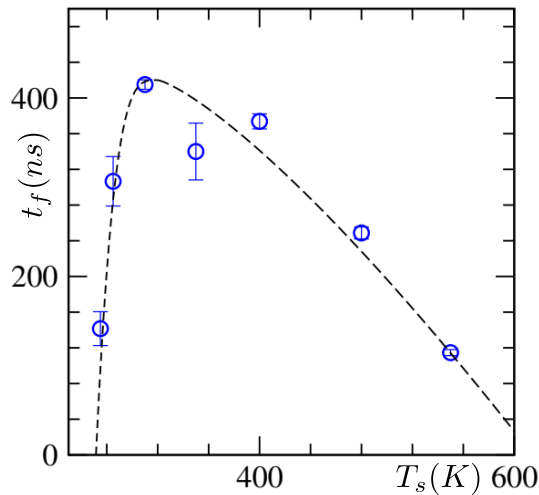


Figure 5.9: The freezing time, t_f , averaged over 8 runs for each T_s , is plotted as a function of T_s . The dashed line is a guide to the eye.

from independent equilibrated configurations, were performed. In Fig. 5.8 (a), potential energy (PE) plots, against time, are shown for three different runs starting from three different initial temperatures, viz. $T_s = 400K, 480K$ and $550K$. These are runs that gave rise to the fastest freezing for each of these temperatures. The symbols denote the freezing times noted for other different trajectories. Generally, faster freezing for a higher T_s can be appreciated. In part (b) of the figure, log-scale is used for the time axis, only to show initial fast decay of energy at early times. Interestingly, here also we have found somewhat faster decay in energy for higher T_s .

We have presented our key results on t_f , average freezing time, in Fig. 5.9. Here we have plotted t_f as a function of the starting temperature T_s . This plot strongly points toward the presence of the ME and nicely resembles the non-monotonic behavior, where the dashed line is a guide to the eye, seen in the original work [8]. The nonmonotonicity reflects that when a starting point is very close to the final one, another system from a very far away state cannot overtake the relaxation or evolution of the former.

5.4 Conclusion

In this chapter, we have studied fluid-to-solid transitions in a model water system via molecular dynamics (MD) simulations, with the objective of investigating the presence of the Mpemba effect. Systems with 96 water molecules were first equilibrated at different initial temperatures T_s , above the melting temperature, ranging between $275K$ and $550K$. These were quenched to $T_f = 230K$, for which the dynamics were probed. We have found that following the quenches, systems enter a metastable state. The metastable state can persist for a very long time, depending upon the value of T_s , leading to the ME. Considering the fact that the temperature settles down to the desired value very early, when compared to the freezing times, the phenomenon of heat transport or cooling rate is very unlikely to have any role to play in the exhibition of the effect.

For water, ME is related to the jump from metastable intermediates to the Ice phase. Thus, to understand the origin of the effect, we need to carefully investigate various different properties of the metastable states. Of course, the longevity at an intermediate level is decided by the property at the corresponding initial state. Very systematic studies are necessary to probe and understand such a dependence

via considerations of molecular orientation, hydrogen bonding, etc. In natural situations, the system size can be thermodynamically large for which the contribution from growth can be significant. For big systems, there will be a large number of nucleation sites. It will be interesting to undertake studies by combining the distribution of nuclei in space and of their occurrences in time with the growth process.

In future we would also like to take up studies by varying the final temperature T_f . For such a variation the nucleation barrier should change, giving rise to quantitative differences. This will provide a better understanding of an interplay of dynamics with metastability.

Our study is by considering a fairly small size of system. Thus, we do not claim to have probed the true kinetics of transformation from a fluid to the ice phase. Our conclusion can be treated as an outcome for dependence of delay of nucleation with the variation of initial temperature. In future we will consider much bigger systems to see if we can pick up similar dependence in kinetics.

Our study is related to ice nucleation in homogeneous condition. Observation of ice formation, from liquid water, under such homogeneous condition was also reported previously [30]. In some other studies [31] ice formation was studied by introducing nuclei above a critical size. We did not take that avenue. Furthermore, our observation suggests that Mpemba effect can be observed without impurities. Impurities, however, can alter the quantitative outcomes.

The primary results from this chapter are now available in an article submitted to arXiv. The link is given below:

<https://doi.org/10.48550/arXiv.2407.06954>

Bibliography

- [1] T. C. Hansen, Nature Comm. **12**(2041-1723), 3161 (2021).
- [2] M. V. Moore, E., Nature **479**, 506 (2011).
- [3] A. J. Bermúdez di Lorenzo, M. A. Carignano, and R. G. Pereyra, Chemical Physics Letters **635**, 45 (2015).
- [4] J. Bechhoefer, A. Kumar, and R. Chétrite, Nat. Rev. Phys. **3**, 534 (2021).
- [5] A. Kumar and J. Bechhoefer, Nature **584**, 64 (2020).
- [6] S. K. Das, Langmuir **39**, 10715 (2023).
- [7] M. Jeng, Am. J. Phys. **74**, 514 (2006).
- [8] E. B. Mpemba and D. G. Osborne, Physics Education **4**, 172 (1969).
- [9] Aristotle, *Meteorologica* (Harvard University Press, 1962).
- [10] J. Jin and W. A. I. Goddard, J. Phys. Chem. C **119**(5), 2622 (2015).
- [11] X. Z. et al., Phys. Chem. Chem. Phys. **16**(22995) (2014).
- [12] A. Gijón, A. Lasanta, and E. R. Hernández, Phys. Rev. E **100**, 032103 (2019).
- [13] M. Vynnycky and S. Kimura, Int. J. Heat Mass Transf. **80**, 243 (2015).
- [14] D. Auerbach, Am. J. Phys. **63**(882) (1995).
- [15] J. L. F. Abascal, E. Sanz, R. García Fernández, and C. Vega, The Journal of Chemical Physics **122**(23), 234511 (2005).
- [16] J.-P. Ryckaert, G. Ciccotti, and H. J. Berendsen, Journal of Computational Physics **23**(3), 327 (1977).

-
- [17] M. P. Allen and D. J. Tildesley, *Computer Simulation of Liquids* (Oxford University Press, 1991).
- [18] M. Chen, H.-Y. Ko, R. C. Remsing, M. F. C. Andrade, B. Santra, Z. Sun, A. Selloni, R. Car, M. L. Klein, J. P. Perdew, *et al.*, Proc. Natl. Acad. Sci. **114**(41), 10846 (2017).
- [19] P. M. Piaggi and R. Car, J. Chem. Phys. **152**(20), 204116 (2020).
- [20] V. Buch, P. Sandler, and J. Sadlej, J. Phys. Chem. B **102**(1520-6106), 44 (1998).
- [21] A. P. Thompson, H. M. Aktulga, R. Berger, D. S. Bolintineanu, W. M. Brown, P. S. Crozier, P. J. in 't Veld, A. Kohlmeyer, S. G. Moore, T. D. Nguyen, *et al.*, Comp. Phys. Comm. **271**, 108171 (2022).
- [22] D. Frenkel and B. Smit, *Understanding Molecular Simulation* (Academic Press, 2002).
- [23] S. Nose, J. Phys. Condens. Matter **2**, SA115 (1990).
- [24] G. J. Martyna, D. J. Tobias, and M. L. Klein, J. Chem. Phys. **101**(5), 4177 (1994).
- [25] <https://github.com/simongravelle/lammps-input-files>.
- [26] P. Rein ten Wolde, M. J. Ruiz-Montero, and D. Frenkel, The Journal of Chemical Physics **104**(24), 9932 (1996).
- [27] P. J. Steinhardt, D. R. Nelson, and M. Ronchetti, Phys. Rev. Lett. **47**, 1297 (1981).
- [28] T. Li, D. Donadio, G. Russo, and G. Galli, Phys. Chem. Chem. Phys. **13**, 19807 (2011).
- [29] E. B. Moore, E. de la Llave, K. Welke, D. A. Scherlis, and V. Molinero, Phys. Chem. Chem. Phys. **12**, 4124 (2010).
- [30] M. Matsumoto, S. Saito, and I. Ohmine, Nature **416**, 409 (2002).
- [31] J. R. Espinosa, E. Sanz, C. Valeriani, and C. Vega, J. Chem. Phys. **141**, 18C529 (2014).

Chapter 6

Initial Temperature Dependence of Ordering in Long-range Ising Model

6.1 Introduction

In the previous chapter, we have discussed the Mpemba Effect (ME) [1], i.e., faster freezing of a hotter body of fluid water, than a colder one, when quenched below the freezing temperature. In recent times, in efforts to generalize the effect, several other experimental systems and theoretical models were shown to exhibit Mpemba-like effect. Examples include cooling granular gases [2, 3], clathrate hydrates [4], anti-ferromagnets [5] and spin glasses [6], as well as, even more surprisingly, pure ferromagnetic systems [7–9]. For ferromagnets, when quenched to a final fixed temperature, T_f , systems initially at a higher temperature, T_s , reaches equilibrium faster compared to a colder one.

The difference in the initial temperature, T_s , should give rise to differences in structural properties in the system [9]. Indeed, the correlation length of the system depends on the temperature T_s . In the context of critical phenomenon [10, 11] it is well known that

$$\xi \sim |T_s - T_c|^{-\nu}. \quad (6.1)$$

Recently it has been shown [9] that the strength of the effect exhibits scaling with respect to ξ . Such studies are with short-range interaction. In this chapter, we aim to identify the ME in the nonconserved Ising model with long-range interactions. Because of technical difficulties, in this case, it is difficult to confirm such a scaling.

Thus, the primary objective in this chapter is to identify the effect. In addition, we will present some more results concerning rather general interest.

6.2 Model and Methods

The model used for this study is similar to the one we have used in some of the previous chapters. Here, unlike those chapters, we will study non-conserved order parameter dynamics. We will briefly discuss the model for the sake of completeness. We deal with a 2D square lattice of length L and lattice spacing of 1. Spins that can take either up or down state sit on lattice points and interact with the Hamiltonian [12, 13]

$$H = -\frac{1}{2} \sum_i \sum_{j \neq i} J(r) S_i S_j; \quad J(r) = \frac{1}{r^{d+\sigma}}, \quad (6.2)$$

$J(r)$ being interaction strength that depends upon the inter-spin separation r .

First, we equilibrate the systems at various different starting temperatures, T_s . In the vicinity of the critical temperature T_c , relaxation time increases rapidly, resulting in the equilibration process being highly time consuming. To overcome difficulty due to this, we have used the Fukui-Todo Monte Carlo (MC) Cluster algorithm [14], where instead of flipping one spin at a time, multiple clusters of like spins are flipped at once.

Initial configurations prepared at T_s ($> T_c$), with nearly 50 : 50 compositions of up and down spins, including the ones with randomly placed up and down spins, mimicking infinite temperature scenario, are quenched to a fixed final temperature $T_f = 0.3T_c$, inside the ordered regime. For quenches to T_f , we perform MC simulations using the Glauber spin-flip dynamics [15, 16], leading to a non-conserved order-parameter dynamics.

In MC simulations with Glauber dynamics [15], a spin is randomly selected and flipped, which is called a trial move. Then the change in energy is calculated and the trial move is accepted or rejected depending on a probability, discussed in detail in the Introductory chapter. In this way, total order parameter of the system changes as the system evolves with time. We have chosen a few different values of σ . For the study of ME, however, we confine ourselves to $\sigma = 0.8$ only. For this choice of σ , $T_c \simeq 9.765$ [17]. As mentioned earlier, we have performed our MC simulations on a 2D $L \times L$ system with $L = 1024$. Unless otherwise mentioned, we will present results that are averaged over 100 independent initial configurations. Note that, time is measured in units of MC steps (MCS), one MCS being equivalent to L^2 trial

moves. We have parallelized our in-house codes with OpenACC [18] and carried out our simulations for the kinetic part on GPUs (Tesla V100).

6.3 Results

We start discussing the results by showing the growing length-scale in Fig. 6.1 following a quench to $T_f = 0.3T_c$ from a random initial configuration. In order to study the morphology of the domains, two-point equal-time correlation function is calculated as [19]

$$C(r, t) = \langle \psi(\vec{r}, t) \psi(\vec{0}, t) \rangle - \langle \psi(\vec{r}, t) \rangle \langle \psi(\vec{0}, t) \rangle, \quad (6.3)$$

where ψ (equivalent to a spin) is a time and space-dependent order-parameter. In Fig. 6.2 (a), we have shown plots of $C(r, t)$ as a function of distance r , for three different times. If the growing patterns are self-similar, which is true for most of the cases, $C(r, t)$ should satisfy a scaling form [19]

$$C(r, t) \equiv \tilde{C}(r/\ell(t)), \quad (6.4)$$

$\ell(t)$ being the domain length at time t . In part (b) of Fig. 6.2, we have plotted $C(r, t)$, for the same set of t , but now against r/ℓ . Overall, the collapse of the data from different times looks good, but at larger r , there exists some deviation from the scaling. In Fig. 6.3, we have plotted domain lengths as a function of time for two different σ values, viz., $\sigma = 0.6$ and 0.8 . The solid lines are power-laws with exponents $1/(1 + \sigma)$, theoretically predicted values of the growth exponent for non-conserved order-parameter dynamics [12, 20].

Next, we have compared the behavior of the simulation obtained correlation function for different σ with the analytical function obtained by Ohta, Jasnow, and Kawasaki [21] (OJK) for nonconserved order-parameter dynamics. This function is known to describe the situation in the nearest neighbor Ising case rather well. A general expression for the OJK function can be written as [22]

$$C_{OJK}(r, t, t_w) = \frac{2}{\pi} \sin^{-1} \left(\frac{2\sqrt{tt_w}}{t + t_w} \right)^{d/2} \exp \left[\frac{-r^2}{4D(t + t_w)} \right], \quad (6.5)$$

D being a diffusion constant. For equal-time cases, i.e., $t = t_w$, relevant for us, Eq.

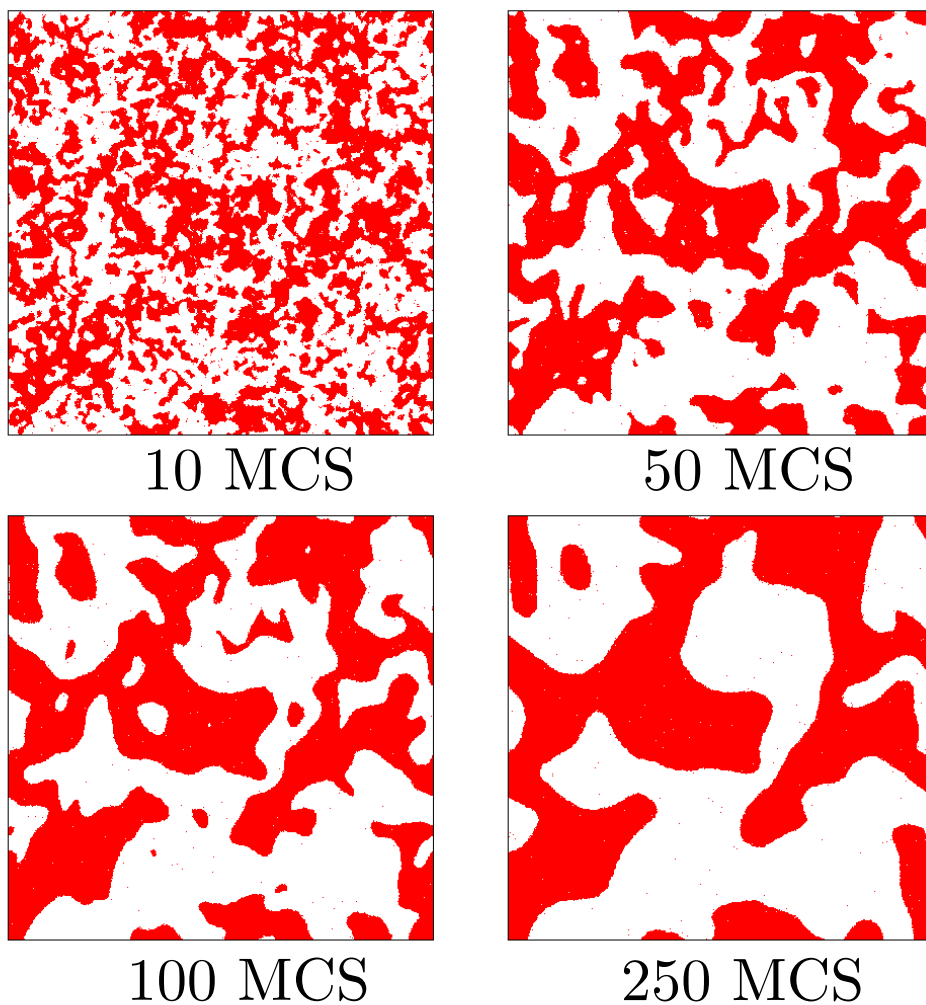


Figure 6.1: Snapshots of an evolving system, with $\sigma = 0.8$, taken at different times when quenched from a very high temperature to a final temperature $T_f = 0.3T_c$. Positions of the $+1$ spins are marked with red, while -1 spins are left unmarked.

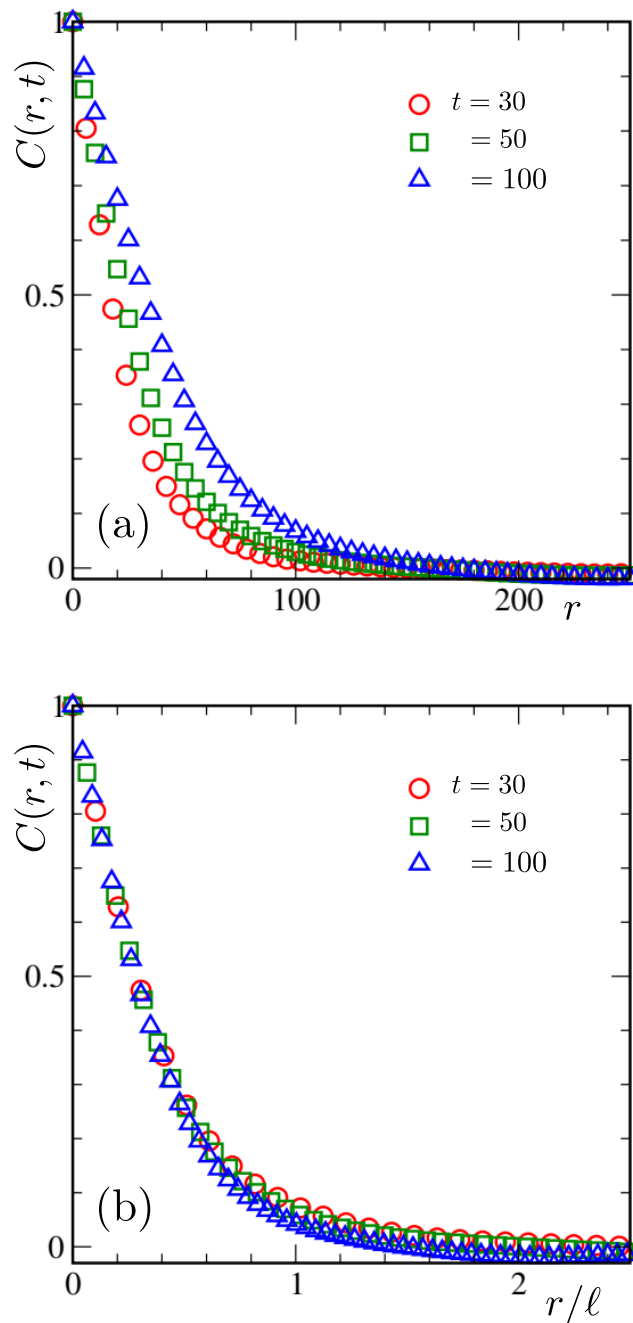


Figure 6.2: (a) Correlation function, $C(r, t)$, from three different times are plotted, versus distance, r , for $\sigma = 0.8$ and $L = 1024$. In (b), r is scaled by the domain length, ℓ , at corresponding times.

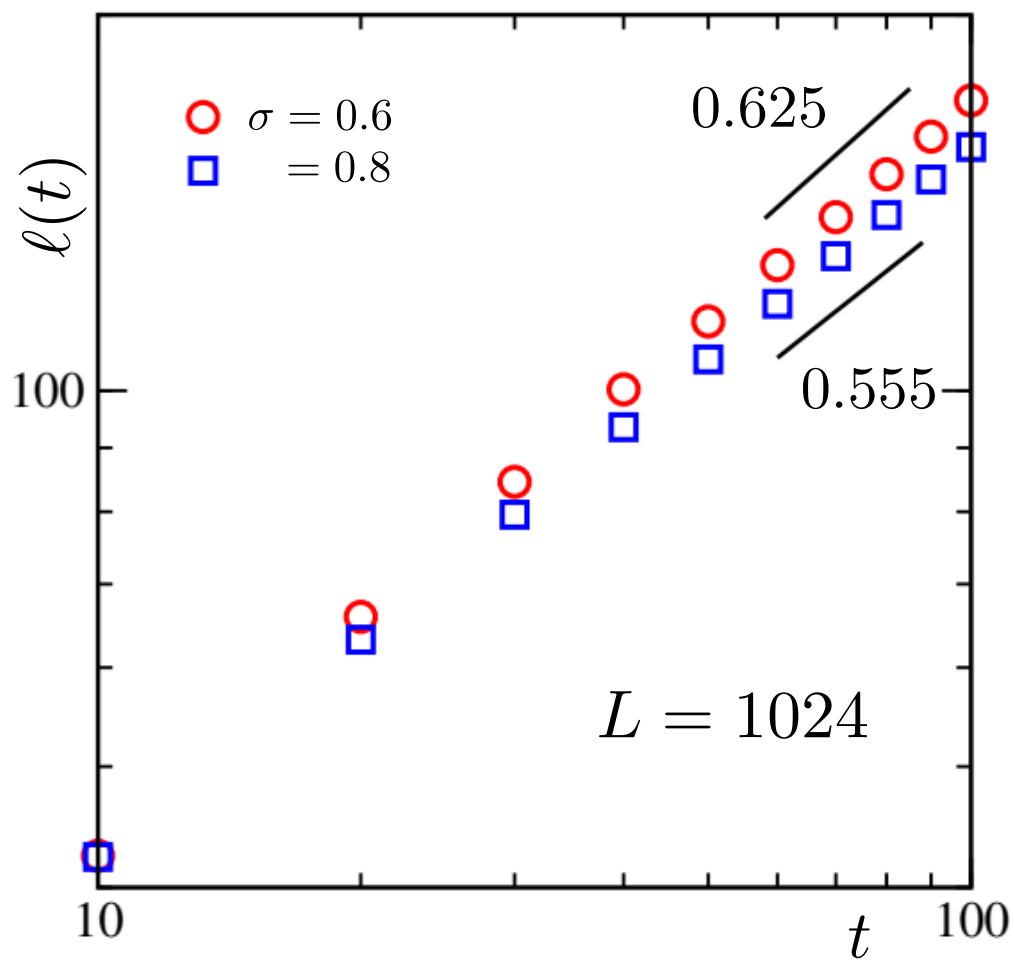


Figure 6.3: Average domain lengths, $\ell(t)$, in log-log scale, for $\sigma = 0.6$ and 0.8 , are plotted versus time, t . The ordinate of the data for $\sigma = 0.8$ is shifted artificially for better visualization of the difference in growth. These results have similarities with those in Ref. [12].

(6.5) reduces to

$$C_{OJK}(r, t) = \frac{2}{\pi} \sin^{-1} \left[\exp \left(\frac{-r^2}{8Dt} \right) \right]. \quad (6.6)$$

In Fig. 6.4, we have shown simulation plots of $C(r, t)$, as a function of distance r , with symbols, for $\sigma = 0.6$, and 0.8 , as well as for the nearest neighbor (NN) Ising model. We have tried to match the OJK function, with each of them, by varying t . The solid lines, shown in the same plot, are the best agreements that we have obtained. The fitting of the function is excellent for the NN case, whereas for the other two considered cases, the fitting is not as good. Another interesting fact that comes out is that for a smaller σ , we find a poorer agreement. This overall picture needs to be tested for longer times. This will, however, require much larger systems. Note that the growth for long-range interactions being very fast [20, 23], finite-size effects appear very soon. On the other hand, simulations of these systems require better resources than the nearest-neighbor case.

Our main objective in this chapter is to find the effect of the initial temperatures, T_s , on the dynamics, if there exists any, when all are quenched to a fixed final temperature, T_f . Fig. 6.5 shows a (fixed) fraction of systems at two different temperatures, one at $T_s = 1.2T_c$ and another one with randomly placed up and down spins, imitating $T_s = \infty$. The positions of the up spins (+1) are marked by red and blue dots in Fig. 6.5(a) and (b), respectively. The difference in the structure is clear from the snapshots. Next, in Fig. 6.6, we have plotted structure factors, $S(k, t)$, of systems, as a function of wave number k , at different starting temperatures, T_s , viz., $1.2T_c$, $2.0T_c$, and ∞ . The enhancement of critical fluctuation with the lowering in temperature is clear.

We have carried out instantaneous quenches, to a final temperature $T_f = 0.3T_c$, with such configurations. In Fig. 6.7, we have presented domain lengths following the quench from different initial temperatures. These lengths are estimated by calculating the distance between two consecutive domain boundaries while scanning the systems along different coordinate axes. The lower panel of the plot shows the domain lengths from an early time regime, where lower T_s corresponds to bigger domains. The upper panel of the same plot shows the late-time behavior. Here we can see a reverse trend. The average domain size for the one with the highest T_s is largest at late times, and it systematically decreases with a reduction in T_s . This fact implies crossings among the curves at some points in time. These results indicate that systems starting at higher initial temperatures relax faster than the colder ones.

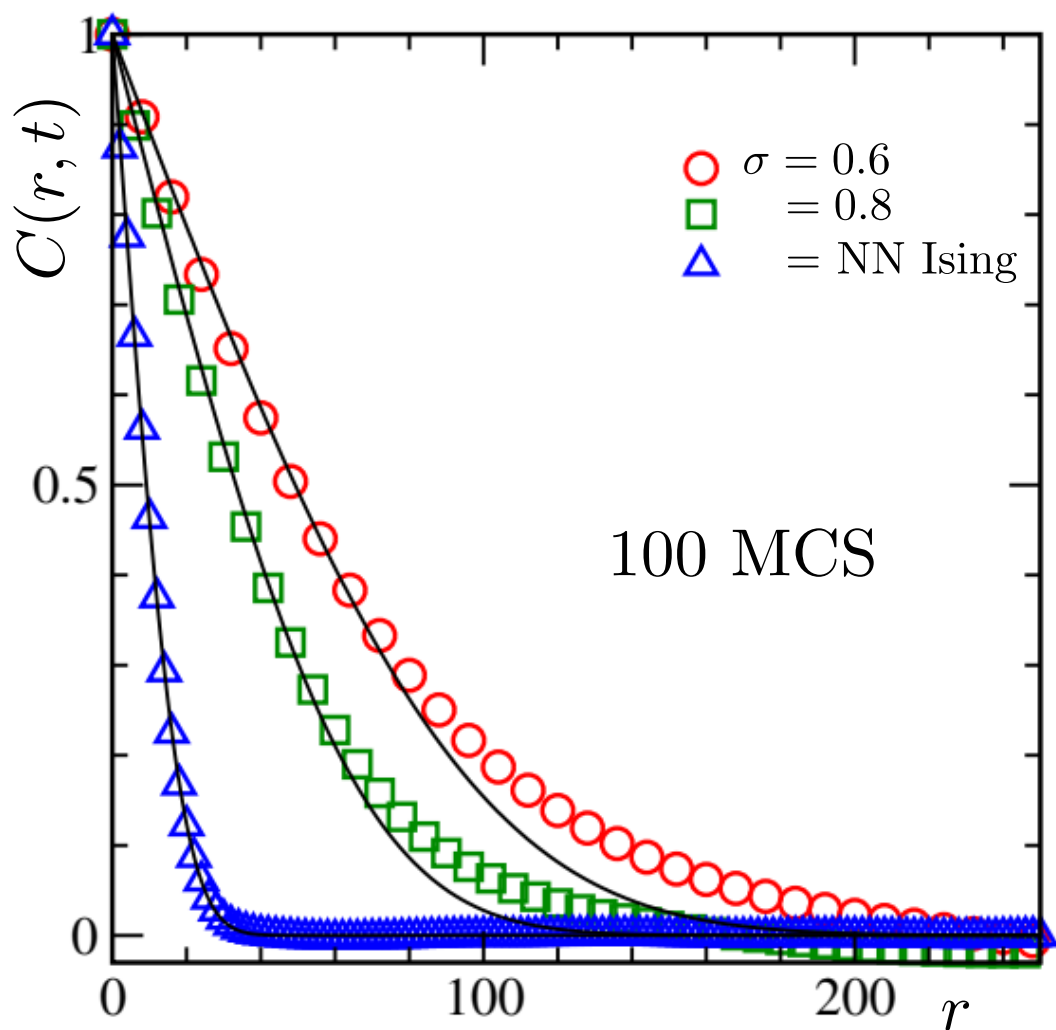


Figure 6.4: The correlation function, $C(r, t)$, is plotted versus distance r for systems with two different σ values, viz., $\sigma = 0.6$ and 0.8 , as well as a nearest neighbor (NN) Ising model. The solid lines represent Ohta-Jasnow-Kawasaki function.

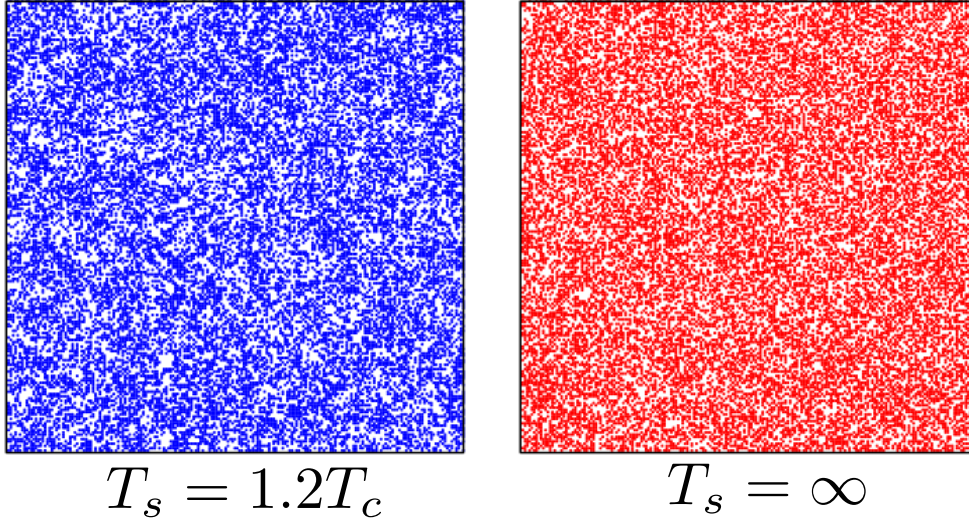


Figure 6.5: Equilibrium snapshots, prepared at two different starting temperatures, viz., $1.2T_c$ and ∞ , are shown. These results are for $\sigma = 0.8$.

A necessary condition for comparing the domain sizes is the existence of similarity in structures of the evolving domains [19] for systems starting from different initial temperatures at any given point in time. In this case, around the crossing times, at the least. The similarity in structure can be captured via the scaling property [19] of the two-point equal time correlation function:

$$C(r, T_s) \equiv C(r/\ell), \quad t \text{ fixed.} \quad (6.7)$$

In Fig. 6.8, we have plotted the two-point correlation function, $C(r, t)$, as a function distance r , scaled by the domain length ℓ . In part (a), we have plotted the simulation data from 50 MCS, for the same set of T_s values used in Fig. 6.7. At this time, no domain length plots have crossed each other and can be identified as a pre-crossover regime. On the other hand, in part (b), we have plotted the same quantity but from time $t = 240\text{MCS}$. At this point in time, all possible crossings have already happened. So, we can call it a post-crossover regime. The interesting outcome of this exercise is that the scaling of data from different T_s is excellent at both pre- and post-crossover regimes, signifying a similar structure of the domains.

We looked at another important quantity, the total energy of the system. While evolving to reach the same equilibrium state, a system with lower energy, true for lower T_s , is considered to be closer to the final state. In Fig. 6.9, we have plotted the total energy for systems with the same T_s as in Fig. 6.7, as a function of time t .

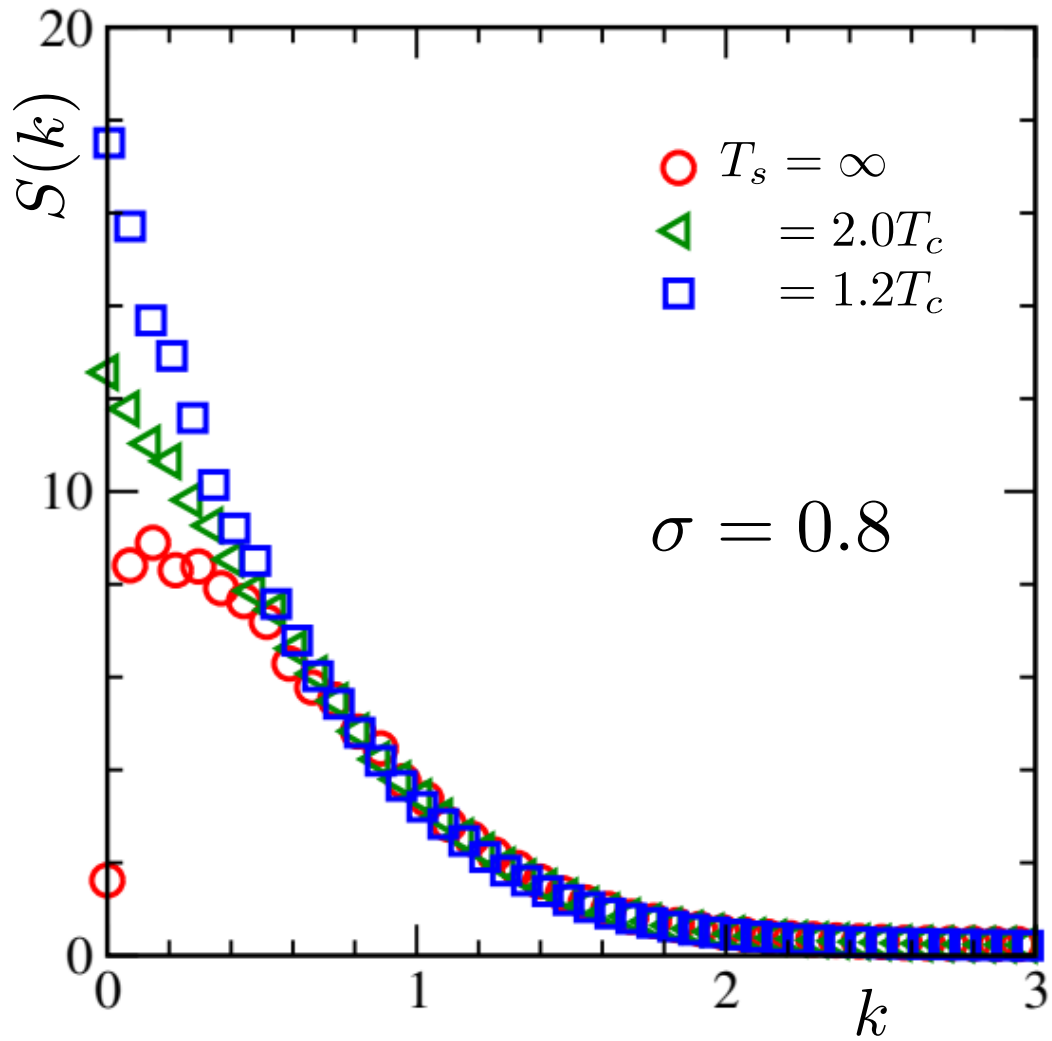


Figure 6.6: Structure factor, $S(k, t)$, is plotted as a function of wavenumber, k . Results from three different initial temperatures are included. Note that the structure factor is defined as $S(k, t) = \langle \phi_k(t) \phi_{-k}(t) \rangle$ [19].

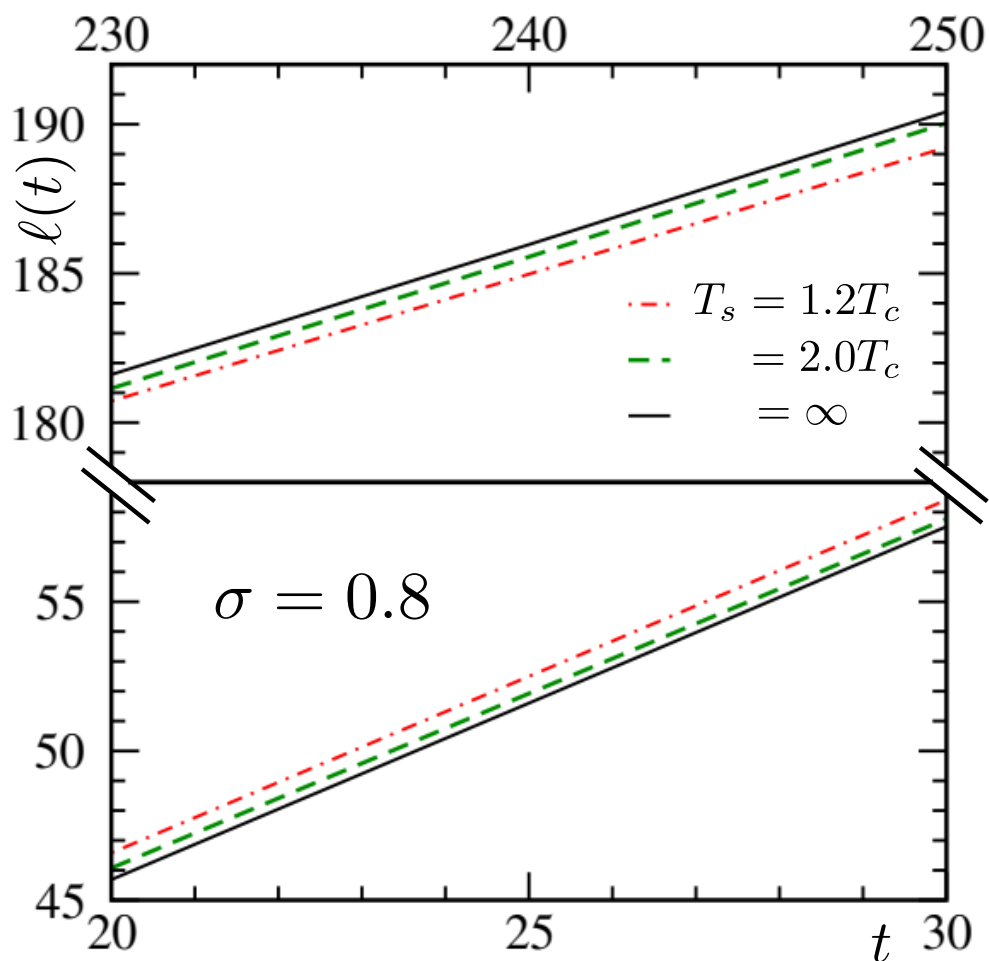


Figure 6.7: Average domain lengths, $\ell(t)$, when quenched to a final temperature, $T_f = 0.3T_c$, from three different T_s are shown as a function of time t . The lower panel shows very early time data, whereas the upper panel shows data from late times.

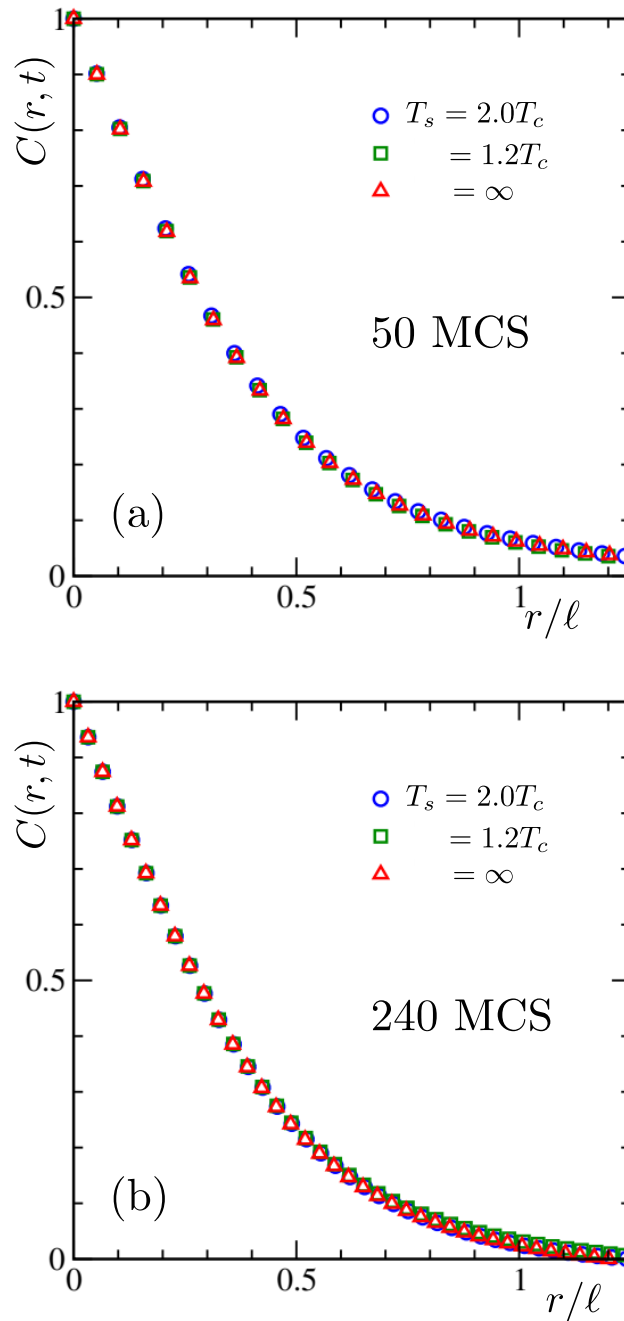


Figure 6.8: The correlation function, $C(r, t)$, is plotted as a function of r/ℓ for three different starting temperatures, T_s . (a) Data from the pre-crossing time are shown. (b) Here scaling of data at a post-crossover time is shown. These results are for $\sigma = 0.8$.

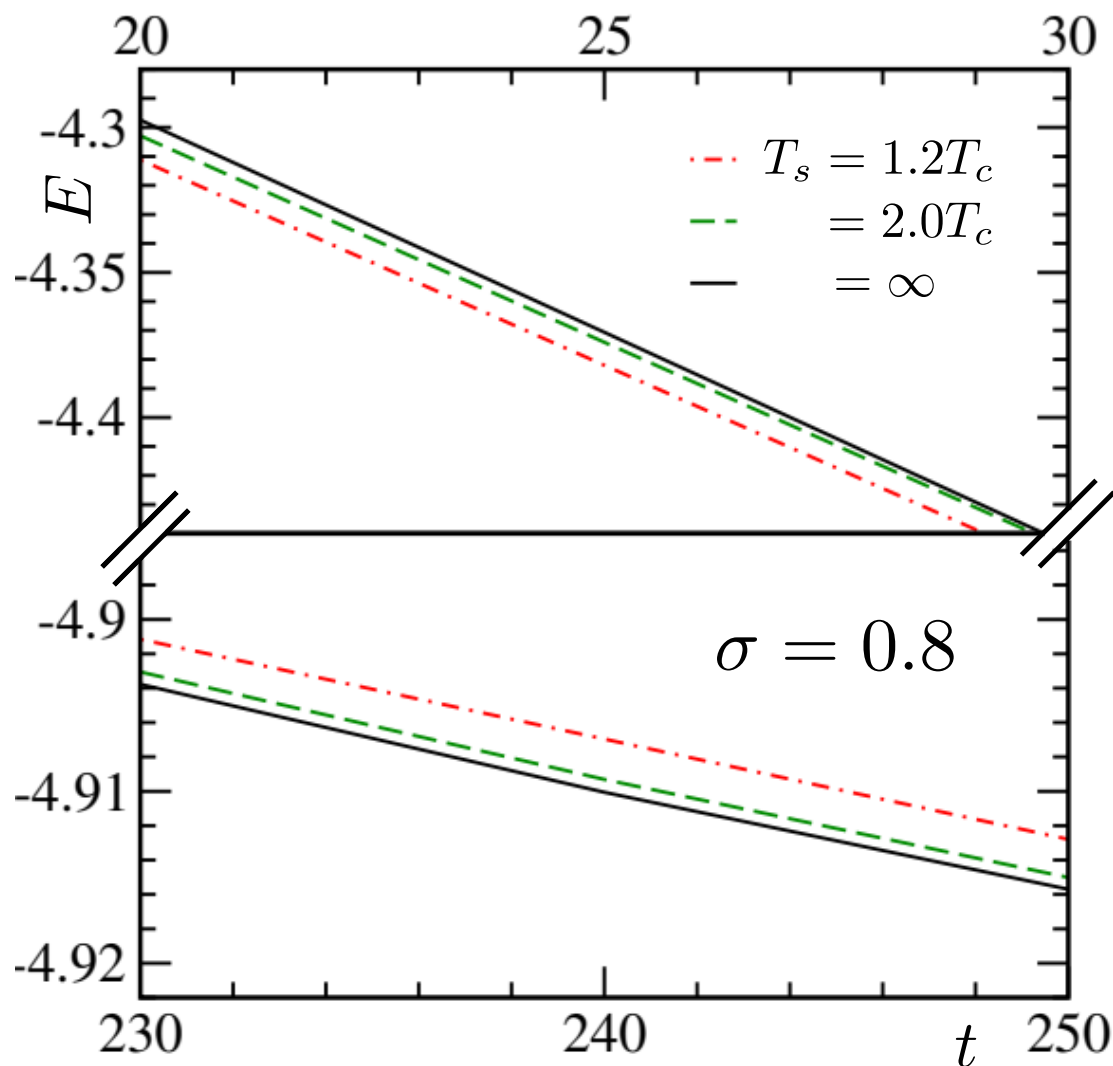


Figure 6.9: Total energy per spin, E , is plotted against time, t , for three different starting temperatures, T_s . The upper and lower panels show data from early and late times, respectively.

The upper panel shows the early-time scenario, where the systems with the lower T_s have the lower energy, which is quite expected. The lower panel, on the other hand, shows late-time behavior. At late times, the system with the highest T_s attains the lowest energy state, crossing others at some points in time. Fig. 6.9 suggests that the larger the initial temperature, the faster the system tries to reach final equilibrium, which indeed is the essence of the Mpemba Effect (ME) [1, 6–8].

6.4 Conclusion

In this chapter, we have studied the dynamics of phase transition in 2D Ising ferromagnet, where interaction between the lattice sites is long-range in nature [23, 24]. To mimic the evolution in ferromagnets, where the total order-parameter is not conserved, we have performed Glauber spin-flip Monte Carlo [15] simulations. Our main objective was to investigate the presence of a Mpemba-like effect [2, 3, 5–9] in a system where the Hamiltonian does not contain any in-built frustration but contains long-range interaction. We have prepared our systems at three different initial temperatures, all in the paramagnetic phase, and quenched them to a final temperature $T_f < T_c$. While the system evolves in order to reach the final equilibrium state, we have found that the one with the higher initial temperature relaxes faster and seems closer to the final equilibrium state within our observational time window than the one that started from lower temperatures. A faster equilibration of a hotter system than a colder one – This is the conclusion of this work.

In the previous chapter, we showed the presence of the Mpemba Effect in bulk water. We have talked about the metastable state and delay in nucleation due to the presence of the supercooled state of water. Here, in the long-range Ising model metastability may not be responsible for the effect. It should be noted here that metastability exists in simple nearest neighbor Ising model also. However, a preliminary study by discarding the metastable trajectories still show the Mpemba effect [25].

It will be interesting to introduce finite cooling rates in future studies. There for an accurate quantitative understanding of results from different σ one may need to adjust the cooling rates appropriately.

The results from this chapter are now published as:

Sohini Chatterjee, **Soumik Ghosh**, Nalina Vadakkayil, Tanay Paul, Sanat K. Singha and Subir K. Das, “Mpemba effect in pure spin systems: Role of initial correlation and a universality”, Phys. Rev. E **110**, L012103 (2024)

We have reproduced the results here following the policy of the American Physical Society. The article can be found online with the link below:

<https://doi.org/10.1103/PhysRevE.110.L012103>

Bibliography

- [1] E. B. Mpemba and D. G. Osborne, *Physics Education* **4**, 172 (1969).
- [2] A. Lasanta, F. Vega Reyes, A. Prados, and A. Santos, *Phys. Rev. Lett.* **119** (2017).
- [3] A. Biswas, V. V. Prasad, O. Raz, and R. Rajesh, *Phys. Rev. E* **102** (2020).
- [4] Y.-H. Ahn, H. Kang, D.-Y. Koh, and H. Lee, *Korean J. Chem. Eng.* **33**(1903) (2016).
- [5] Z. Lu and O. Raz, *Proc. Natl. Acad. Sci. U. S. A.* **114**(5083) (2017).
- [6] M. Baity-Jesi et. al., *Proc. Natl. Acad. Sci. U. S. A.* **116**(31), 15350 (2019).
- [7] S. K. Das, *Langmuir* **39**, 10715 (2023).
- [8] N. Vadakkayil and S. K. Das, *Phys. Chem. Chem. Phys.* **23**, 11186 (2021).
- [9] S. Chatterjee, S. Ghosh, N. Vadakkayil, T. Paul, S. K. Singha, and S. K. Das, *Phys. Rev. E* **110**, L012103 (2024).
- [10] A. Onuki, *Phase Transition Dynamics* (Cambridge University Press, 2002).
- [11] M. E. Fisher, *Reports on Progress in Physics* **30**(2), 615 (1967).
- [12] H. Christiansen, S. Majumder, M. Henkel, and W. Janke, *Phys. Rev. Lett.* **125**, 180601 (2020).
- [13] S. Ghosh and S. K. Das, *Phys. Rev. E* **109**, L052102 (2024).
- [14] K. Fukui and S. Todo, *Journal of Computational Physics* **228**(7), 2629 (2009).
- [15] R. J. Glauber, *Journal of Mathematical Physics* **4**(2), 294 (1963).

-
- [16] D. Frenkel and B. Smit, *Understanding Molecular Simulation* (Academic Press, 2002).
 - [17] T. Horita, H. Suwa, and S. Todo, Phys. Rev. E **95**, 012143 (2017).
 - [18] <https://github.com/OpenACCUserGroup/openacc-users-group>.
 - [19] A. J. Bray, Adv. Phys. **51**, 481 (2002).
 - [20] A. J. Bray, Phys. Rev. E **47**, 3191 (1993).
 - [21] T. Ohta, D. Jasnow, and K. Kawasaki, Phys. Rev. Lett. **49**, 1223 (1982).
 - [22] C. Yeung and D. Jasnow, Phys. Rev. B **42**, 10523 (1990).
 - [23] H. Christiansen, S. Majumder, and W. Janke, Phys. Rev. E **99**, 011301 (2019).
 - [24] F. Müller, H. Christiansen, and W. Janke, Phys. Rev. Lett. **129**, 240601 (2022).
 - [25] N. Vadakkayil and S. K. Das, To be published .

Chapter 7

Summary of the Thesis

This thesis contains results from studies on structure and dynamics in various nonequilibrium systems, having long-range inter-particle interactions. We have considered two well-known models, viz., the long-range Ising model (LRIM) and the TIP4P/Ice model of water (see the work chapters for related references). In the case of water, we have studied the phenomenon of freezing (into ice) from fluid phases. With LRIM, we have investigated the kinetics of phase separation in binary mixtures, as well as ordering from para- to ferromagnetic phase. For water, we have carried out molecular dynamics simulations. In the case of LRIM, the two different requirements were achieved via implementations of appropriate dynamics that either conserves the overall order-parameter (binary mixture) or not (ferromagnetic ordering). A brief summary of the outcomes is provided below.

In Chapters 2, 3 and 4, using LRIM Hamiltonian, we have studied the structure, growth, and aging during phase separation in binary mixtures, following quenches of configurations imitating the temperature $T = \infty$, to state points inside the appropriate coexistence regime. We have obtained results for significant variation in the range of interaction in the Hamiltonian. In the short-range situation, the results largely follow the established picture from the nearest neighbor Ising model. We found, however, that above a cut-off for the range of interactions, all the above-mentioned properties depend upon further micro variation of the interaction range [1]. This is unlike the case of static critical phenomena where the critical exponents for the long- and short-range universality classes are independent of such micro variations. Furthermore, the boundary for the studied nonequilibrium dynamics appears to be different from the reported picture in the static case. While there exist no theoretical results on structure and aging, our results on growth are in agreement with the

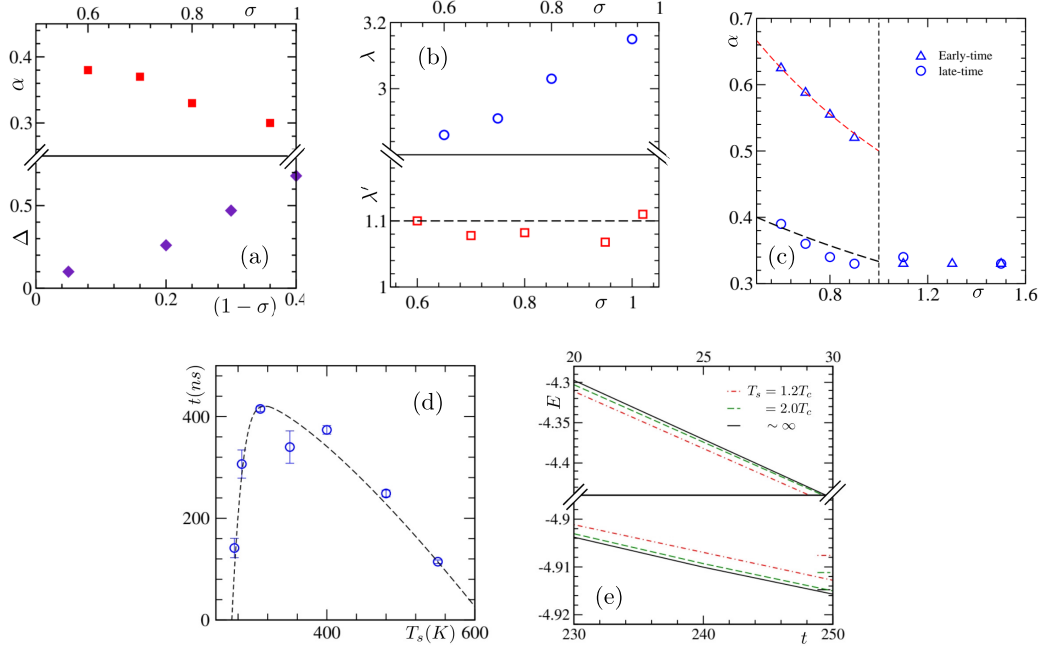


Figure 7.1: (a) The upper half shows a plot of the growth exponent, α , in the long time limit, for conserved order-parameter dynamics in the LRIM, that we have obtained from our simulations, as a function of σ . In the lower half, we have plotted the deviation, Δ , from the expected Porod exponent, in some intermediate wave number region, versus $(1 - \sigma)$. (b) Here, in the upper part, we have shown our estimated values of the aging exponent, λ , for the LRIM with conserved order-parameter dynamics, as a function of σ . The lower part shows the variation in the quantity $\lambda' (= \alpha\lambda)$ with the variation in σ . (c) The simulation estimated early and late time values of α , for the same system as in (a) and (b), are plotted as a function of σ , with symbols. The lines correspond to the existing theoretical predictions. (d) Freezing times, t_f , for the TIP4P/Ice model, are shown as a function of the starting temperatures, T_s . The dashed line is drawn for a better visualization of the trend. (e) Decay of energy per spin, E , in the LRIM with nonconserved order-parameter dynamics, as a function of time, for different starting temperatures, T_s . The upper and lower halves show data from early and late time regimes, respectively.

available theoretical literature [1]. For domain growth in the LRIM, we have also investigated the scaling at early times [2]. Even though the dynamics is conserved, we, to much surprise, find that the early time behavior matches with theoretical prediction for nonconserved dynamics, on the long-range side of the interaction! The key results from these chapters are put in parts (a), (b), and (c) of the adjacent figure. In these three chapters our new observations are nonuniversal features in different aspects of far-from-equilibrium dynamics with long-range interactions. Such interactions are common in nature. Examples include self-assembling active devices [5] and systems with dipoles [6]. Our studies can be of relevance in such practically relevant systems in other disciplines.

In Chapters 5 and 6 we address the issue of the Mpemba effect concerning two types of transitions - (1) Fluid to solid transition in TIP4P/Ice model and (2) Para-to-Ferromagnetic transition in the LRIM. We observe the effect in both situations [3, 4]: Configurations prepared at higher temperatures equilibrate at the new state point, following sudden quenches, quicker. In both the cases, our studies suggest that the cooling rate difference and presence of impurity, that may lead to heterogeneous nucleation, should not be necessary criteria for the exhibition of the effect. In the case of water, it appears that differences in longevity of metastability for different starting temperatures lead to the effect. In the magnetic case, we believe, the driving force comes from the differences in spatial correlations among the initial states. These issues we will address in details in the future. Key results from these chapters are put in parts (d) and (e) of the adjacent figure.

The references related to these works are provided below. The text and the results of the thesis often overlap with some of these published works. The related background literature can be found in the work chapters.

Bibliography

- [1] **S. Ghosh** and S. K. Das, Nonuniversal aging during phase separation with long-range interaction, Phys. Rev. E **109**, L052102 (2024).
- [2] **S. Ghosh** and S. K. Das, arXiv:2407.06954 (2024).
- [3] **S. Ghosh**, P. Pathak, S. Chatterjee and S. K. Das, Simulations of Mpemba Effect in WATER, Lennard-Jones and Ising Models: Metastability vs Critical Fluctuations, arXiv:2407.06954 (2024).
- [4] S. Chatterjee, **S. Ghosh**, N. Vadakkayil, T. Paul, S. K. Singha and S. K. Das, Mpemba effect in pure spin systems: Role of initial correlation and a universality, Phys. Rev. E **110**, L012103 (2024).
- [5] R. H. French et al., Long range interactions in nanoscale science, Soft Matter **82**, 1887 (2010).
- [6] A. K. Singh and V. Banerjee, Accelerated inertial regime in the spinodal decomposition of magnetic fluids, Soft Matter **19**, 2370 (2023).



Re: Regarding reuse of our published work in my thesis

From Tanay Paul <tanaypaul9492@gmail.com>

Date Mon 11/25/2024 6:37 PM

To Chatterjee Sohini <schatterjee@jncasr.ac.in>

Cc Nalina VADAKKAYIL <nalina.vadakkayil@uni.lu>; Ghosh Soumik <soumik@jncasr.ac.in>; sksingha <sksingha@rgipt.ac.in>; Subir K Das <das@jncasr.ac.in>

Dear Soumik,

You can surely add in your thesis the portion you reproduced from the paper. I am perfectly fine with it.

All the best wishes for your defence.

Tanay.

On Mon, 25 Nov, 2024, 6:33 am Chatterjee Sohini, <schatterjee@jncasr.ac.in> wrote:

Dear Soumik,

I agree. You may use it from the published paper in PRE.

Regards
Sohini

From: Nalina VADAKKAYIL <nalina.vadakkayil@uni.lu>

Sent: Monday, November 25, 2024 4:37 PM

To: Ghosh Soumik <soumik@jncasr.ac.in>; Chatterjee Sohini <schatterjee@jncasr.ac.in>; tanaypaul9492@gmail.com <tanaypaul9492@gmail.com>; sksingha <sksingha@rgipt.ac.in>; Subir K Das <das@jncasr.ac.in>

Subject: Re: Regarding reuse of our published work in my thesis

Dear Soumik,

You can surely use that. Infact, according to the APS copyright policy you can use it in the thesis without requesting the permission from APS. When we were including the results from paper published in pre in the thesis, we provided the citation and attached the relevant pages of copyright policy at the end of the thesis. I hope you are doing the same.

Regards,
Nalina

From: Ghosh Soumik <soumik@jncasr.ac.in>

Sent: Monday, November 25, 2024 11:21 AM

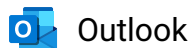
To: Chatterjee Sohini <schatterjee@jncasr.ac.in>; Nalina VADAKKAYIL <nalina.vadakkayil@uni.lu>; tanaypaul9492@gmail.com <tanaypaul9492@gmail.com>; sksingha <sksingha@rgipt.ac.in>; Subir K Das <das@jncasr.ac.in>

Subject: Regarding reuse of our published work in my thesis

Dear all,

I have reproduced a part of our published work {S. Chatterjee et al., Phys. Rev. E **110**, L012103 (2024)} and want to add it to my Ph.D. thesis. May I have your permission for that?

Thanks and regards,
Soumik Ghosh



Re: Regarding reuse of our published work in my thesis

From Dr. Sanat Kumar Singha <sksingha@rgipt.ac.in>

Date Mon 11/25/2024 10:01 PM

To Ghosh Soumik <soumik@jncasr.ac.in>

Cc Chatterjee Sohini <schatterjee@jncasr.ac.in>; Nalina VADAKKAYIL <nalina.vadakkayil@uni.lu>; tanaypaul9492@gmail.com <tanaypaul9492@gmail.com>; Subir K Das <das@jncasr.ac.in>

Dear Soumik,

You can certainly use it.

Best wishes,
Sanat

On Mon, Nov 25, 2024 at 3:51 PM Ghosh Soumik <soumik@jncasr.ac.in> wrote:

Dear all,

I have reproduced a part of our published work {S. Chatterjee et al., Phys. Rev. E **110**, L012103 (2024)} and want to add it to my Ph.D. thesis. May I have your permission for that?

Thanks and regards,
Soumik Ghosh



RightsLink

**The everlasting hunt for new ice phases****Author:** Thomas C. Hansen**Publication:** Nature Communications**Publisher:** Springer Nature**Date:** May 26, 2021*Copyright © 2021, The Author(s)***SPRINGER NATURE****Creative Commons**

This is an open access article distributed under the terms of the [Creative Commons CC BY](#) license, which permits unrestricted use, distribution, and reproduction in any medium, provided the original work is properly cited.

You are not required to obtain permission to reuse this article.

To request permission for a type of use not listed, please contact [Springer Nature](#)

AIP PUBLISHING LICENSE TERMS AND CONDITIONS

Jul 22, 2024

This Agreement between Soumik Ghosh ("You") and AIP Publishing ("AIP Publishing") consists of your license details and the terms and conditions provided by AIP Publishing and Copyright Clearance Center.

| | |
|------------------------------|--|
| License Number | 5834150116449 |
| License date | Jul 22, 2024 |
| Licensed Content Publisher | AIP Publishing |
| Licensed Content Publication | Journal of Chemical Physics |
| Licensed Content Title | A potential model for the study of ices and amorphous water: TIP4P/Ice |
| Licensed Content Author | Abascal, J. L. F.; Sanz, E. |
| Licensed Content Date | Jun 23, 2005 |
| Licensed Content Volume | 122 |
| Licensed Content Issue | 23 |
| Type of Use | Thesis/Dissertation |
| Requestor type | Student |
| Format | Print and electronic |

| Portion | Figure/Table |
|---|--|
| Number of figures/tables | 1 |
| Will you be translating? | No |
| Title of new work | Kinetics of Phase Transitions in a few Systems with Long-range Interactions |
| Institution name | Jawaharlal Nehru Centre for Advanced Scientific Research |
| Expected presentation date | Jul 2024 |
| Portions | FIG. 1 |
| The Requesting Person / Organization to Appear on the License | Soumik Ghosh |
| Requestor Location | Mr. Soumik Ghosh JNCASR Rachenahalli Lake Road Jakkur Bangalore, Karnataka 560064 India Attn: Mr. Soumik Ghosh |
| Billing Type | Invoice |
| Billing Address | Mr. Soumik Ghosh JNCASR Rachenahalli Lake Road Jakkur Bangalore, India 560064 Attn: Mr. Soumik Ghosh |
| Total | 0.00 USD |
| Terms and Conditions | |

AIP Publishing -- Terms and Conditions: Permissions Uses

AIP Publishing hereby grants to you the non-exclusive right and license to use and/or distribute the Material according to the use specified in your order, on a one-time basis, for the specified term, with a maximum distribution equal to the number that you have ordered. Any links or other content accompanying the Material are not the subject of this license.

1. You agree to include the following copyright and permission notice with the reproduction of the Material: "Reprinted from [FULL CITATION], with the permission of AIP Publishing." For an article, the credit line and permission notice must be printed on the first page of the article or book chapter. For photographs, covers, or tables, the notice may appear with the Material, in a footnote, or in the reference list.
2. If you have licensed reuse of a figure, photograph, cover, or table, it is your responsibility to ensure that the material is original to AIP Publishing and does not contain the copyright of another entity, and that the copyright notice of the figure, photograph, cover, or table does not indicate that it was reprinted by AIP Publishing, with permission, from another source. Under no circumstances does AIP Publishing purport or intend to grant permission to reuse material to which it does not hold appropriate rights.
You may not alter or modify the Material in any manner. You may translate the Material into another language only if you have licensed translation rights. You may not use the Material for promotional purposes.
3. The foregoing license shall not take effect unless and until AIP Publishing or its agent, Copyright Clearance Center, receives the Payment in accordance with Copyright Clearance Center Billing and Payment Terms and Conditions, which are incorporated herein by reference.
4. AIP Publishing or Copyright Clearance Center may, within two business days of granting this license, revoke the license for any reason whatsoever, with a full refund payable to you. Should you violate the terms of this license at any time, AIP Publishing, or Copyright Clearance Center may revoke the license with no refund to you. Notice of such revocation will be made using the contact information provided by you. Failure to receive such notice will not nullify the revocation.
5. AIP Publishing makes no representations or warranties with respect to the Material. You agree to indemnify and hold harmless AIP Publishing, and their officers, directors, employees or agents from and against any and all claims arising out of your use of the Material other than as specifically authorized herein.
6. The permission granted herein is personal to you and is not transferable or assignable without the prior written permission of AIP Publishing. This license may not be amended except in a writing signed by the party to be charged.
7. If purchase orders, acknowledgments or check endorsements are

issued on any forms containing terms and conditions which are inconsistent with these provisions, such inconsistent terms and conditions shall be of no force and effect. This document, including the CCC Billing and Payment Terms and Conditions, shall be the entire agreement between the parties relating to the subject matter hereof.

This Agreement shall be governed by and construed in accordance with the laws of the State of New York. Both parties hereby submit to the jurisdiction of the courts of New York County for purposes of resolving any disputes that may arise hereunder.

V1.2

Questions? customercare@copyright.com.

RE: Regarding permission for using a figure in a Ph. D. Thesis

AIPRights Permissions <Rights@aip.org>

Mon 7/22/2024 6:22 PM

To: Ghosh Soumik <soumik@jncasr.ac.in>

Dear Dr. Soumik,

Thank you for requesting permission to reproduce material from AIP Publishing publications. We are delighted to be able to assist.

Material for which permission is requested:

J. L. F. Abascal, E. Sanz, R. García Fernández, C. Vega; A potential model for the study of ices and amorphous water: TIP4P/Ice. *J. Chem. Phys.* 15 June 2005; 122 (23): 234511. <https://doi.org/10.1063/1.1931662>; Figure 1

To be reproduced in the following new work:

Soumik Ghosh, PhD Thesis, Jawaharlal Nehru Centre for Advanced Scientific Research; 2024

Permission is granted subject to these conditions:

1. AIP Publishing grants you non-exclusive world rights in all languages and media. This permission extends to all subsequent and future editions of the new work.
2. The following notice must appear with the material (please fill in the information indicated by capital letters):

“Reproduced from [FULL CITATION], with the permission of AIP Publishing.”

When reusing figures, photographs, covers, or tables, the notice may appear in the caption, in a footnote, or in the reference list.

In cases where the new publication is licensed under a Creative Commons license, the full notice as stated above must appear with the reproduced material.

3. If the material is published in electronic format, we ask that a link be created pointing back to the abstract of the article on the journal website. This can be accomplished using the article’s DOI.

4. This permission does not apply to any materials credited to another source.

For content reuse requests that qualify for permission under the STM Permissions Guidelines, which may be updated from time to time, the STM Permissions Guidelines supersede the terms and conditions contained in this license.

For future permission requests, we encourage you to use RightsLink, which is a tool that allows you to obtain permission quickly and easily online. To launch the RightsLink application, simply access the appropriate article on the journal site, click on “Tools”, and select “Reprints & Permissions.”

Please let us know if you have any questions. Congratulations on the completion of your thesis and your degree!

Sincerely,

Suzanne Inge

From: Ghosh Soumik <soumik@jncasr.ac.in>

Sent: Monday, July 22, 2024 5:33 AM

To: AIPRights Permissions <rights@aip.org>

Subject: Regarding permission for using a figure in a Ph. D. Thesis

Dear Sir/Madam,

I want to include 'FIG. 1' of the article "Journal of Chemical Physics 122(23), 234511 (2005)." in my Ph. D. thesis.
May I have your permission for that?

Regards,
Soumik Ghosh
Ph.D. Student
Jawaharlal Nehru Centre for Advanced Scientific Research
Bangalore, India

PHYSICAL REVIEW JOURNALS (/).

Published by the American Physical Society

[Journals \(/about\)](#) [Authors \(/authors\)](#) [Referees \(/referees\)](#) [Collections \(/collections\)](#)
[Browse \(/browse\)](#) [Search \(/search\)](#) [Press \(/press\)](#) [RSS \(/feeds\)](#)

December 2017

APS Copyright Policies and Frequently Asked Questions

- [What is copyright?](#)
- [What does copyright protect?](#)
- [How is a copyright different from a patent or a trademark?](#)
- [What is the difference between copyright infringement and plagiarism?](#)
- [Why should I transfer copyright to APS?](#)
- [Does transferring copyright affect my patent rights?](#)
- [As the author of an APS-published article, may I post my article or a portion of my article on my own website?](#)
- [What happens if the author has posted an APS-published article on a free access e-print server or on the authors' or institutions' web pages and subsequently a fee is imposed for access to those sites?](#)
- [As the author of an APS-published article, may I post my article or a portion of my article on an e-print server?](#)
- [As the author of an APS-published article, can I post my article or a portion of my article on a web resource like wikipedia or quantiki?](#)
- [As the author \(or the author's employer\) of an APS-published article, may I use copies of part or all of my articles in the classroom?](#)
- [As the author of an APS-published article, may I use figures, tables, graphs, etc. in future publications?](#)
- [As the author of an APS-published article, may I include my article or a portion of my article in my thesis or dissertation?](#)
- [As the author of an APS-published article, may I give permission to a colleague or third party to republish all or part of the article in a print publication?](#)
- [As the author of an APS-published article, may I give permission to a colleague or third party to republish all or part of the APS-published version in an online journal, book, database compilation, etc.?](#)

- As the author of an APS-published article, may I provide a PDF of my paper to a colleague or third party?
- As a third party (not an author), may I republish an article or portion of an article published by APS?
- As a third party, may I use articles published by APS for lecture and classroom purposes?
- How do I request permission to republish APS-copyrighted material?

What is copyright? <http://www.copyright.gov/> (<http://www.copyright.gov/>)

Copyright is a form of legal protection for original works of authorship. Copyright covers both published and unpublished works.

What does copyright protect?

Copyright, a form of intellectual property law, protects original works of authorship including literary, dramatic, musical, and artistic works, such as poetry, novels, movies, songs, computer software, and architecture. Copyright does not protect facts, ideas, systems, or methods of operation, although it may protect the way these things are expressed. See Circular 1, Copyright Basics, section "What Works Are Protected", see <http://www.copyright.gov/circs/circ01.pdf> (<http://www.copyright.gov/circs/circ01.pdf>).

How is a copyright different from a patent or a trademark?

Copyright protects original works of authorship, while a patent protects inventions or discoveries. Ideas and discoveries are not protected by the copyright law, although the way in which they are expressed may be. A trademark protects words, phrases, symbols, or designs identifying the source of the goods or services of one party and distinguishing them from those of others.

What is the difference between copyright infringement and plagiarism?

Copyright infringement occurs when an author's work is reused or republished without the permission of the copyright owner, whether or not author attribution accompanied the reuse.

Plagiarism occurs when an author's work has been reused or republished in such a manner as to make it appear as someone else's work, e.g., without quotation marks and citation of the original work.

Why should I transfer copyright to APS?

Like many other scientific publishers, the American Physical Society (APS) requires authors or their employers to provide transfer of copyright prior to publication. This permits APS to publish the article and to defend against improper use (or even theft) of the article. It also permits APS to publish the article online and to use the article in other forms or media, such as PROLA. By the APS transfer agreement, authors and their employers retain substantial rights in the work, as specified in the agreement <https://journals.aps.org/authors/transfer-of-copyright-agreement> (<https://journals.aps.org/authors/transfer-of-copyright-agreement>) and discussed in your copyright permission letter.

Does transferring copyright affect my patent rights?

No. Copyright is separate from any patent rights, and the APS transfer agreement specifically states that patent rights are not affected. However, you should be aware that submitting a manuscript to a journal without first taking steps to protect your patent rights (e.g., filing for a patent) could endanger those rights. Consult your patent attorney.

As the author of an APS-published article, may I post my article or a portion of my article on my own website?

Yes, the author or the author's employer may use all or part of the APS published article, including the APS-prepared version (e.g., the PDF from the online journal) without revision or modification, on the author's or employer's website as long as a fee is not charged. If a fee is charged, then APS permission must be sought. In all cases, the appropriate bibliographic citation and notice of the APS copyright must be included.

What happens if the author has posted an APS-published article on a free access e-print server or on the authors' or institutions' web page and subsequently a fee is imposed for access to those sites?

When a fee is imposed, the author must either obtain permission from APS or withdraw the article from the e-print server or Institutional Repository.

As the author of an APS-published article, may I post my article or a portion of my article on an e-print server?

The author has the right to post and update the article on a free-access e-print server using files prepared and formatted by the author. Any such posting made or updated after acceptance of the article for publication by APS should include a link to the online APS journal article abstract. In all cases, the appropriate bibliographic citation and notice of the APS copyright must be included.

As the author of an APS-published article, can I post my article or a portion of my article on a web resource like wikipedia or quantiki?

Sites like wikipedia and quantiki are strict about permissions and require that authors hold copyright to articles that they post there. In order to allow authors to comply with this requirement, APS permits authors to hold copyright to a "derived work" based on an article published in an APS journal as long as the work contains at least 10% new material not covered by APS's copyright and does not contain more than 50% of the text (including equations) of the original article. The APS will extend the author of a "derived work" the right to all papers published in APS journals.

As the author (or the author's employer) of an APS-published article, may I use copies of part or all of my article in the classroom?

Yes, the author or his/her employer may use all or part of the APS-prepared version for educational purposes without requesting permission from the APS as long as the appropriate bibliographic citation is included.

As the author of an APS-published article, may I use figures, tables, graphs, etc. in future publications?

Yes, as the author you have the right to use figures, tables, graphs, etc. in subsequent publications using files prepared and formatted by you or the APS-prepared versions. The appropriate bibliographic citation must be included.

As the author of an APS-published article, may I include my article or a portion of my article in my thesis or dissertation?

Yes, the author has the right to use the article or a portion of the article in a thesis or dissertation without requesting permission from APS, provided the bibliographic citation and the APS copyright credit line are given on the appropriate pages.

As the author of an APS-published article, may I give permission to a colleague or third party to republish all or part of the article in a print publication?

Yes, as the author you may grant permission to third parties to republish print versions of the article provided the APS-published version (e.g., the PDF from the online journal, or a copy of the article from the print journal) is not used for this purpose. The article may not be published in another journal, and the third party may not charge a fee. The appropriate bibliographic citation and notice of the APS copyright must be included.

As the author of an APS-published article, may I give permission to a colleague or third party to republish all or part of the APS-published version in an online journal, book, database compilation, etc.?

No, an author may not grant permission in this case. To request permission to republish APS-copyrighted material, please refer to the "Reuse & Permissions" link that can be found on each APS article page.

As the author of an APS-published article, may I provide a PDF of my paper to a colleague or third party?

The author is permitted to provide, for research purposes and as long as a fee is not charged, a PDF copy of his/her article using either the APS-prepared version or the author prepared version.

As a third party (not an author), may I republish an article or portion of an article published by APS?

Yes, APS will grant permission to republish articles or portions of articles (e.g., tables, graphs, excerpts) published by APS. Depending on the reuse and medium APS has the right to grant permission subject to APS terms and conditions and a fee may be assessed.

As a third party, may I use articles published by APS for lecture and classroom purposes?

Yes, you may use photocopied articles published by APS for lecture and classroom purposes without asking permission from APS as long as you remain an Authorized User of the APS online research per your institution's site license. Also, there is no limitation on the use of APS articles using links to the material accessible through institutional subscriptions.

How do I request permission to republish APS-copyrighted material?

APS uses Aptara's SciPris™ platform to manage rights and permission requests. APS will continue to support the STM guidelines for all copyright needs. To request permission to republish APS-copyrighted material, please refer to the "Reuse & Permissions" link that can be found on each APS article page.

Once directed to the SciPris™ platform, the following information is required:

1. The format in which the material will be republished, e.g., print, online, CD-ROM, and/or other format
2. How much of the article you want to republish, e.g., all or portion of article; if a portion describe the specific material, e.g., figure numbers, excerpt
3. How the material will be used, e.g., in a book, journal, proceeding, thesis, etc.
4. The title of the article/thesis/chapter etc., and the name of the publication in which your work will appear
5. The name of the publisher
6. Indicate whether or not a fee will be charged for the publication

Upon submission, a letter of permission will be generated, specifying all guidelines and regulations to follow.

Blanket permissions are not granted. Please note all requests are subject to APS [terms and conditions \(/info/terms.html\)](#) and a fee may be assessed.

If your questions have not been addressed and you need further assistance, please email customercare@aps.org (<mailto:customercare@aps.org>).

Further information

For further information about copyright in general, please refer to the Library of Congress FAQ at <https://www.copyright.gov/help/faq/> (<https://www.copyright.gov/help/faq/>).

Journals published by the American Physical Society can be found at <https://journals.aps.org/> (<https://journals.aps.org/>).

FAQ Version: December 12, 2017

Sign up to receive regular email alerts from *Physical Review Journals*

Sign up (<https://info.aps.org/journals-emails>).

AUTHORS[General Information \(/authors\)](/authors)[Submit a Manuscript \(https://authors.aps.org/Submissions/\)](https://authors.aps.org/Submissions/)[Publication Rights \(/pub_rights.html\)](/pub_rights.html)[Open Access \(/open_access.html\)](/open_access.html)[Tips for Authors \(/authors/tips-authors-physical-review-physical-review-letters\)](/authors/tips-authors-physical-review-physical-review-letters)[Professional Conduct \(/authors/professional-conduct-ethics\)](/authors/professional-conduct-ethics)**REFEREES**[General Information \(/referees\)](/referees)[Submit a Report \(http://referees.aps.org/\)](http://referees.aps.org/)[Update Your Information \(http://referees.aps.org/\)](http://referees.aps.org/)[Referee FAQ \(/referees/faq.html\)](/referees/faq.html)[Outstanding Referees \(/OutstandingReferees\)](/OutstandingReferees)**LIBRARIANS**[General Information \(https://librarians.aps.org/\)](https://librarians.aps.org/)[Subscriptions \(https://librarians.aps.org/subscriptions\)](https://librarians.aps.org/subscriptions)[Online License Agreement \(https://librarians.aps.org/sitelicense.pdf\)](https://librarians.aps.org/sitelicense.pdf)[Usage Statistics \(https://librarians.aps.org/login\)](https://librarians.aps.org/login)[Your Account \(https://librarians.aps.org/account\)](https://librarians.aps.org/account)**STUDENTS**[Physics \(https://physics.aps.org\)](https://physics.aps.org)[PhysicsCentral \(http://www.physicscentral.com/\)](http://www.physicscentral.com/)[Student Membership \(https://www.aps.org/membership/student.cfm\)](https://www.aps.org/membership/student.cfm)**APS MEMBERS**[Subscriptions \(https://www.aps.org/membership/aps-publications.cfm\)](https://www.aps.org/membership/aps-publications.cfm)[Article Packs \(https://journals.aps.org/article-packs\)](https://journals.aps.org/article-packs)[Membership \(https://www.aps.org/membership/index.cfm\)](https://www.aps.org/membership/index.cfm)[FAQ \(https://www.aps.org/membership/faq.cfm\)](https://www.aps.org/membership/faq.cfm)[APS News \(https://www.aps.org/publications/apsnews/index.cfm\)](https://www.aps.org/publications/apsnews/index.cfm)[Meetings & Events \(https://www.aps.org/meetings/index.cfm\)](https://www.aps.org/meetings/index.cfm)

[Privacy \(https://www.aps.org/about/webpolicies.cfm#privacy\)](https://www.aps.org/about/webpolicies.cfm#privacy)[Policies \(/policies\)](/policies)[Contact Information \(/contact.html\)](/contact.html)[Feedback \(mailto:feedback@aps.org\)](mailto:feedback@aps.org)

©2024 American Physical Society. (<https://www.aps.org/>) All rights reserved. *Physical Review*[™], *Physical Review Letters*[™], *Physical Review X*[™], *Reviews of Modern Physics*[™], *Physical Review A*[™], *Physical Review B*[™], *Physical Review C*[™], *Physical Review D*[™], *Physical Review E*[™], *Physical Review Applied*[™], *Physical Review Fluids*[™], *Physical Review Accelerators and Beams*[™], *Physical Review Physics Education Research*[™], *Physical Review Materials*[™], *Physical Review Research*[™], *PRX Energy*[™], *PRX Life*[™], *PRX Quantum*[™], *APS Physics logo*, and *Physics logo* are trademarks of the American Physical Society. Information about registration may be found [here \(/legal\)](/legal). Use of the American Physical Society websites and journals implies that the user has read and agrees to our [Terms and Conditions \(/info/terms.html\)](/info/terms.html) and any applicable [Subscription Agreement \(https://librarians.aps.org/sitelicense.pdf\)](https://librarians.aps.org/sitelicense.pdf).